The forgotten Mesoproterozoic of Northern Australia: a chemostratigraphy and detrital zircon study of the greater McArthur Basin.

Word Count: 7748

Thesis submitted in accordance with the requirements of the University of Adelaide for an Honours Degree in Geology

Darwinaji Subarkah

November 2018

THE UNIVERSITY of ADELAIDE

THE FORGOTTEN MESOPROTEROZOIC OF NORTHERN AUSTRALIA: A CHEMOSTRATIGRAPHY AND DETRITAL ZIRCON STUDY OF THE FAVENC PACKAGE, GREATER MCARTHUR BASIN.

CONSTRAINTS ON GEOCHRONOLOGY AND PALAEOGEOGRAPHY OF THE GREATER MCARTHUR BASIN

ABSTRACT

The informally named greater McArthur Basin is a regionally extensive Proterozoic 'super basin' system located across northern Australia. The region hosts large and proven hydrocarbon reservoirs as well as high grade mineralisation. The deposition system is divided into 'packages'; rocks of similar lithology, age and stratigraphic position. Although studies have begun to constrain intra-basin correlation, tectonic setting and depositional environments of the enclosing Wilton and Glyde Packages, very little is known about the Favenc Package. In this study, we present new, high resolution geochemical isotopic data (rare earth, trace and majors elements) as proxies for the palaeoenvironment and redox conditions of the Mount Rigg Carbonates. Cerium anomalies, Y/Ho and Zn/Fe ratios of carbonate-rich facies show evidence for restrictive and anoxic basin-wide conditions through the deposition of the Dook Creek, Limmen and Mainorou Formations. Furthermore, rare earth elements and yttrium (REY) distribution patterns of these carbonates also reflected a lacustrine environment. In addition, new U–Pb, Hf and REE data of detrital zircons within the Favenc and Wilton Packages are also presented to investigate correlation and provenance of stratigraphically similar groups. Using the youngest concordant grain, the Dook Creek Formation is interpreted to have a maximum depositional age of 1614 ± 78 Ma. $\varepsilon_{Hf}(t)$ values of the unit ranges between -28.09 to 18.89. Findings in this study were then incorporated together to develop a tectonic and deposition model for the Mesoproterozoic greater McArthur Basin.

KEYWORDS

GREATER MCARTHUR BASIN, REDOX, GEOCHRONOLOGY

Table of Contents

LIST OF FIGURES AND TABLES

INTRODUCTION

The informally-named greater McArthur Basin is a large-scale, multiphase deposition system formed during the Proterozoic (Close, 2014). It extends over a significant portion of the Northern Territory, from the northeast of Western Australia to northwest of Queensland (Figure 1). The region hosts large and proven hydrocarbon reserves, high grade mineralisation (Ahmad & Munson, 2013; Close, 2017; Dunster, 1998) as well as an unperturbed sedimentary record of its geological era (Cox et al., 2016; Shen et al., 2002). Further insight on the rocks of the greater McArthur Basin can provide a better understanding on how the basin formed, developed, as well as the palaeoenvironment during the deposition of its sedimentary units.

The greater McArthur Basin consists of five distinct Palaeoproterozoic to Neoproterozoic sedimentary packages (Rawlings, 1999) comprising of successions from the McArthur Basin, Birrindudu Basin and the Tomkinson Province that have been correlated in the subsurface (Munson, 2016; compiled in Figure 2). These packages are the Wilton, Favenc, Glyde and the Redbank Packages. Each package represents basin-wide rocks of similar age, lithology and stratigraphic position. Intra-basin chemostratigraphic and physical correlations between the Glyde Package and the Wilton Package throughout the Greater McArthur Basin have been recently established and refined (Bullen, 2017; Close, 2017; Cox et al., 2016; Munson, 2016; Yang et al. 2018: in review). However, the rocks of the Favenc Package are still poorly constrained. Very little is known about the age, provenance as well as the palaeogeography of these units.

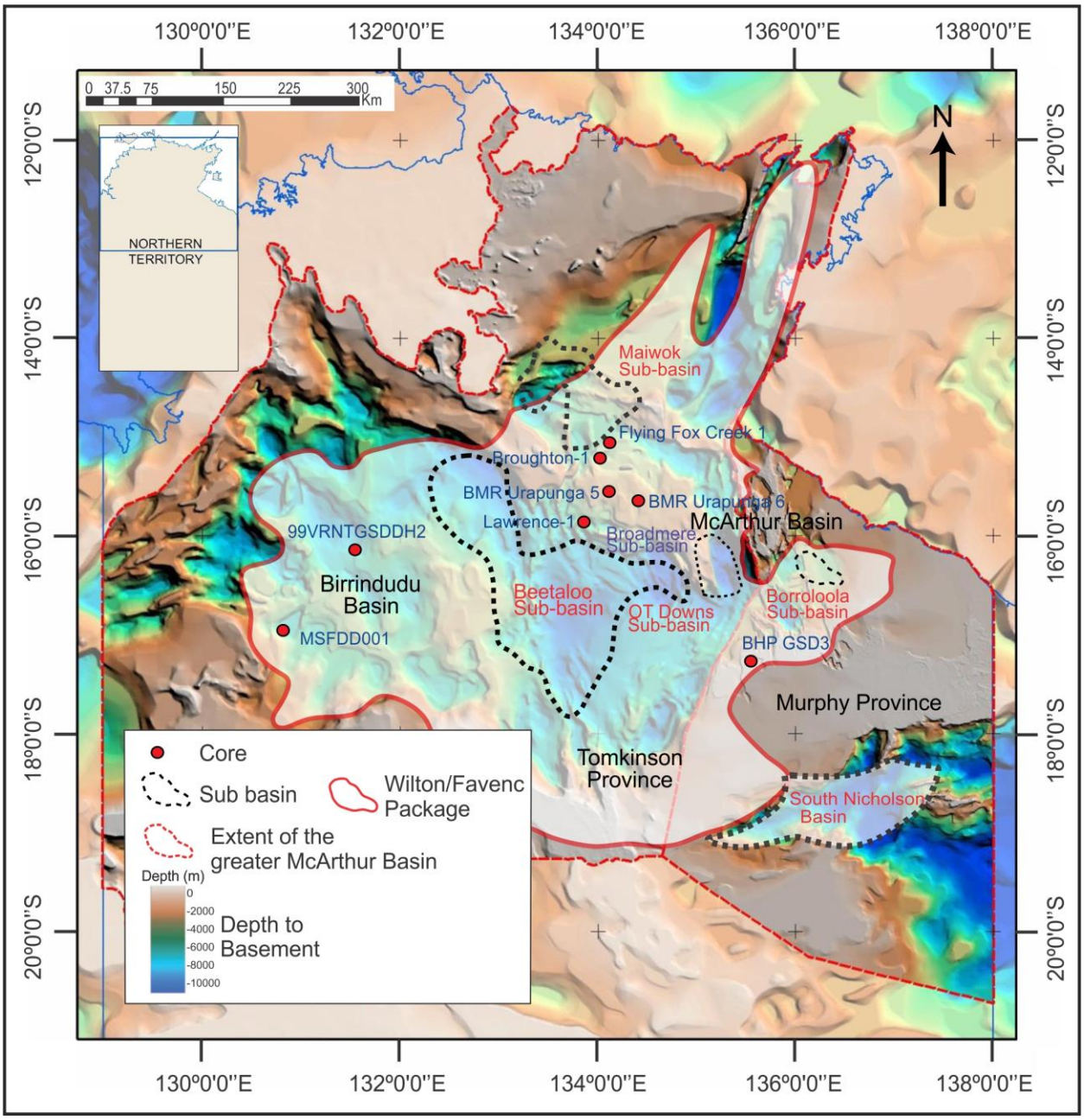

Figure 1: Proterozoic SEEBASE™ basement surface map showing the extent of the greater McArthur Basin as well as the locations of drillholes used in this sample.

The interpreted correlation between the Favenc Package units within the Birrindudu Basin and the McArthur Basin is weak at best. Within the Birrindudu Basin, only three tentative maximum depositional ages (MDA) have been identified. These were derived from the Wickham Formation (1639 ± 16 Ma), the Neave Sandstone (1622 ± 32 Ma) and the Weaner Sandstone (MDA = 1600 ± 24 Ma) by Carson (2012). In the McArthur Basin, studies by Geoscience Australia (Ahmad & Munson, 2013) indicated that the oldest dated formation of the Nathan Group is the Smythe Sandstone (1613 ± 24 Ma) while the youngest is the Balbirini Dolostone (1589 ± 3 Ma). There are no known age constraints for the Mount Rigg Group, which is the proposed equivalent of the Nathan Group in the northern region of the McArthur Basin.

Palaeoenvironment studies of the greater McArthur Basin have largely focused on packages enclosing the Favenc Package. A compilation by Munson (2016) concluded that geochemical isotopic studies done on the Wilton Package as well as presence of synaeresis cracks in multiple units suggests that the sediments were deposited in a restricted to partially restricted anoxic environment with fluctuating salinities. Meanwhile, results from Bullen (2017) on the Limbunya Group (Glyde Package equivalent) have also been interpreted to imply deep water anoxia with periods of open water conditions during the deposition of minor dolomitic units. Both studies propose a depositional model of an enclosed marine basin, partially cut off from the open ocean and causing cycles of water stratification. No such enquiries have been made on any of the formations in the Favenc Package.

This study aims to fill this knowledge gap to develop a palaeoenvironmental and palaeogeographic interpretation of northern Australia during the deposition of the Favenc Package. Specifically, by integrating new geochronological data with existing literature, this study constrains sedimentary provenance, the maximum depositional ages and improves intra-basin correlations. In addition, this study will explore the geochemical properties of the Mount Rigg Group in order to create a complete chemostratigraphic profile for its palaeoenvironment. The palaeoenvironment will be investigated using trace and major elemental data from the carbonate-rich successions. $\delta^{18}O$ and $\delta^{13}C$ signatures, Ce anomalies as well as Zn/Fe ratios can determine biological activity and redox conditions of the water column. Rare earth elements and yttrium (REY) distribution patterns and Y/Ho ratios of the carbonate facies reflects the environmental setting during deposition. Intra-basin correlation is established by age constraints derived from detrital zircons (maximum deposition age) in addition to linking changes in sedimentary provenance. Rare earth elements (REE) as well as hafnium isotopic data in zircons can be powerful tools to analyse these changes. Findings in this study are then combined to form a tectonic model to explain the palaeogeography during the deposition of the Favenc Package.

	Birrindudu Basin	McArthur Basin	Tomkinson Province
Wilton Package	Tijunna Group	Roper Group	Renner Group
Favenc Package	Bullita Group Wattie Group	Nathan Group Mt. Rigg Group	
Glyde Package	Limbunya Group	McArthur Group	Namerinni Group
Redbank Package	Birrindudu Group	Tawallah Group	

Figure 2: Intra-basin correlation within the greater McArthur Basin summarised from Rawlings (1999) and Munson (2016). The figure shows the proposed equivalent groups within different regions of the greater McArthur Basin.

BACKGROUND

The Favenc Package

The Favenc Package is a regionally extensive succession ranging from 50 to 1600 m in thickness and is comprised of largely evaporitic dolostone and subordinate siliciclastic rocks deposited in a shallow marine marginal-shelf (Rawlings, 1999; Ahmad & Munson 2013). It lies uncomformably on top of the Glyde package and underlies the Wilton package. The Favenc Package consists of the Bullita Group in the Birrindudu Basin, the widespread Nathan Group deposited in most of the McArthur Basin as well as the Mount Rigg Group in the northeast of the McArthur Basin (Figure 2). The age of the package has initially been constrained by the enclosing Glyde and Wilton packages. This constrains deposition to between 1599 ± 11 Ma (SHRIMP U–Pb zircon age of upper Balma Group: Haines, 1994) and 1492 ± 4 Ma (SHRIMP U–Pb zircon age of the Showel Member of the Mainoru Formation: Munson et al., 2013). However, recent studies have started to internally constrain the Favenc package. SHRIMP zircon dating of the lower and upper Balbirini Dolostone in the Nathan Group gave ages of 1632 ± 4 Ma and 1589 ± 3 Ma respectively (Page et al., 2000). A tentative maximum depositional age of 1600 ± 24 Ma (Carson, 2010) was also given by detrital zircon grains in the Weaner Sandstone of the Bullita Group. The correlated formations, as well as their respective maximum depositional ages compiled in this study are shown in Figure 3.

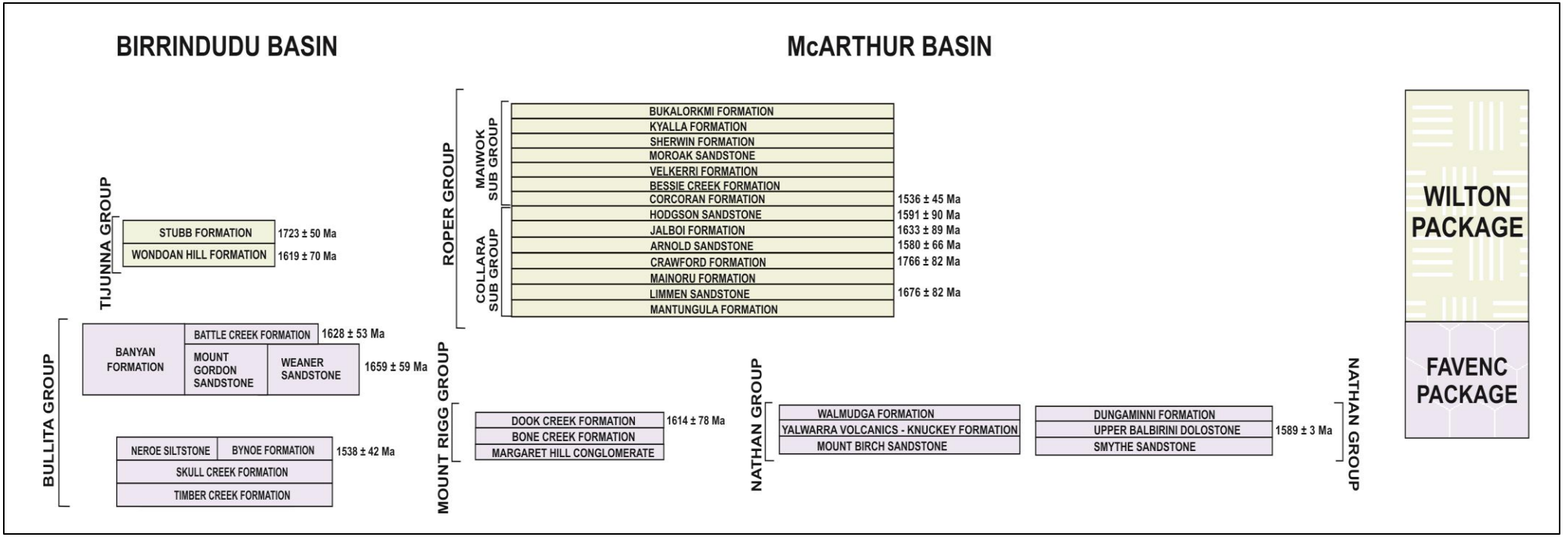

Figure 3: MDA of the Dook Creek Formation displayed alongside other stratigraphically similar formations. The maximum depositional age is defined as the youngest concordant age of a single grain as there should be no reason why one zircon has the same age of another. Roper Group data are from Cassidy (2018) and Birrindudu Basin data are from Yang et al. (2018).

McArthur Basin

The McArthur Basin contains rocks aging from Palaeo-to-Mesoproterozoic and are exposed over an area of 180000 km^2 in the northeastern of the Northern Territory. It unconformably overlies the metamorphosed Pine Creek Orogeny to the northwest and the Arnhem Province to the east (Ahmad & Munson, 2010). A geographic high called the Murphy Inlier separates the McArthur Basin from the South Nicholson Basin (Plumb & Wellman, 1987). Initial models represented the basin as a number of north-trending asymmetric rifts separated by north-west trending faults that divided the basin into depositional 'troughs' and 'shelves' (Plumb, Derrick, & Wilson, 1980). However, seismic data discussed in Rawlings (2004) indicated that these structures show no evidence of a separate depocentre and the sedimentary successions continue laterally in both directions from the implied boundaries, arguing against grouping the basin into these sub-sections. All of the subdivisions of the McArthur Basin are shown in Figure 2.

The Nathan Group is recognised to lie above a regional unconformity, separating it from the underlying McArthur Group. The overlying Roper Group sits above a second unconformity (Ahmad & Munson 2013). The Nathan Group crops out extensively from the southern McArthur Basin and northwards into eastern Arnhem Land (Rawlings, 1999). The bottom of the group is made of thin, basal siliciclastic and sometimes conglomeratic unit followed by thicker carbonate formations that pass up into siliciclastic rocks.

The Mount Rigg Group crops out mostly on the Arnhem Shelf in the margin of the northern McArthur Basin (Kruse et al., 1994) and is interpreted to correlate with the Nathan Group (Ahmad & Munson 2013). It lies unconformably above the Katherine River Group, with the

Roper Group unconformably overlying it. The group is dominated by stromatolitic and oolitic dolostone and sandstone and is thought to be deposited in a shallow shelf setting.

The Collara Subgroup is defined as the lower portion of the Roper Group, consisting of formations from the base of the Roper Group to the top of the Hodgson Sandstone (Abbott et al., 2001). The basal unit of the subgroup differs depending on location varying from the Phelp Sandstone in northwestern McArthur Basin, Limmen Sandstone or the Mantungula Formation elsewhere. The subgroup consists of eight different formations which were largely deposited within a marine shelf or tidal platforms (Ahmad & Munson 2013).

Birrindudu Basin

The sedimentary packages of the Birrindudu Basin are similar in age and lithology to the McArthur Basin and crop out over 35000 km^2. The first geological mapping of the area was undertaken by Woods and Brown in 1895. It unconformably overlies the metamorphosed and deformed Pine Creek Orogen in the north and the Tanami Region in the south (Ahmad & Munson, 2013). The basin was interpreted to have formed by rifting and lithospheric tilting during subduction arc processes in Central Australia (Southgate et al., 2000) and correlates with parts of the Kimberley Basin in Western Australia (Blake et al., 2000). Although initial workers had recognised that the Birrindudu Basin and the overlying Victoria Basins were different deposition systems (Blake, Hodgson, & Smith, 1975; Sweet 1977), there was no consensus on where to put the break between the two. Currently, the basins were redefined by Ahmad and Munson (2013) who has inserted the break at the base of the Auvergne Group. The Birrindudu Basin contains six main groups and all are separated by unconformities. In stratigraphic order, these groups are the Tijunna, Bullita, Wattie, Limbunya, Birrindudu and the Tolmer Group.

Rocks of the Birrindudu Basin are largely unmetamorphosed and undeformed, with minor igneous activity recorded in the Limbunya Group. Exposure of oldest rocks in the centre of the basin in addition to strata dipping away from depocentres indicate a major basin inversion (Ahmad & Munson 2013).

The Bullita Group is a sequence of mainly stromatolitic carbonates and sandstone successions. There is a clear cessation to basin-wide carbonate deposition followed by a transition to siliciclastic deposition between the lower and upper part of the group (Ahmad & Munson, 2013). This group is made of eight different formations that reflected varying depositional environments, from shallow-marine evaporitic conditions to relatively deeper, stable environments.

The Tijunna Group unconformably overlies the Bullita Group and is itself uncomformably overlain by the Auvergne Group in the Victoria Basin (Cutovinos, et al., 2002). The group varies in thickness throughout the basin ranging from 200–300 m of preserved beds in the south of the basin to totally absent in northeastern Waterloo 1:250K map sheet. The Tijunna Group is largely composed of sandstone and mudstone assemblages.

METHODS

Extended instructions for the methodology used in this study can be found in the Appendix.

Sample Selection

Samples used in this study were taken from the Dook Creek Formation in the Mount Rigg Group and compared with rocks stratigraphically higher from the Collara Subgroup (Cassidy, 2018) as well as supposed spatial equivalents from the Bullita Group and the Tijunna Group in the Birrindudu Basin (Yang et al., 2018). Detrital zircons were acquired from sandstone formations to improve age constraints while carbonate-rich strata were analysed for their geochemical properties. The locations of drillholes used in this study are shown in Figure 1.

For detrital zircon analysis, two sandstone samples were collected from the Flying Fox Creek borehole in the McArthur Basin. U–Pb, REE and Hf isotopic data from both samples were then compared to possible equivalents across the greater McArthur Basin. For trace and major element analysis as well as δ^{13}Carbon and δ^{18}O isotopic investigation, 25 carbonate-rich samples were collected from Mountain Valley borehole, which contains an undisturbed record of the formations relevant to this study, described as the Mount Rigg Carbonates. The samples were collected to give a resolution of approximately 10 metre intervals. The samples are largely homogeneous and have no visible signs of alteration. The resultant geochemical profile produced was then compared to other carbonate-rich formations lower in the stratigraphy.

Uranium—Lead detrital zircon analysis

Procedure for this stage was done following Blades (2013) and Yang et al. (2018). Grains were separated from crushed samples by standard panning, magnetic as well as heavy liquid techniques. Individual grains were then handpicked and mounted onto a non-reactive epoxy resin which were polished to expose the surface. The mounts were then carbon coated to prepare for cathodoluminesence (CL) imaging using a FEI Quanta 600 Scanning Electron Microscope (SEM) with attached Gatan CL Detector and examined using a Laser Ablation Inductively Coupled Plasma-Mass Spectrometer (LAICP-MS). Data were reduced and processed using Iolite and plotted using Excel add-in Isoplot (Ludwig, 2003). Zircon standard GEMOC GJ–1 (TIMS normalisation data: $^{207}Pb/^{206}Pb$ = 607.7 ± 4.3 Ma, $^{206}Pb/^{238}U$ = 600.7 ± 1.1 Ma and $^{207}Pb/^{235}U$ = 602.0 ± 1.0 Ma, Jackson et al., 2004) was used to correct for mass bias and instrumental fractionation and accuracy was checked using Plesovice zircon standard ($^{206}Pb/^{238}U$ = 337.13 ± 0.37, Slama et al., 2008). A total of 52 Plesovice internal standard were analysed yielding a weighted average $^{207}Pb/^{206}Pb$ age of 338.2 ± 2.7 Ma (95% confidence, MSWD = 1.3). For estimating age of detrital grains, the $^{207}Pb/^{206}Pb$ age was chosen for ages older than 1.2 Ga (Gehrels, 2014 and Yang, 2018). Maximum depositional ages were then defined using single grain ages, as there should be no reason that any two zircon grains should have the same age in any sandstone (Spencer & Kirkland, 2016).

Hafnium isotope determination

Hafnium isotope examination were based on Payne (2013) where zircon grains were selected for ablation and analyses based on concordance and age populations in each sample. Analyses were undertaken using a New Wave UP–193 Laser with attached Thermo-Scientific Neptune Multi-Collector ICP-MS at University of Adelaide. Ablation times were ~25 seconds for 200 cycles at

a 6Hz repetition rate, with laser power of 100mJ/pulse and a spot size of 50μm for each measurement. Data reduction was done using a Hf isotope data reduction Excel add-in, Hf TRAX (Payne et al. 2013). Data were normalised to $^{179}Hf/^{177}$ Hf = 0.7325 with an exponential correction accounting mass bias. Internal standards were analysed for a range between $^{176}Yb/^{177}Hf$ and $^{176}Lu/^{177}Hf$ to check for accuracy and stability, with the resultant $^{176}Lu/^{177}Hf$ used to calculate initial $^{176}Hf/^{177}Hf$ ratios. A total of 25 standards were analysed, producing an MT average of 0.282512 ± 0.00001.

Trace and major element analysis of carbonates

Trace and major element analysis was modified from conventional procedures (Bullen, 2017; Halverson et al., 2010; Liu et al., 2014) to ensure prevention of contamination from clay minerals, altered carbonate and other mineral phases. Samples were crushed and ~70mg of rock powder were weighed and placed into 15mL centrifuge tubes. They were then cleansed twice using 1 M ammonium acetate solution to extract loose ions from mineral surfaces (Bailey et al., 2000) prior to leaching. Leaching was done in a 3-step process, twice with 0.2M acetic acid and once with 2% nitric acid to restrict partial dissolution of clays within the sample. For each step, sample tubes sat in a sonicating bath for 20 minutes and centrifuged at 4000rpm for 10 minutes. The residue was kept for further leaching while the supernatant was collected and digested with 2% nitric acid again into aliquots of ~1:1500 and ~1:100000 dilutions for trace and major element analysis respectively. A calibration for matrix effects was done using standards prepared from multi-element stock standards solutions ranging from 0.3–300 μg/L and accuracy was determined by a calibration curve established for five samples for concentrations from 0–500 ppb. The standard used was JDO–1.

δ^{13}Carbon and δ^{18}Oxygen isotope analysis of carbonates

Carbon and oxygen isotopic analysis was done following Bullen (2017) and Cox et al. (2016). Samples were crushed and ~25mg of rock powder was weighed and placed into 1mL glass septa vials. The vials were then cleansed with He. Next, 10 drops of H_3PO_4 (1 M) was added at 90˚C for 1 hour to purify the samples. The resultant CO_2 produced was then collected cryogenically and isotope ratios were measured against an in-house reference gas using a Nu Perspective Dual-Inlet Isotope Ratio Mass Spectrometer (DI-IRMS) connected to a NuCarb carbonate preparation system at McGill University Stable Isotope Laboratory in Montréal, Canada. Samples were calibrated to Vienna Pee Dee Belemnite (VPDB) and errors are ~0.05‰ (1σ) for both $\delta^{13}C$ and $\delta^{18}O$.

OBSERVATIONS AND RESULTS

Detrital Zircon Analysis

U–PB GEOCHRONOLOGY

Samples FF01 and FF02 were collected from the Jamberline Sandstone, a silicilastic member within the Dook Creek Formation. Both samples were quartz sandstone, medium-to-coarse grained with pebbly clasts up to 0.5 mm. The Dook Creek Formation makes up the bulk of the Mount Rigg Group and has been interpreted to be deposited under a proximal fluvial to shallow marine setting. The ages of detrital zircons were examined to define maximum depositional ages and establish correlation with supposed equivalents within the basin system. Zircon grains examined in this study vary in shapes and sizes but almost all show oscillatory zoning under CL (Figure 4), characteristic of growth within a magma chamber (Corfu et al. 2003). A majority of the grains were also rounded, elongated and not prismatic indicating a history of sedimentary processes. A total of 224 analyses were conducted. This yielded 53 and 38 concordant data from samples FF01 and FF02 respectively. Both the kernel density estimation (KDE) (Figure 5) and U–Pb concordia (Figure 6) plots demonstrate the main age population of zircons within the sample to be ca. 1800 Ma, ca. 2100 Ma and ca. 2500 Ma. Three youngest concordant grains were calculated to give a weighted average population age of 1646 ± 44 Ma. The single youngest concordant age was 1614 ± 78 Ma and this is interpreted to be the maximum depositional age. A number of analyses are discordant, apparently with approximately zero intercepts. This suggests a pattern of modern lead loss, which is surprising as these samples were collected from depths below the effects of modern weathering.

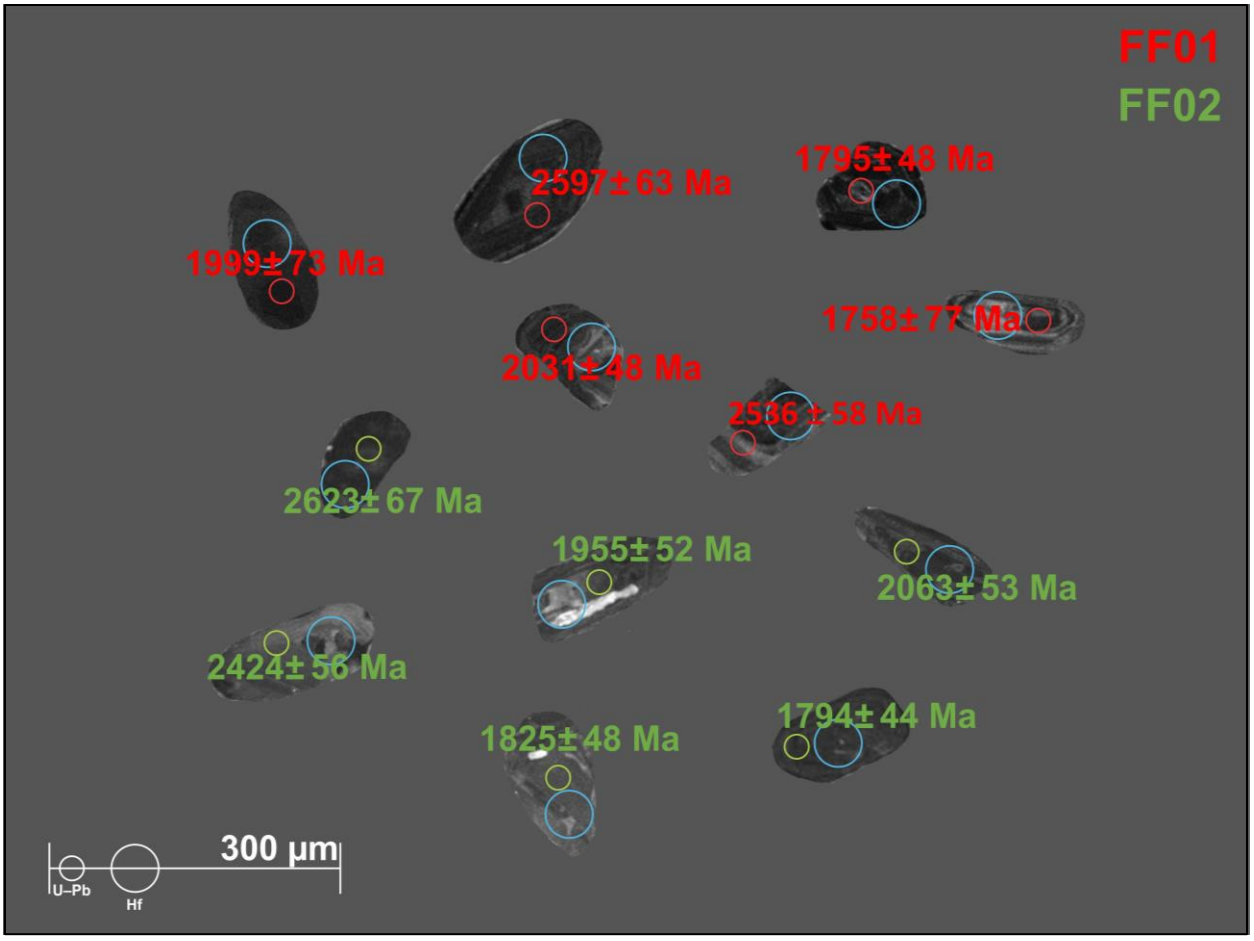

Figure 4: CL images of detrital zircon grains from FF01 and FF02, a quartz sandstone from the Dook Creek Formation, Mount Rigg Group. They show oscillatory zoning and are rounded to sub-rounded, indicative of a magmatic origin followed by sedimentary processes. U–Pb and Hf analyses laser spots are indicated by the smaller and larger circles respectively.

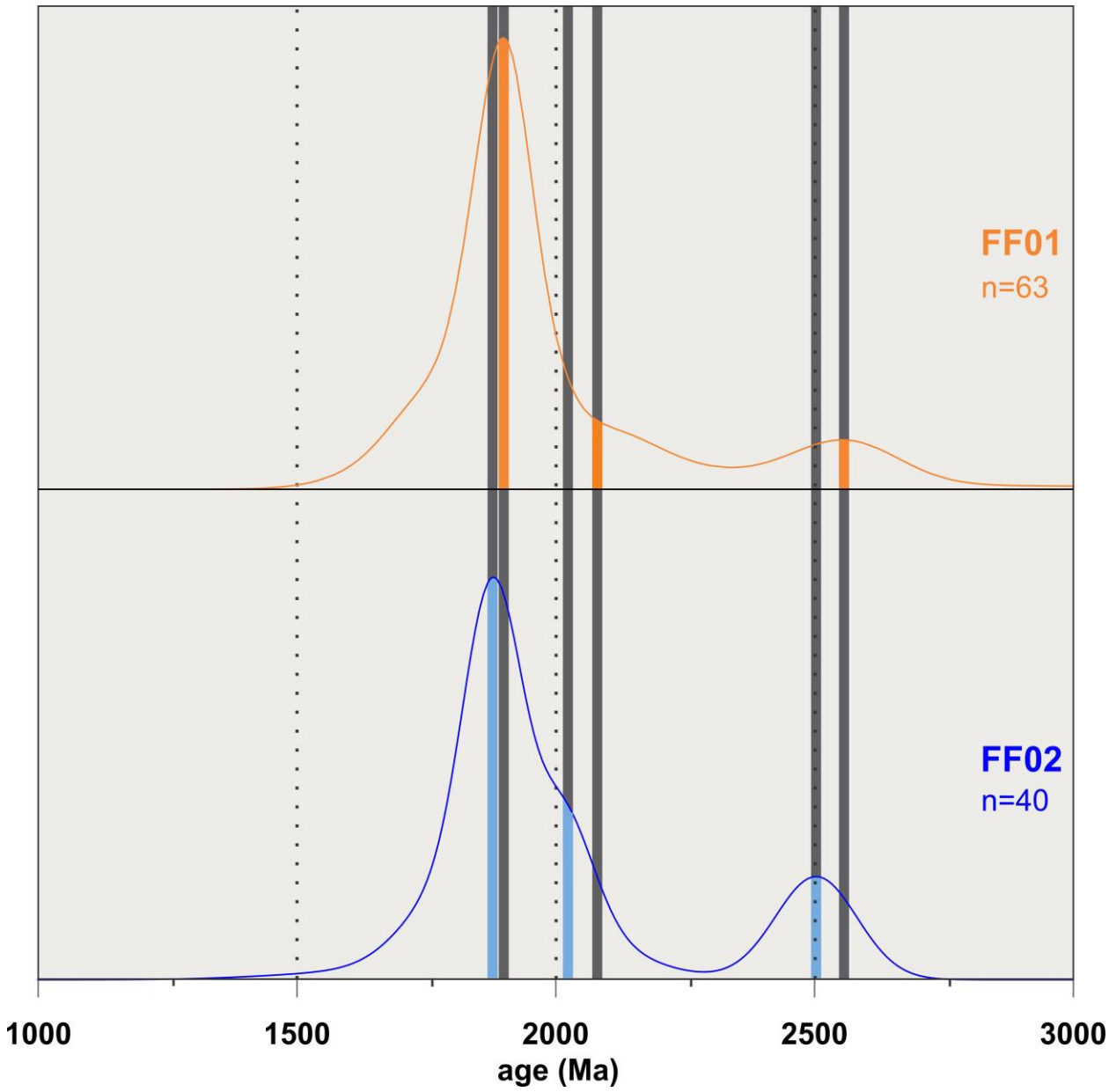

Figure 5: Kernel Density Estimation (KDE) plots for samples FF01 and FF02. $^{207}Pb/^{206}Pb$ ages were used, showing major peaks of ca. 1800 Ma. There are minor peaks of ca. 2100 Ma and ca. 2500 Ma as well, both of which are more prominent in FF02. This is possibly an effect due to fewer analyses.

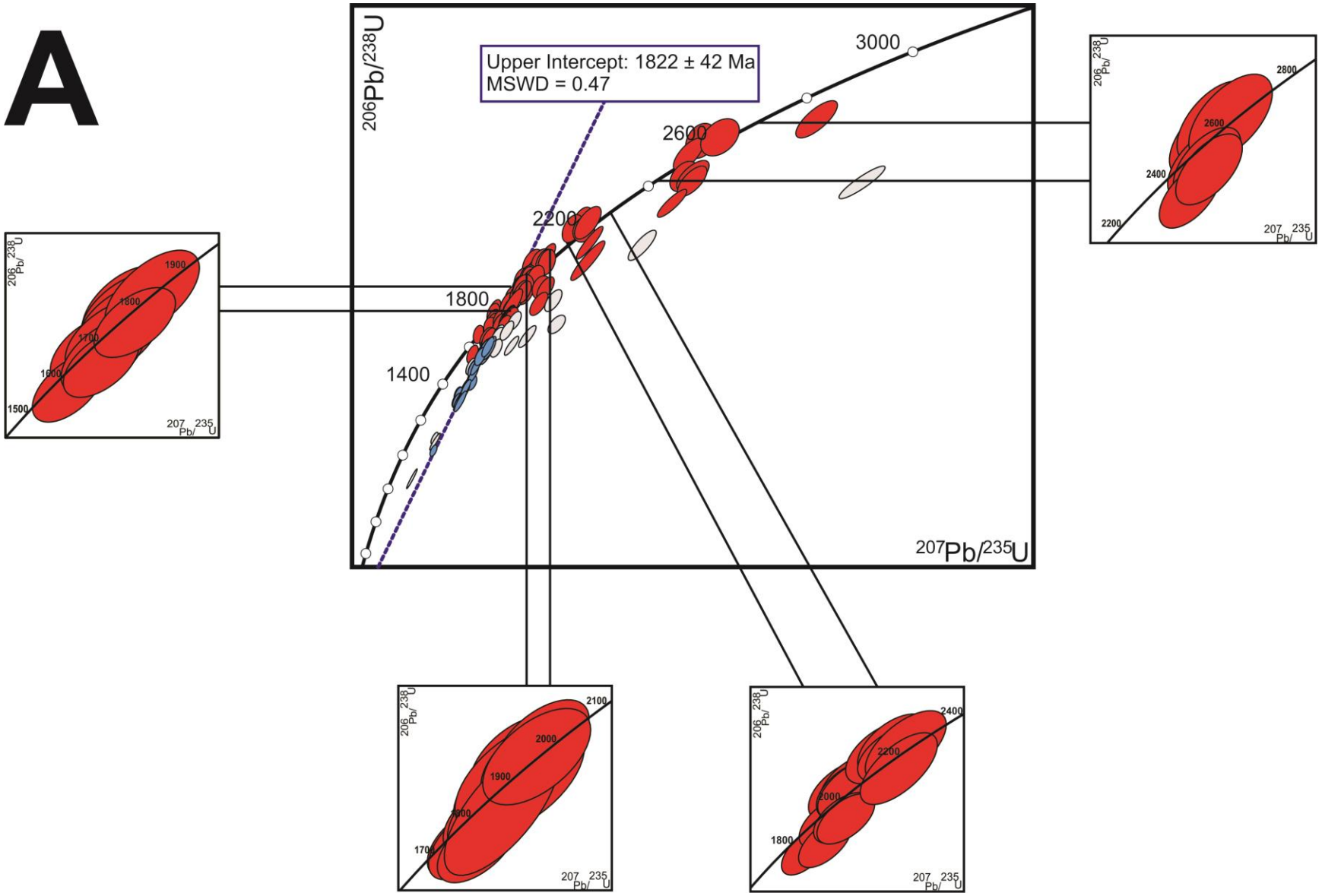
A
Upper Intercept: 1822 ± 42 Ma
MSWD = 0.47
206Pb/238U
207Pb/235U
3000
2600
2200
1800
1400
2800
2400
2200
2600
1900
1800
1700
1600
1500
2100
2000
1900
1800
1700
2400
2200
2000
1800
207 235
Pb/ U
206 238
Pb/ U

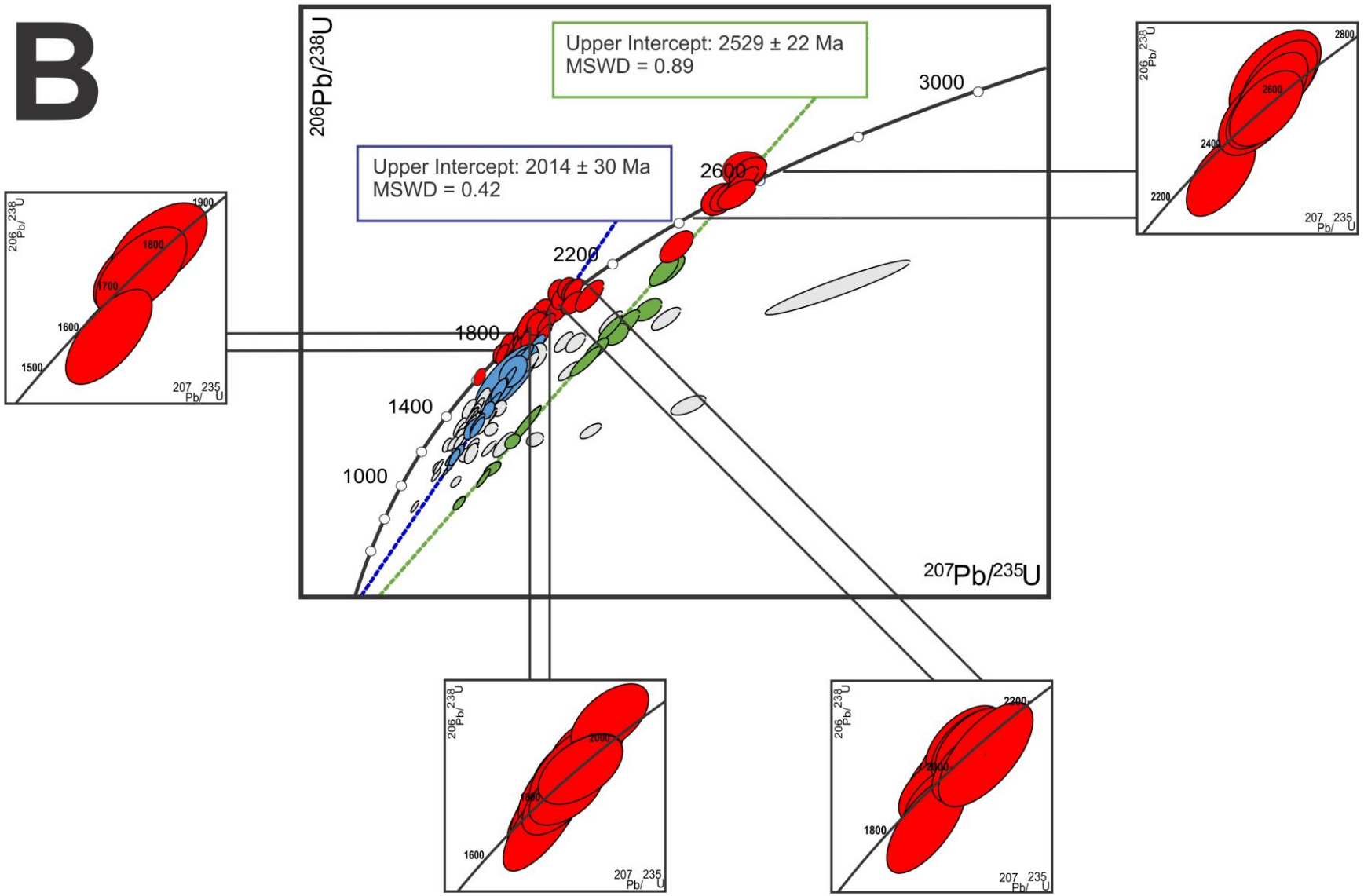

Figure 6: Concordia plots for samples FF01 and FF02 (A and B respectively). The ellipses represent one-sigma errors for each analysis. The centroid of the red ellipses are >90% confidence concordant data. Blue and green ellipses are discordant analyses and a line of best fit has been plotted through them. These lines are interpreted as a discordia line representing open system lead loss from the zircon. Concordant ages cluster around ca. 1800 Ma, ca. 2100 Ma and ca. 2500 Ma in both samples. Discordia line in sample FF01 has an upper intercept of 1822 ± 42 Ma and an MSWD of 0.47. The blue discordia plot of FF02 has an upper intercept of 2014 ± 30 Ma and an MSWD of 0.42. The green discordia plot of the same sample has an upper intercept of 2529 ± 22 Ma and an MSWD of 0.89.

REE CHEMISTRY

Rare earth elements were collected simultaneously with U–Pb to compliment the geochronology data and assist in characterisation of the source rock lithology (Figure 7). Zircon chemistry within a closed, fractionating magma system is expected to reflect the compositional changes within a magma as fractionation occurs (Dabard et al., 1996). Both samples have similar REE patterns. There is a slightly lower light REE (La–Nd) abundance in comparison to middle REE (Sm–Tb). However, a noticeable increase towards heavy REE values is present, producing similar $[Yb/Gd]^N$ mean values; 6.176 for FF01 and 6.701 for FF02. No significant Eu anomalies occur in either samples (Eu* > 0.59, Hoskin & Ireland, 2000), with an average Eu* of 0.448 and 0.4699 respectively. On the other hand, a Ce anomaly does occur and is slightly more prominent in FF01 comparative to FF02. Ce anomaly values range from 1.24 to 32.82 and 1.879 to 21.46 in FF01 and FF02 respectively.

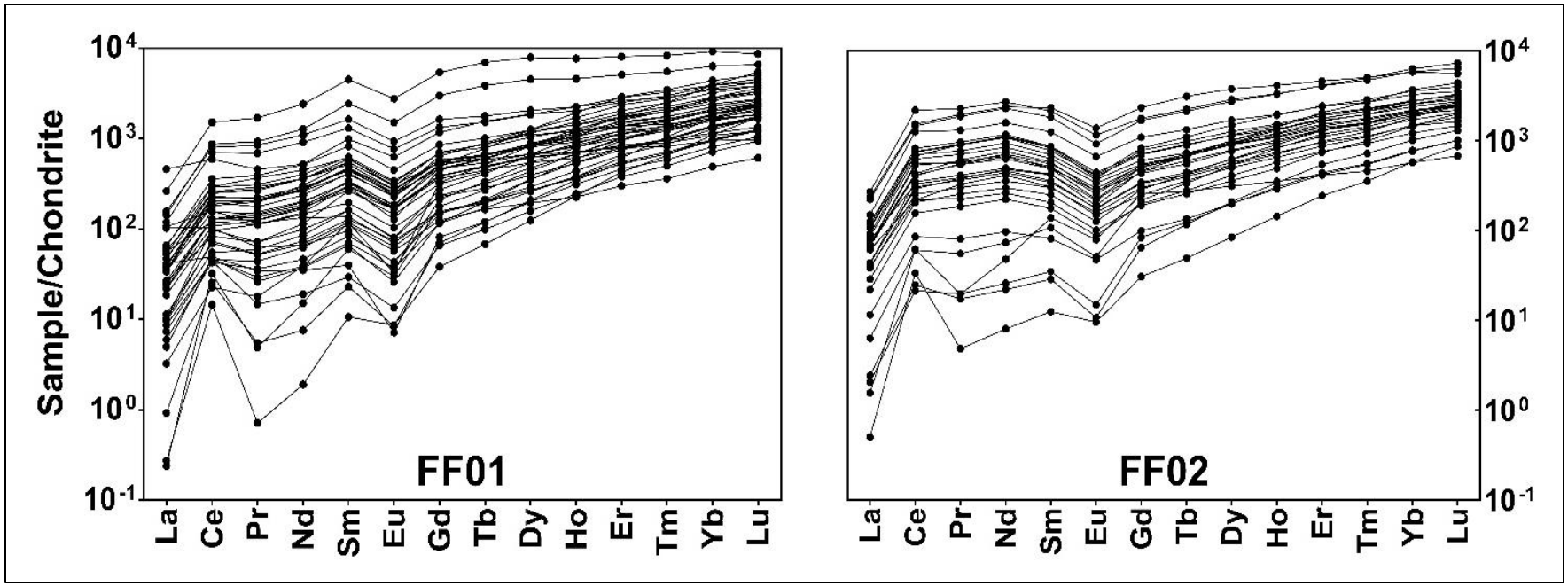

Figure 7: Chondrite-normalised rare earth element patterns for detrital zircon grains from the Dook Creek Formation. Chondrite values are from McDonough and Sun (1995).

ZIRCON HF ISOTOPES

Fractionation of Lu from Hf occurs during the magma generation phase and can be used to reflect the history of chemical differentiation between the crust and the mantle (Hawkesworth & Kemp, 2006). The Hf isotopic system in zircons records the $^{176}Hf/^{177}Hf$ ratios of the environment it grew in at the time of crystallization and are often used as a parameter to also assist in provenance identification (Hawkesworth & Kemp, 2006). 84 concordant analyses were then selected by age populations in order to investigate their Hf isotopic composition. The resultant data were then plotted against their $^{207}Pb/^{206}Pb$ ages (Figure 8). In both samples, the $\varepsilon_{Hf}(t)$ values become more positive from younger to older populations. For FF01, analyses yielded average $\varepsilon_{Hf}(t)$ values of +8.31 for ca. 2500 Ma, +0.65 for ca. 2100 Ma and -5.67 for ca. 1800 Ma populations respectively. In sample FF02, a similar pattern exists with slightly differing mean $\varepsilon_{Hf}(t)$ results; +10.23, -2.79 and -6.00 for the same age populations. This signals a change from a juvenile nature in the older populations to a larger continental influence in zircons of younger populations.

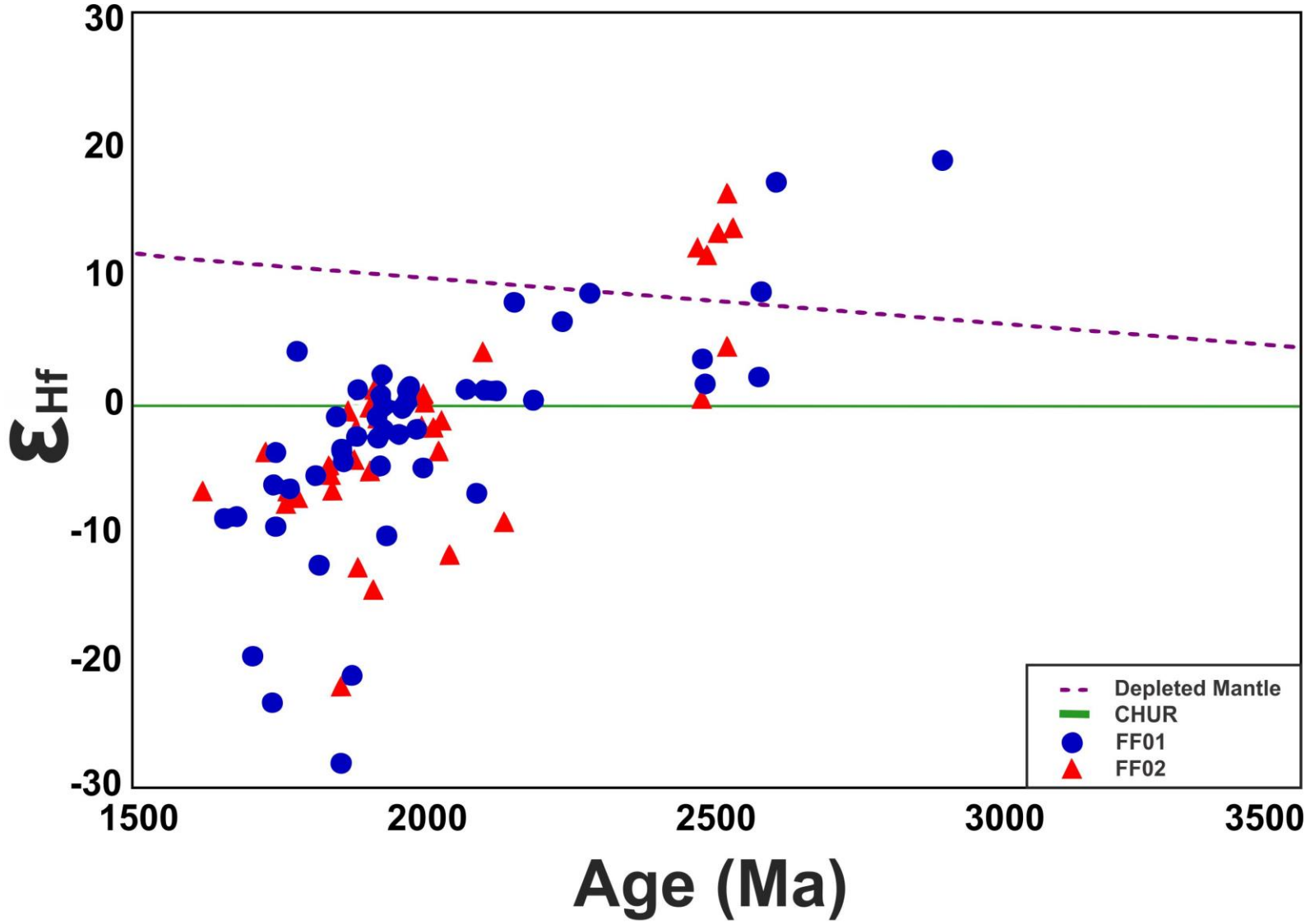

Figure 8: ε_{Hf} versus age plot of samples within the Dook Creek Formation. The blue circles and the red triangles indicate samples FF01 and FF02 respectively. The green solid line represents CHUR and the purple dotted line defines the depleted mantle. There is a trend in both samples showing the ε_{Hf} values becoming more positive with grains of older ages.

Carbonate Geochemistry

Twenty five carbonate samples were measured for their elemental concentrations and the main redox and palaeoenvironment proxies as well as contaminant indicators are plotted against depth (Figure 9). All three leachates examined show the same pattern of results throughout the different elemental phases. Iron shows no systematic change with lithology. Strontium values are comparatively low in all leachates with an average of 14.87 ppm. Ce* values in all leachates has a mean value of +1.05 although negative values occur towards the bottom of the stratigraphy between 500–600 m. Eu* values are relatively constant throughout the formation, except for an anomalous value at one particular point (+2.892 at 482 m). Full table of all elemental concentrations measured can be found in the Appendix.

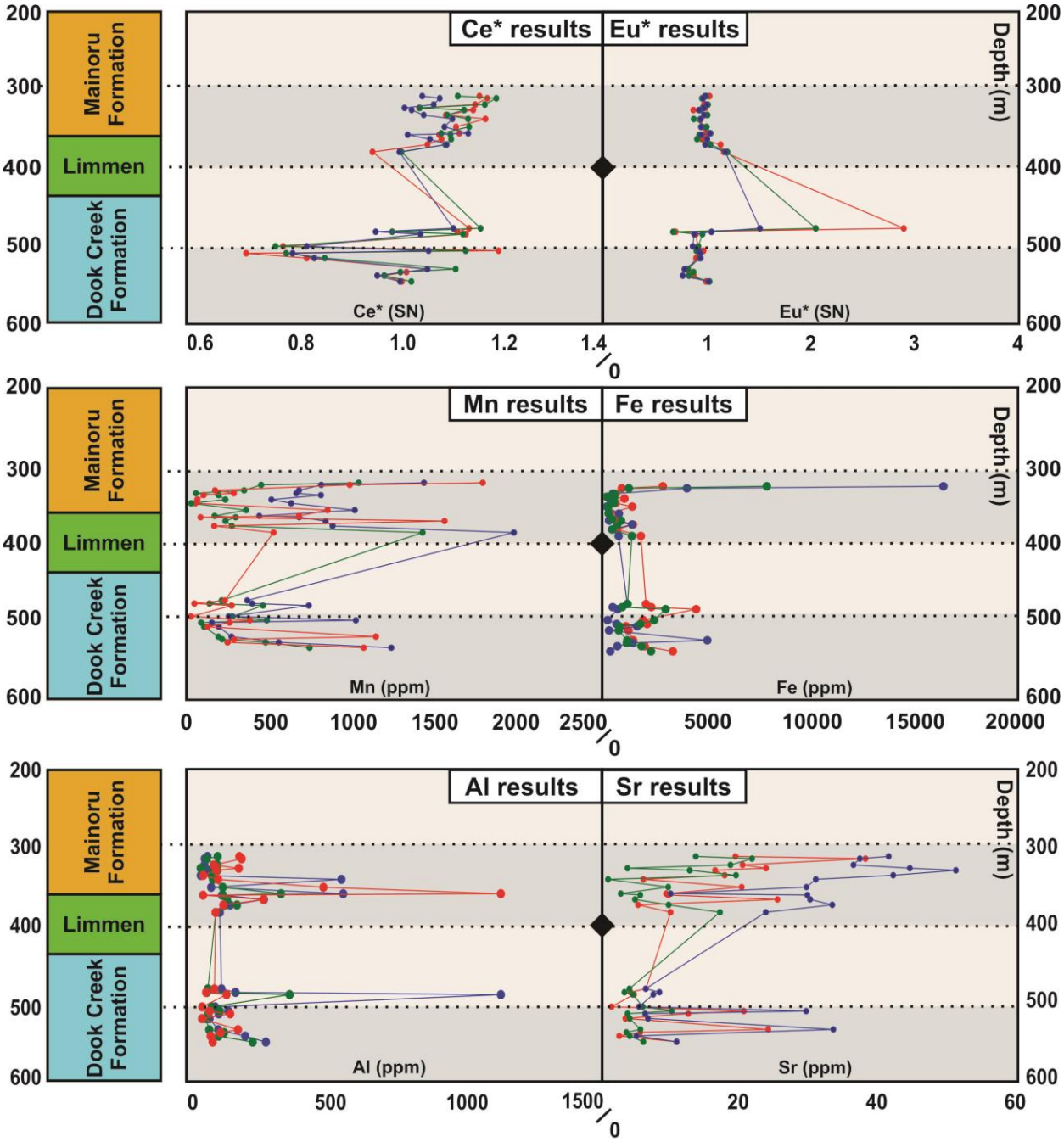

Figure 9: Stratigraphic variation in redox sensitive, major and trace element concentrations within samples from the Broughton Valley borehole. Ce* and Eu* values are calculated using equations from Bau and Dulski (1996) and SN refers to shale normalization using PAAS values (Nance & Taylor, 1976).

DISCUSSIONS

Detrital zircon analyses

CONSTRAINTS ON DEPOSITION

Group	Formation	Sample Name	Drillhole	Total no. of near concordant analyses	Youngest single concordant age (Ma)	Youngest concordant population age (Ma)	MSWD
Tijunna Group[1]	Stubb Formation	MS-4	MSFDD001	52	1723 ± 50	1743 ± 22 (3)	0.58
Tijunna Group[1]	Wondoan Hill Formation	DD2-57 MS-5	99VRNTGSDDH2 MSFD001	101	1619 ± 70	1660 ± 38 (9)	2.1
Collara Subgroup[2]	Munyi/Corcoran Formation	BR04	BROUGHTON 1	7	1530 ± 45	1734 ± 18 (8)	0.23
Collara Subgroup[2]	Hodgson Sandstone	L02	LAWRENCE 1	131	1591 ± 90	1740 ± 25 (5)	0.63
Collara Subgroup[2]	Jalboi Formation	U503	URAPUNGA 5	24	1633 ± 89	1706 ± 40 (5)	1.3
Collara Subgroup[2]	Arnold Sandstone	U506	URAPUNGA 5	20	1580 ± 66	1723 ± 23 (8)	0.072
Collara Subgroup[2]	Crawford Sandstone	U507	URAPUNGA 5	16	1766 ± 82	1782 ± 37 (4)	0.074
Collara Subgroup[2]	Limmen Sandstone	GSD3-02 GSD3-01	GSD003	67	1676 ± 82	1706 ± 44 (3)	0.53
Bullita Group[1]	Battle Creek Formation	MS-6	MSFDD001	41	1628 ± 53	1742 ± 20 (5)	1.7
Bullita Group[1]	Weaner Sandstone	DD2-24	99VRNTGSDDH2	66	1659± 59	1702 ± 31 (3)	1.7
Bullita Group[1]	Bynoe Formation	DD2-1 DD2-2	99VRNTGSDDH2	47	1538 ± 42	1545 ± 28 (3)	0.19
Mount Rigg Group[3]	Dook Creek Formation	FF01 FF02	FLYING FOX CREEK 1	91	1614 ± 78	1646 ± 44 (3)	0.58

Table 1: All the maximum depositional ages of possibly correlated formations within the Favenc Package, greater McArthur Basin. Data from the Bullita and Tijunna Groups (subscript 1) are from Yang 2019 and ages from the Collara Subgroup (subscript 2) are from Cassidy 2019. The results obtained from this study noted by subscript 3. All reported ages are $^{207}Pb/^{206}Pb$ age. Number of grains in each population are noted in brackets.

Constraints on the Favenc Package have been recently proposed with ages from the Balbirini Dolostone in the Nathan Group (1632 ± 4 Ma: Page et al., 2000) and the Weaner Sandstone of the Bullita Group (1600 ± 24 Ma: Carson, 2010). A single youngest concordant analysis with a $^{207}Pb/^{206}Pb$ age of 1614 ± 78 Ma is used to define the maximum deposition age of the Dook Formation. This is well within the range of the equivalent units within the Favenc Package. Furthermore, the age also overlaps (in 2 sigma error) with the maximum depositional U–Pb zircon age of the Limmen Sandstone ($^{207}Pb/^{206}Pb$ age: 1692 ± 43 Ma, Cassidy, 2018). A summary of results for this study as well as literary data for stratigraphically similar units to the Mount Rigg Group is displayed in Table 1.

PROVENANCE ANALYSIS

When comparing their age distributions using a KDE plot (Figure 10), the formations within the Favenc Package look almost identical, with very similar minor and major peaks. These age populations occur ca. 2500 Ma, ca. 2100 Ma and ca. 1800 Ma. This suggests that these particular formations may be sourcing from similar provenance regions. However a shift within the major peaks to a younger ages can be observed up stratigraphy. In the Wilton Package, the pattern continuous, although at the top of the stratigraphy, there is a slight shift back to peaks of slightly older ages. These minor changes can perhaps be taken into account when investigating provenance, although we must acknowledge that the absence of peaks within such plots are just as important as the peaks observed.

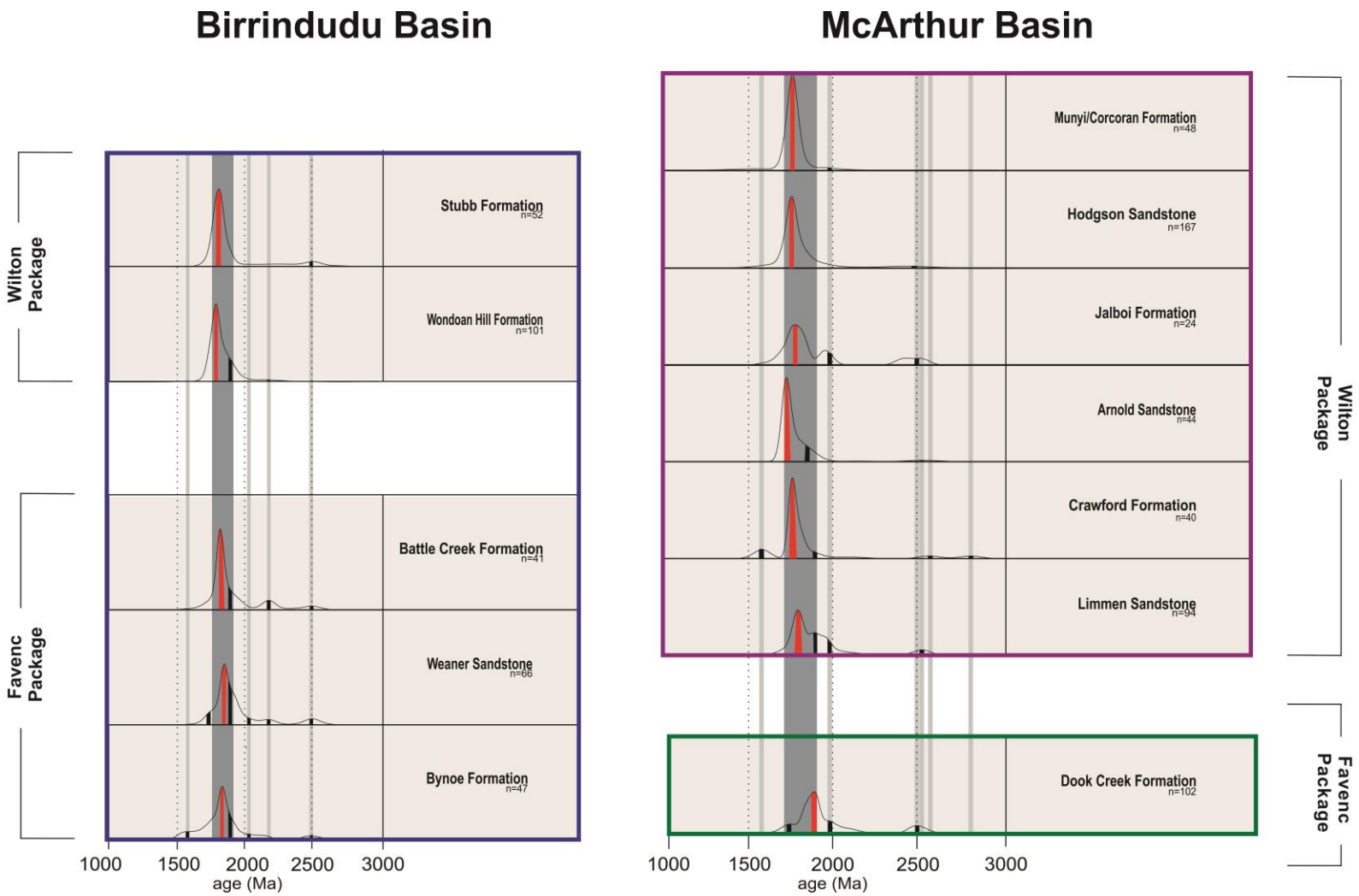

Figure 10: Kernel Density Estimation (KDE) plots of formations discussed in this study. Thin grey bars represent minor peaks while thick grey bars are the age domains where the major peaks of all formations fall within. Major and minor peaks for each formation are displayed by red and black bars respectively. Up stratigraphy, major peaks seems to slightly shift to younger ages and at the top formations shift back to older ages. Formations in purple, and blue are from Cassidy (2018), and Yang et al. (2018) respectively whilst the Dook Creek Formation data were collected in this study.

The MDS plot is a provenance analysis tool developed by Vermesch (2013) in order to compare the similarities and the dissimilarities of large U–Pb age data sets. This technique uses the Kolmogorov-Smirnov (K–S) test and quantifies the dissimilarity between different age distributions. Groups that are more similar will plot closer together; dissimilar groups will plot away from each other.

Using the MDS plot of sedimentary samples from the Birrindudu and the McArthur Basin alongside possible surrounding regions, we can investigate the changes in provenance. Figure 11 shows the sedimentary units compared with provenance sources from the north (Pine Creek Orogen and Halls Creek Orogen), south (Arunta, Tanami and Tennant) and east (Mount Isa Province and the Coen and Georgetown Province) of the basin system. The MDS plot shows that there is a general change from northerly-to-southerly sources up stratigraphy. In the McArthur Basin units, there is a change back towards northern sources right at the youngest units. In the Birrindudu Basin, the trend is not as prominent, with the top unit of the stratigraphy seemingly indicating that it contains both provenance sources. The reason for this spatial difference is unclear, however this plot does show that all of the sedimentary groups seems to be sourcing from similar provenance regions. In addition, data from all units are largely dissimilar to eastern sources. However, even further up stratigraphy, Yang et al. (2018) noted that the age data sets of the Maiwok Subgroup (Kyalla Formation, Moroak Sandstone, Velkerri Formation and the Jamison Sandstone) showed striking similarities with the Mount Isa Province. The inception of input from easterly sources could indicate a tectonic change at this time.

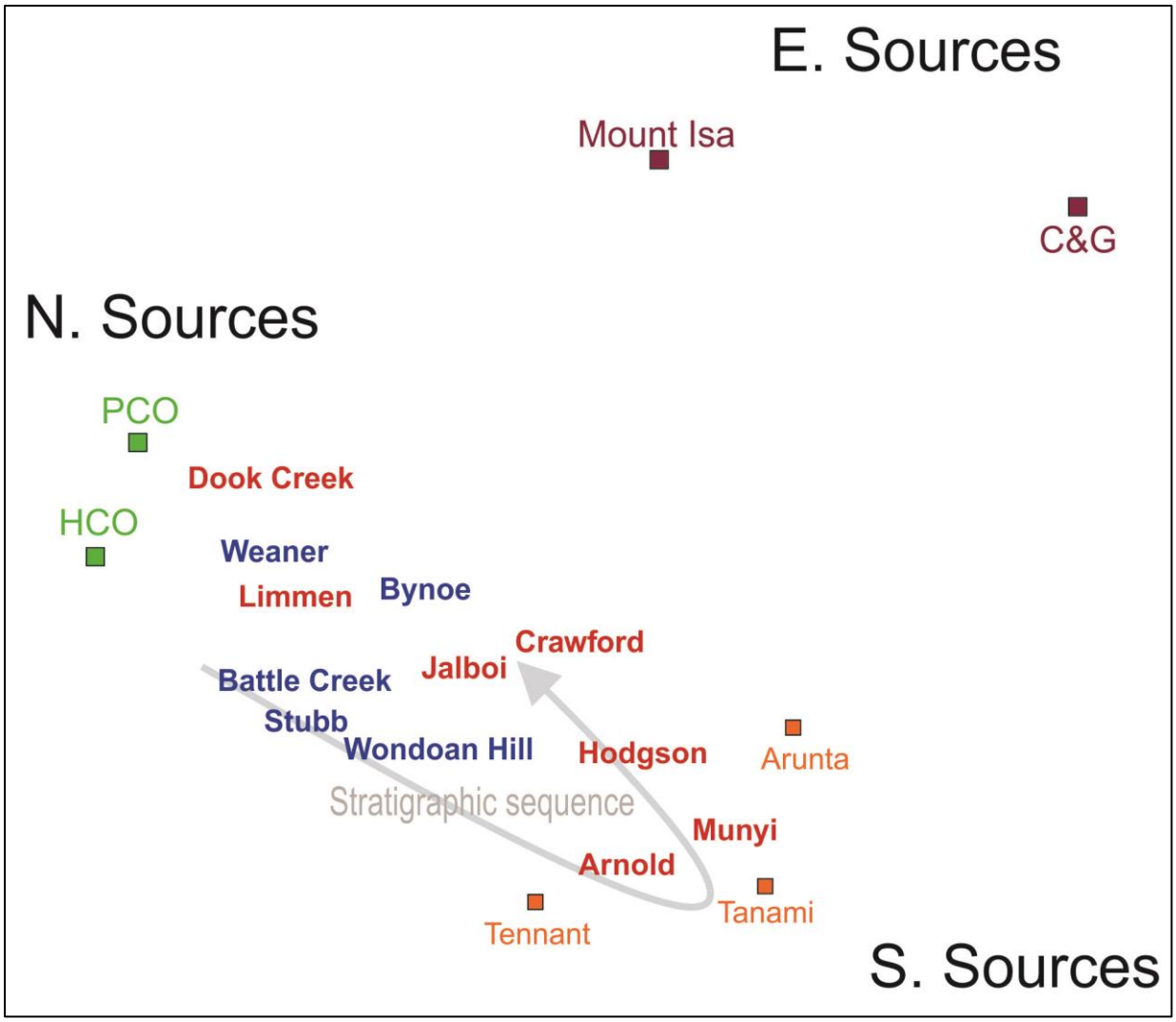

Figure 11: Multidimensional scaling (MDS) plot of sedimentary samples from the McArthur Basin (red) and the Birrindudu SBasin (blue) alongside surrounding source regions around the greater McArthur Basin. Similar samples plot closer together while the opposite is true for dissimilar samples. Samples from both basins exhibit a change in similarity from northern sources (green) to southern sources (orange) up stratigraphy. The plot implies that these comparable units seems to be sourcing from the same regions. No units plot similarly to eastern sources (purple).

Zircon Hf Isotopes

Integration of the U–Pb ages and the Hf-isotopic data of the Dook Creek Formation along with possible stratigraphic and spatial correlations are presented to analyse the crustal evolution of the greater McArthur Basin and northern Australia (Figure 12). All of the detrital zircon data shows a remarkable likeness to each other, further suggesting that these sedimentary units are sourcing similar provenance regions. The Hf-isotope Dook Creek Formation data show that older detrital zircons (ca. 2500–2100 Ma) have positive ε_{Hf} values, while younger grains (ca. 1900–1800 Ma) tend to have more negative values. This similar pattern persists throughout the correlated formations within the Favenc and the Wilton Packages. This indicates that the source regions largely formed in the NeoArchean to Palaeoproterozoic show little evidence for crustal material. On the other hand, there is little evidence of any juvenile magmatic input in the source regions post ca. 2.2 Ga. These later zircons suggest the source region was progressively thermo-tectonically reworked.

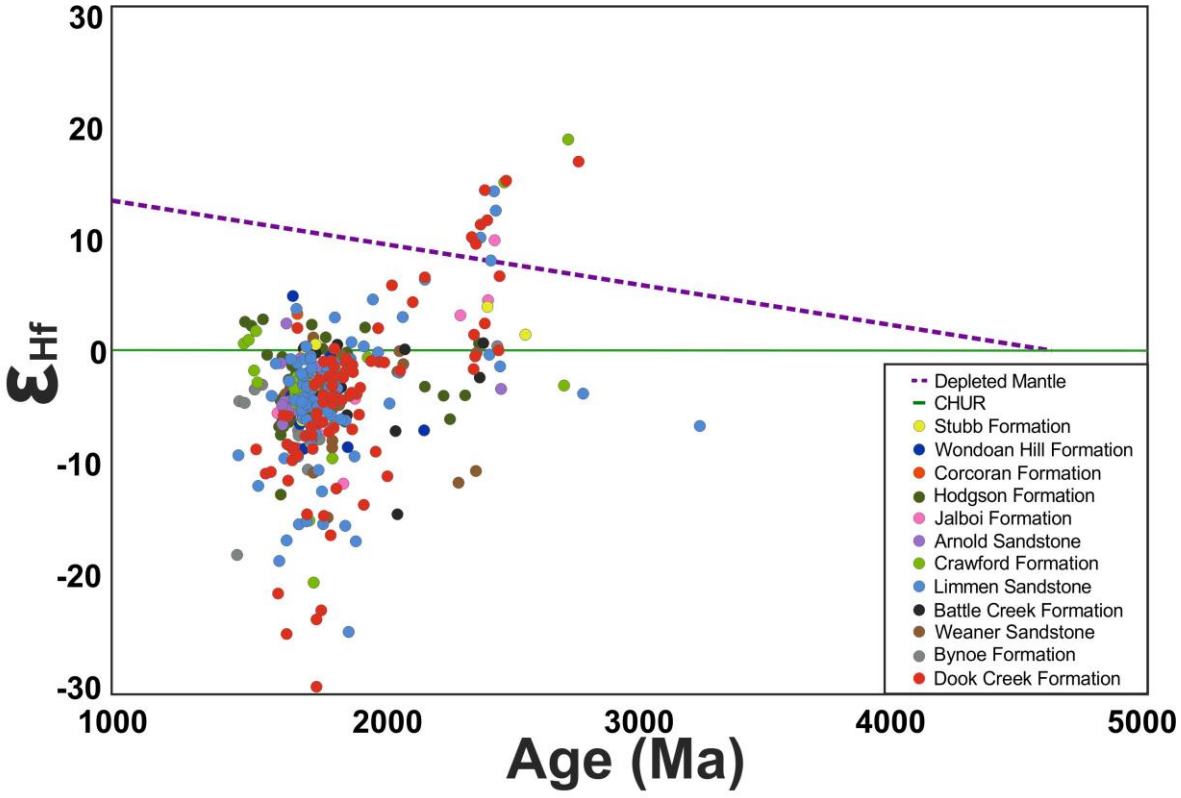

Figure 12: ε_{Hf} values of detrital zircons from the Dook Creek Formation as well as comparable units within the greater McArthur Basin. The zircons of older populations (2500-2100 Ma) displays a largely positive values while the younger populations (1900-1800 Ma) are dominated by negative values.

$\varepsilon_{Hf}(t)$ values are also commonly used in conjunction with U–Pb data sets when analysing provenance. When compared to surrounding source regions, the $\varepsilon_{Hf}(t)$ values of the older and younger populations from all detrital zircon data are most similar to the Arunta Region (Figure 13). The Arunta source data also consists of two restricted zircon populations, an older and a younger group (ca. 2500 Ma and ca. 1800 Ma respectively). The younger population $\varepsilon_{Hf}(t)$ data from the detrital zircons closely resemble that of the younger population for the Arunta. Furthermore, older population $\varepsilon_{Hf}(t)$ data of the detrital zircons are also more similar to the $\varepsilon_{Hf}(t)$ older population of the Arunta. On the contrary, both the Pine Creek Orogeny (PCO) and the Halls Creek Orogeny (HCO) data do not show juvenile $\varepsilon_{Hf}(t)$ values similar to our older population detritus data.

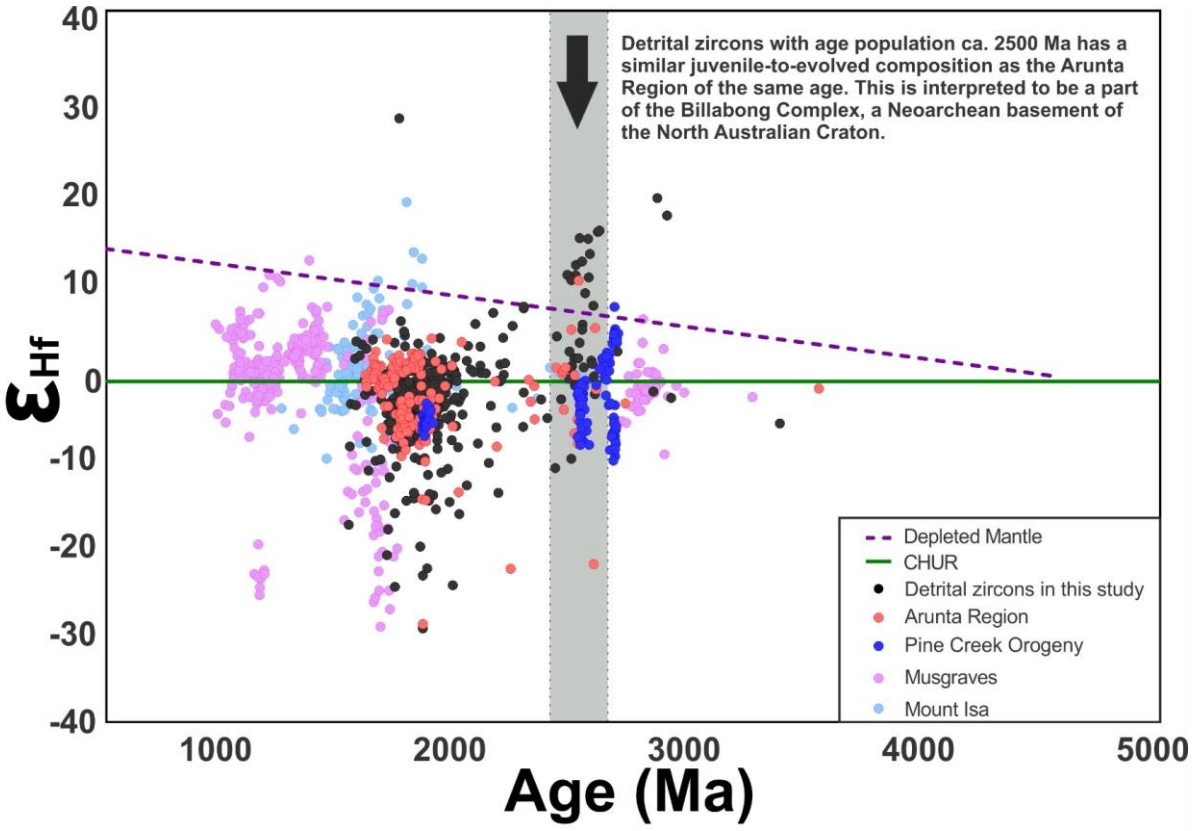

Figure 13: ε_{Hf} values of detrital zircons from the Mesoproterozoic greater McArthur Basin compared to possible surrounding source regions. Detritus data most resemble the different populations of the Arunta Region, located south of the basin.

Hence, when incorporating both U–Pb age and $\varepsilon_{Hf}(t)$ values, we propose that these sedimentary units are sourcing different regions of the Arunta, with age populations that are reflected in our detritus. In the Tanami Region, an area of rocks comprising of juvenile, Archaean material occurs at the Billabong Complex (crystallization age 2514 ± 3 Ma, with two older inherited populations ca. 2550 and 2530 Ma: Ahmad & Munson, 2013). In addition, there are also silicate igneous units within the Aileron Province aged 1860–1790 Ma (Ahmad & Munson, 2013; Leno et al., 2017). Therefore, it is possible that the formations discussed perhaps have not sourced from the PCO and the HCO but instead be sourcing the different populations of the Arunta.

Trace element analysis of zircons

Detrital zircon trace element composition have been initially used as a source-rock lithological identifier alongside chronology and typology (Dabard et al., 1996). Any mineral phase can be used to indicate its whole-rock source if its composition can somehow be related to a melt composition or chemical features of said mineral that can systematically relate to a particular rock type of origin (Hoskin & Ireland, 2000). These applications all assume that the mineral itself was saturated at the liquidus and equilibrium of mineral/melt partitioning was maintained. However such properties are mainly only common in felsic and some intermediate igneous bodies (Watson & Harrison, 1983). Previous studies have noted that such assumptions are most probably invalid as enrichment and growth entrapment or rare earth elements (including Y) at the surface is inevitable (Watson, 1996).

Whilst recognising minor differences between some zircon populations (Figure 14), REE distribution patterns of the Dook Creek Formation all look remarkably similar. Positive Ce anomalies occur throughout all the samples and there is a general slight enrichment of

HREEs as opposed to LREEs. However, previous studies have also found similar results with a wide range of crustal rock types across a number of tectonic settings (Hinton & Upton 1991; Barbey et al., 1995; Hoskin & Ireland, 2000). Their respective trace elemental distribution patterns also do not conform to the chemical discriminants initially declared by Heaman et al.(1990). Therefore, we have not found the REE chemistry of detrital zircon within the Dook Creek Formation to be a generally useful provenance indicator for this study.

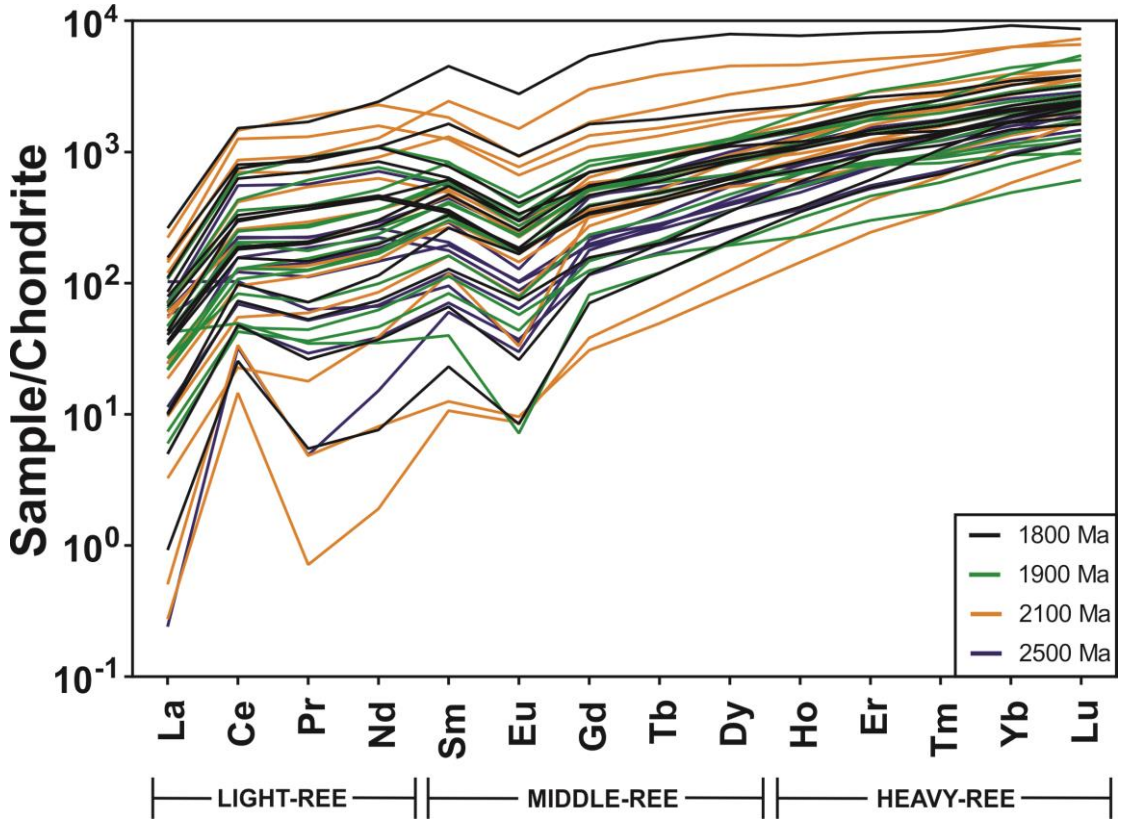

Figure 14: Trace elemental distribution patterns of the Dook Creek Formation discriminated by their populations. All samples exhibit a positive Ce anomaly, a negative Eu anomaly and a minor enrichment of HREEs comparatively to LREEs.

However, we can use REE in detrital zircons to infer characteristics of the magma it grew in. The minimal enrichment of HREE displayed in all the age populations within the Dook Creek Formation (Figure 15) are indicative of zircon growing in competition with garnet (Rubatto, 2002). All normalised Lu/Gd values for fall between 0–50. Positive Ce anomalies are also present in the sample, reflecting an oxidized parental magma chamber (Hoskin & Ireland,

2000). Eu anomalies also exist throughout the samples. Eu anomalies can be indicative of an abundance in plagioclase; as its cations have similar size, charge and behaviour as Ca cations found in the mineral (Trail et al. 2012).

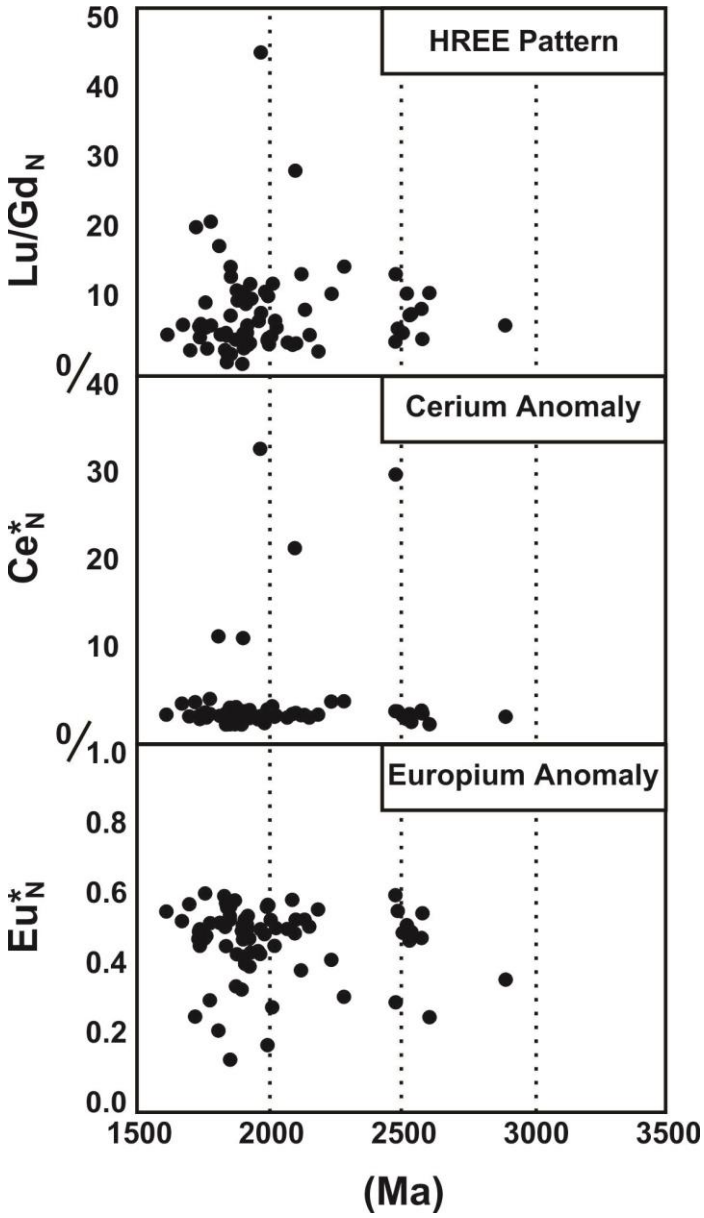

Figure 15: Rare earth proxies for magmatic origin of the detrital zircons within the Dook Creek Formation. The analyses shows no distinct trends between the proxies and age population.

Carbonate Geochemistry

DIAGENESIS AND CONTAMINATION EFFECTS ON PRIMARY SIGNALS

In all carbonate geochemistry, we acknowledge that the potential of diagenetic alteration and contamination from non-carbonate phases is of the utmost concern. Multiple steps of leaching were done to ensure that signals detected were only from the carbonate phase of each sample. The Mount Rigg Carbonates have been leached in three different stages and show consistent trace element patterns throughout all leachates. This is a confident indicator that the signals detected all come from the same mineral phase. Any mixing with non-carbonate phases can result in overwhelming signatures from the authigenic inventory and the development of increased LREEs, masking of Ce anomalies as well as false Eu anomalies (Tostevin et al., 2016). The most common type of contaminants are fine-grained clastics and clay minerals which lack many of the anomalies distinguished in marine deposits (Pourmand et al., 2012). Key comparative parameters were plotted against proxies for silicates (Zr), oxides (Ni) and sulphides (Sc) (Figure 16) and they all show no statistically significant correlation, which indicates that the origin of the signals detected were not from those mineral phases.

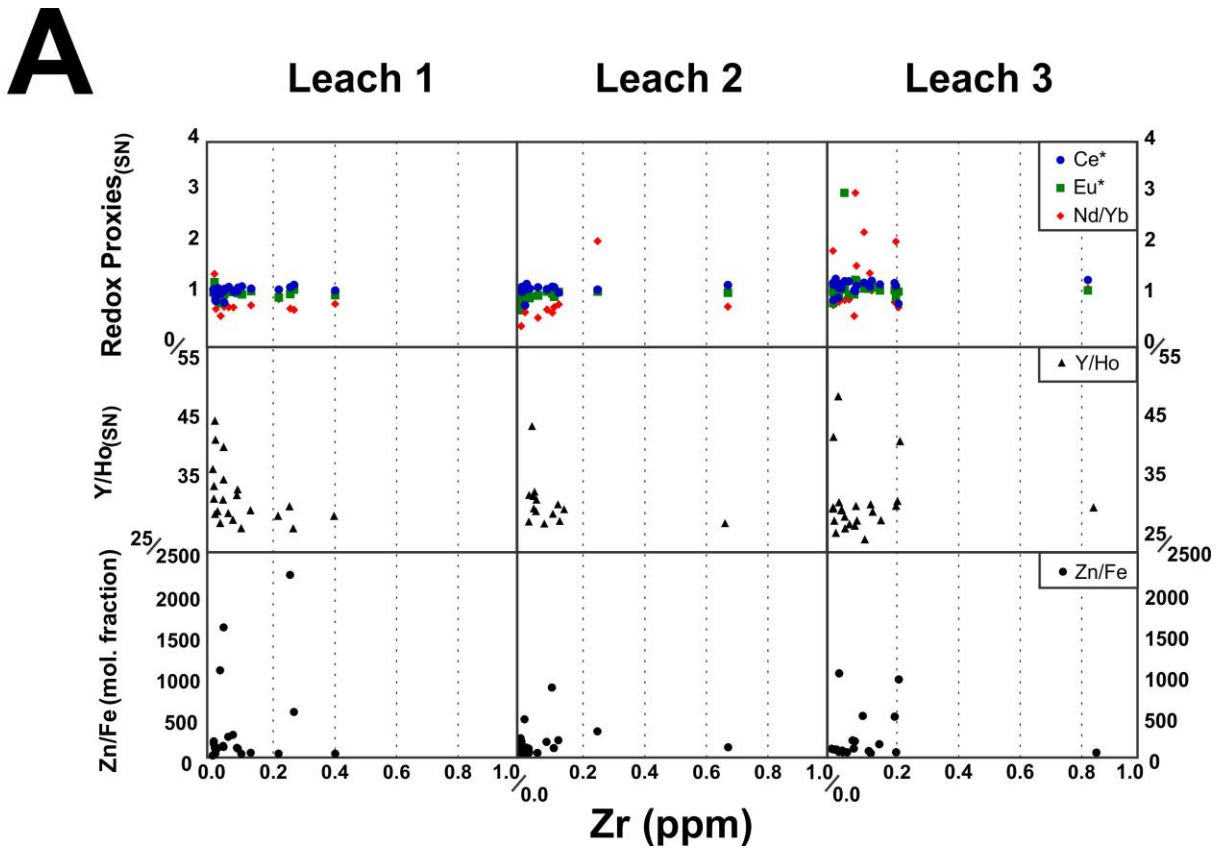
A
Leach 1
Leach 2
Leach 3
Redox Proxies(SN)
Y/Ho(SN)
Zn/Fe (mol. fraction)
Ce*
Eu*
Nd/Yb
Y/Ho
Zn/Fe
Zr (ppm)

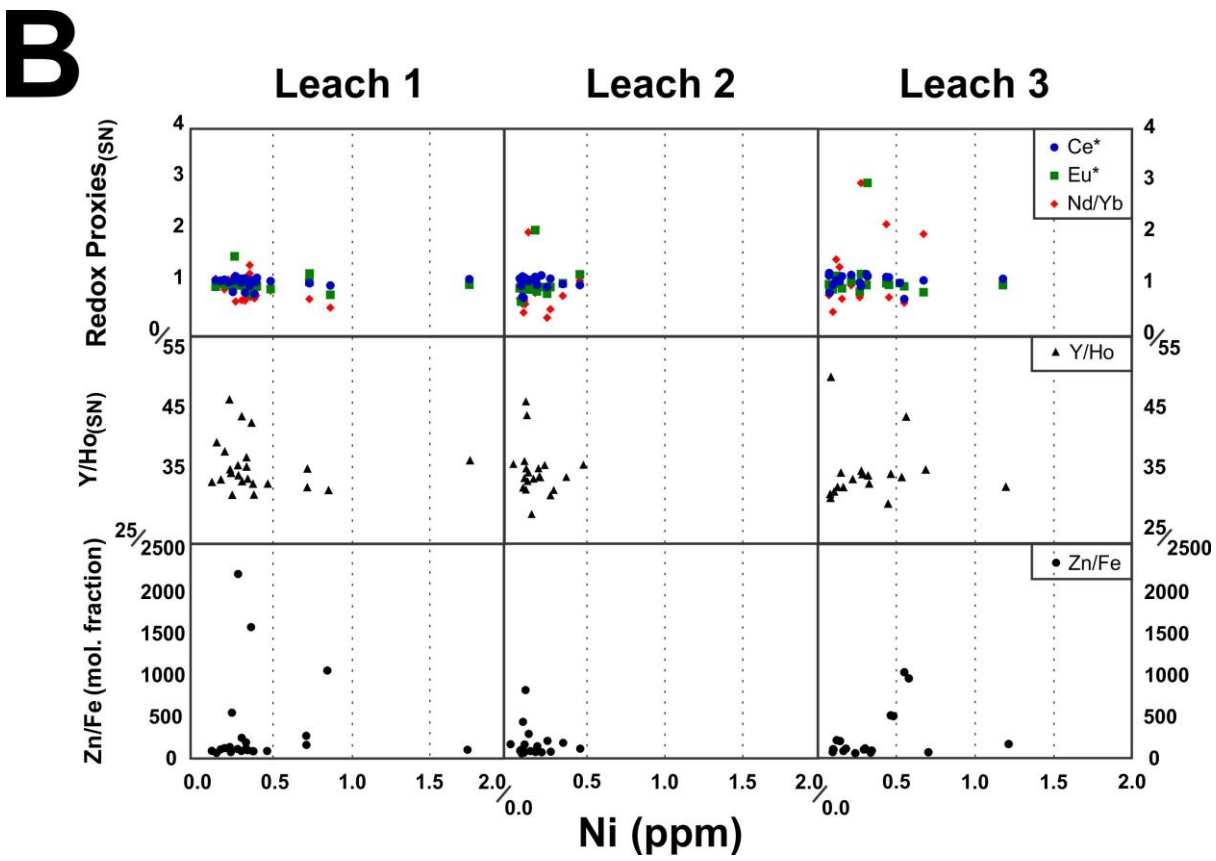
B
Leach 1
Leach 2
Leach 3
Redox Proxies(SN)
Y/Ho(SN)
Zn/Fe (mol. fraction)
Ce*
Eu*
Nd/Yb
Y/Ho
Zn/Fe
Ni (ppm)

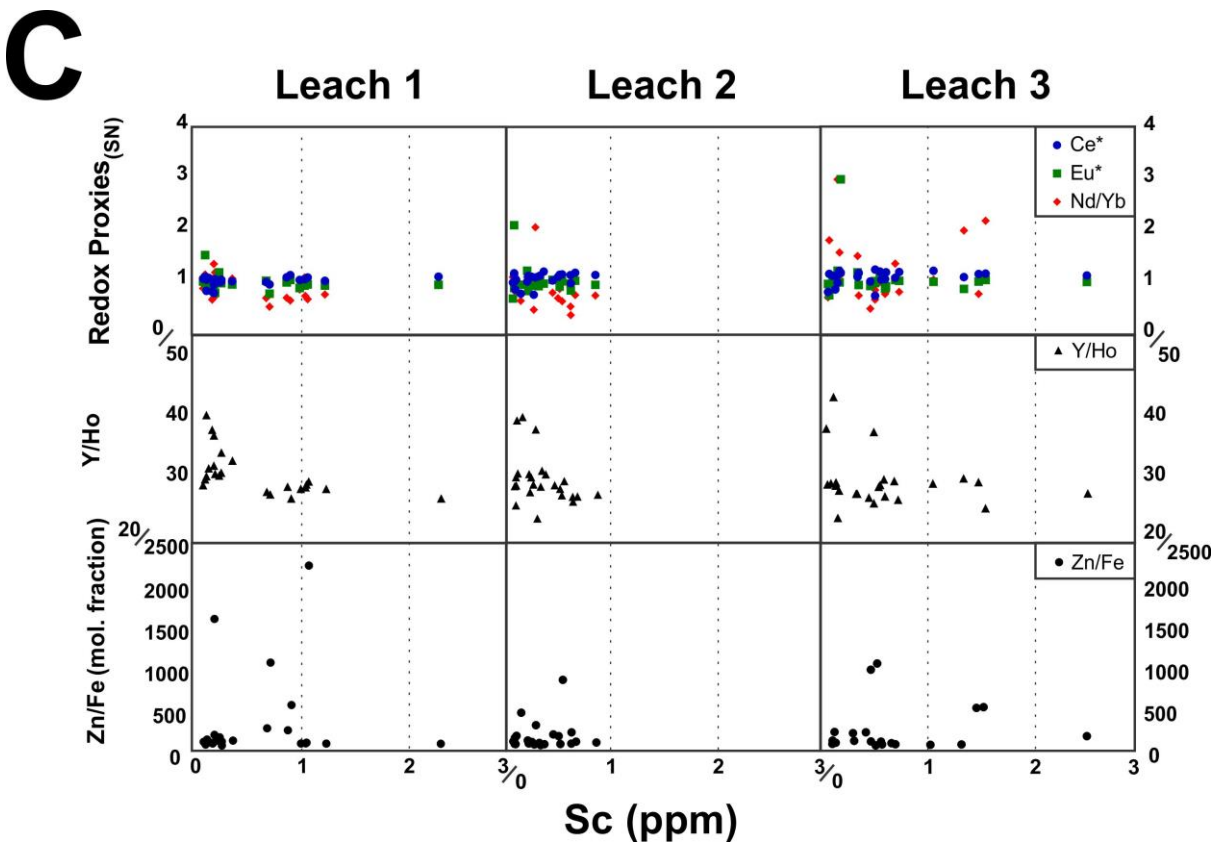

Figure 16: Key trace elemental parameters were plotted against proxies of silicates (A), oxides (B) and sulphides (C) showing no correlation in all 3 leachates. This is a confident indicator that the signals detected all originated from the carbonate phase. Redox proxies as well as Y anomalies (Y/Ho) values are standardised to PAAS. Zn/Fe values shown are in molar fraction. All mineral phase parameter values were in ppm.

Carbonates that have undergone seawater-freshwater mixing and other subsequent fluid-rock interactions will preserve values that represent both diagenetic and marine calcite signals. A comparison of $\delta^{13}C$ and $\delta^{18}O$ is used to test for the mixing between the two carbonate mineral endmembers (Banner & Hanson, 1990). A cross plot of these stable isotopes from the Mount Rigg Carbonates shows a statistically significant correlation. The data for these elements are therefore interpreted to not represent a primary water signature, but instead reflected the effects of diagenesis on those signals (Figure 17). Consequently, we cannot use this data set to depict a reliable chemostratigraphy for the Mount Rigg Carbonates or for any further interpretation.

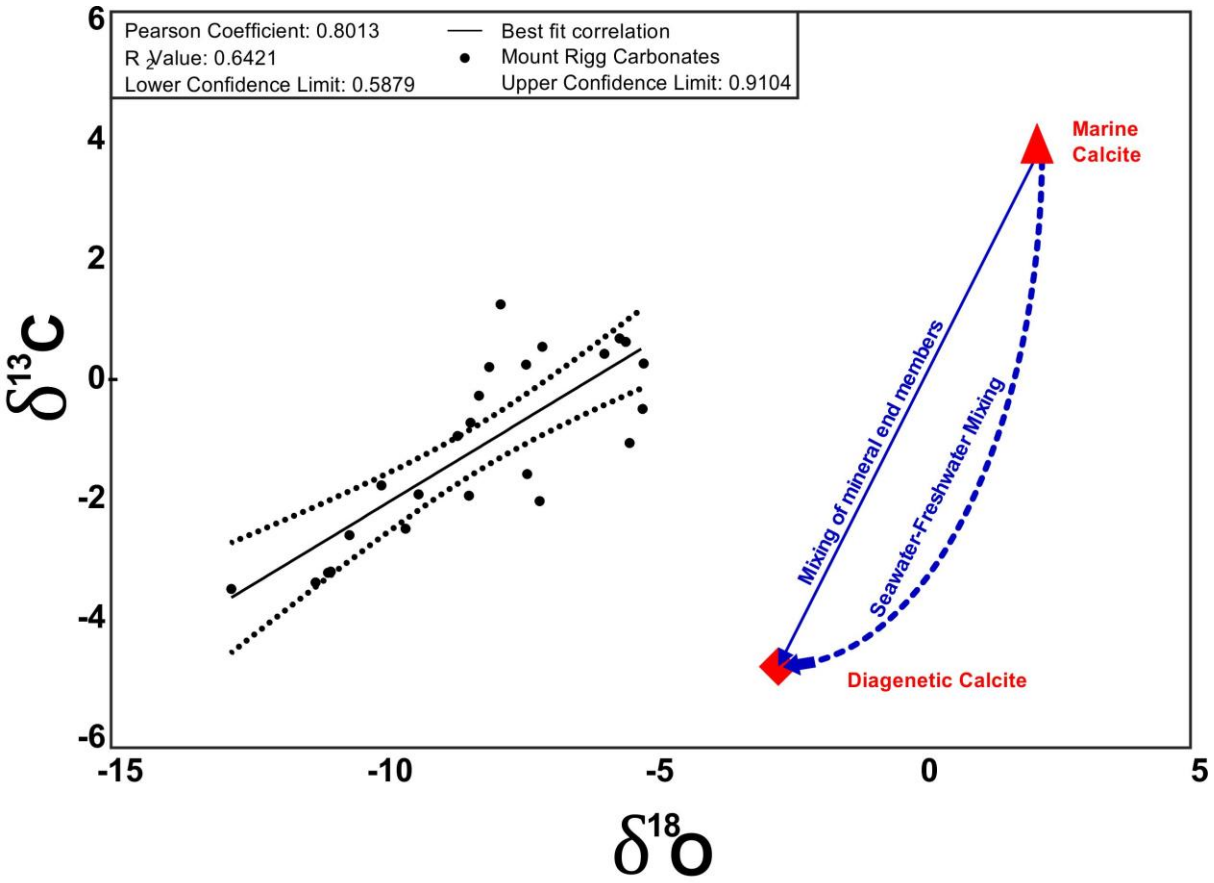

Figure 17: Covariation of carbon vs oxygen isotopic composition values presented in PDB. There is a clear, statistically significant correlation between the two isotopes within the Mount Rigg Carbonates. Isotopic values of marine and diagenetic calcites, as well as the trend illustrated by the interaction between the two end members were also plotted for comparison (Banner and Hanson 1990).

Oxygen as well as carbon are commonly more susceptible to alteration from water-rock interactions because of their smaller cation size (2^+) compared to Rare Earth Elements and Yttrium (REY), which are mainly 3^+ or 4^+. REY ordinarily replaces the calcium ion in the calcite lattice, and can remain stable during diagenesis, including burial dolomitization as well as dissolution from meteoric precipitation (Banner et al., 1988; Webb & Kamber 2000; Webb et al. 2009,). Although alteration of REY patterns during diagenesis cannot be excluded, it can be identified via comparison with known altered elemental data (Tostevin et al., 2016). In order to test whether the trace elemental data were also affected by diagenesis, the same parameters examined against the proxies of mineral phases were also cross plotted against their $\delta^{18}O$ composition (Figure 18).

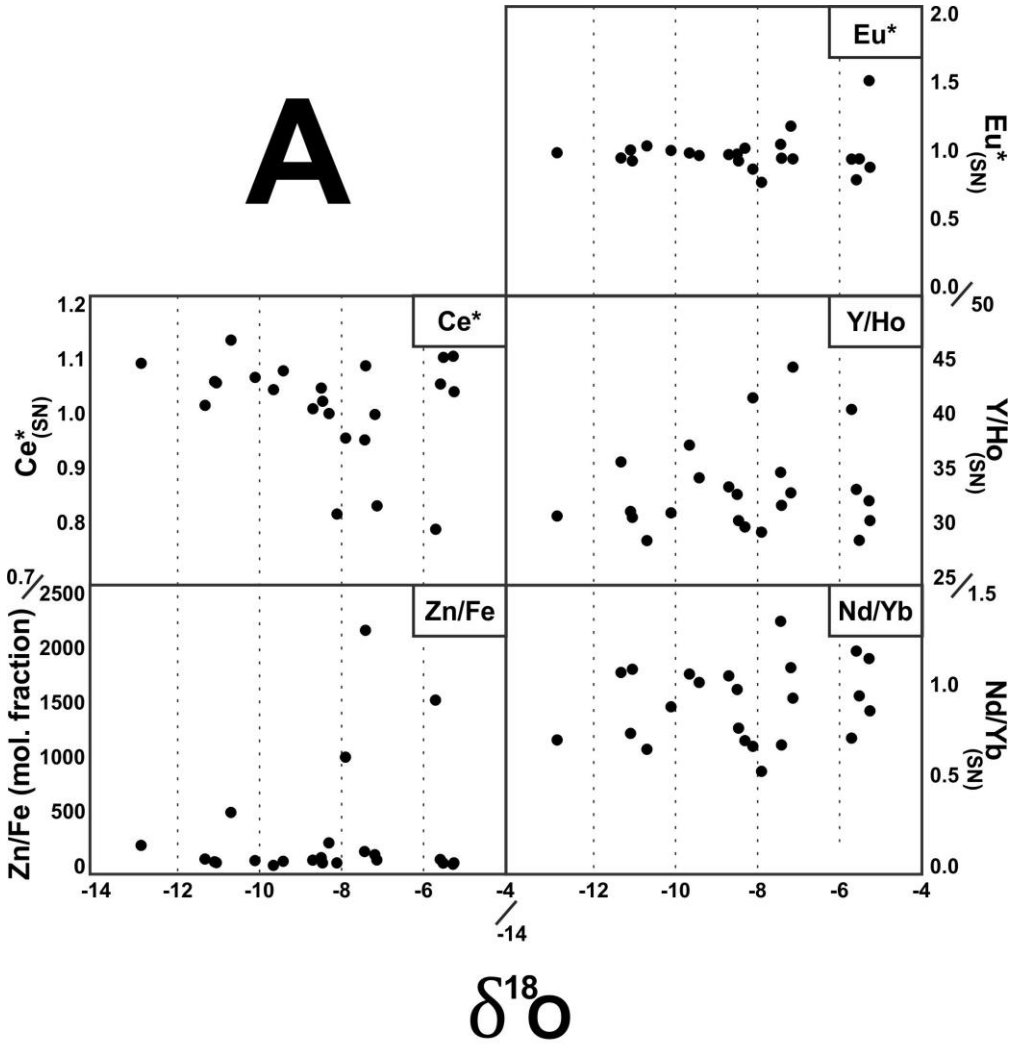

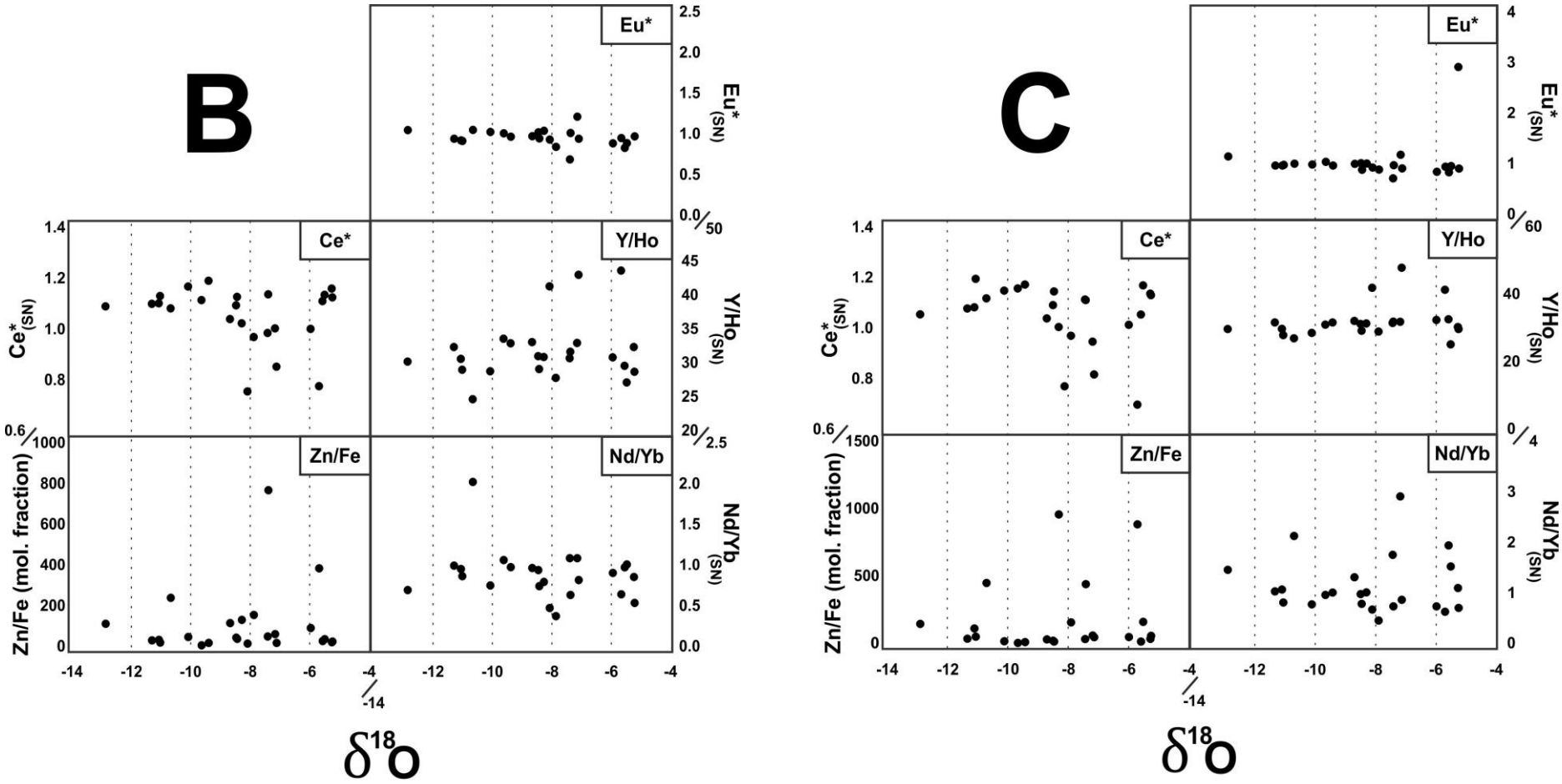

Figure 18: Cross plots of trace elemental parameters against ^{18}O isotope composition for leachates 1-3 (A-C respectively). All plots show no statistically significant relationship. Full column statistics of each plot can be found in the Appendix.

Trace elemental data from all three leachates show no indication of diagenetic effects and therefore is interpreted to still represent primary signal. However, even if we select the most primary signals, we cannot ignore possible diagenetic influences on any of the elemental composition and therefore it is imperative that we treat the data conservatively.

PALAEOREDOX PROXIES

Cerium is an effective palaeoredox proxy because it is a REE that exists in multiple redox states; Ce^{3+} and Ce^{4+}. Ce anomalies can occur relative to La and Pr in different seawater and marine sediments depending on the redox state of the water column (Wilde et al., 1996). Ce anomalies are expressed as Ce* with results normalised to Post Archean Australian Shale (PAAS) in order to remove natural variations in their absolute concentrations (Tostevin et al., 2016).

In a consistent oxygen-rich environment, Ce^{3+} is oxidized to Ce^{4+} which is less soluble and easily removed from the water column by ion (eg: Mn) hydroxide phases (Elderfield & Greaves, 1981; Bau et al., 1996). Hence, authigenic phases precipitated from such conditions will show a negative Ce anomaly. On the other hand, Ce anomalies will not develop under anoxic conditions because Ce has similar properties to La and Pr. This will therefore result in precipitates with similar concentrations in those particular elements (Wang et al., 1986). In redox stratified waters where both conditions occur, negative and positive Ce anomalies can be observed because of iron hydroxide remineralization through the redox cline (Elderfield & Greaves, 1981). In summary, the presence of Ce anomalies themselves indicates active redox cycling within the water column (Slack et al., 2007). To determine whether the Ce anomalies observed were independent of La anomalies, Ce* values were cross plotted against Pr* (Figure 19) following Bau and Dulski (1996).

Throughout all three leachates, a majority of the Ce values display positive anomalies which indicates an anoxic environment. A lack of negative Ce anomalies was expected for Proterozoic biochemical sediments as dissolved oxygen present in the aquatic environments at that time is thought to not be sufficient to oxidize Ce (Derry & Jacobson 1990; Bau & Moler 1993; Kamber & Webb 2001; Bolhar et al., 2005). Some values fall within the intermediate field while few show negative Ce anomalies. The minimal negative Ce* data seemingly represents a local oxidation events within the formations, although mass balance theory indicates that there should be a reservoir of Ce negative signatures somewhere to compliment the data displayed in these samples.

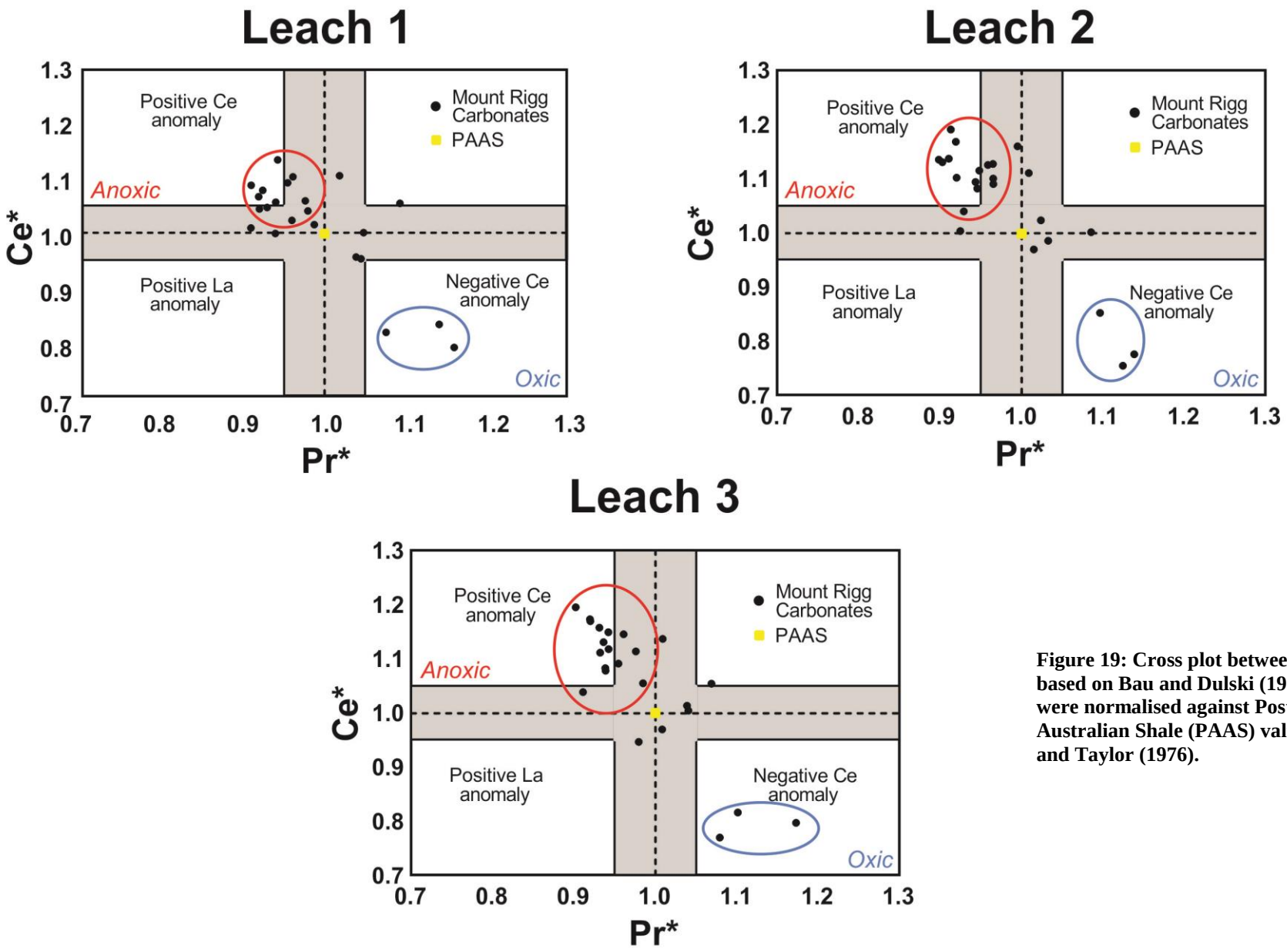

Figure 19: Cross plot between Ce* and Pr* based on Bau and Dulski (1996). All results were normalised against Post Archean Australian Shale (PAAS) values from Nance and Taylor (1976).

Another proxy that can be used to indicate redox conditions are Zn/Fe ratios. Marine carbonates deposited in shallow environments are likely to be in contact with the atmosphere and therefore their elemental ratios are likely to reflect equilibrium with atmospheric conditions. Although Fe and Zn in the shallow ocean are mainly sourced from hydrothermal inputs, their redox sensitivities are significantly different. An increase in Zn/Fe ratios during geological intervals will be indicative of a higher atmospheric O^2 environment (Liu et al. 2016).

The potential use of Zn/Fe ratios in the sedimentary record as a redox evolution proxy can be done if we assume that the hydrothermal inputs of these elements as well as their partition coefficients were stable through time in addition to both ions having the same solubility. Zn/Fe ratios of the Mount Rigg Carbonates were plotted alongside data from literature (Figure 20). All 3 leachates have similar values, ranging from 2.871 to 90.52 with a mean of 29.85 to 45.26. The average values, albeit slightly higher comparatively to data of similar ages from literature, still represent a fairly O_2 poor environment, which is expected for the geological period. The slightly higher values within the sample could be indicative of the local oxygenation events previously as hinted at from Ce anomalies.

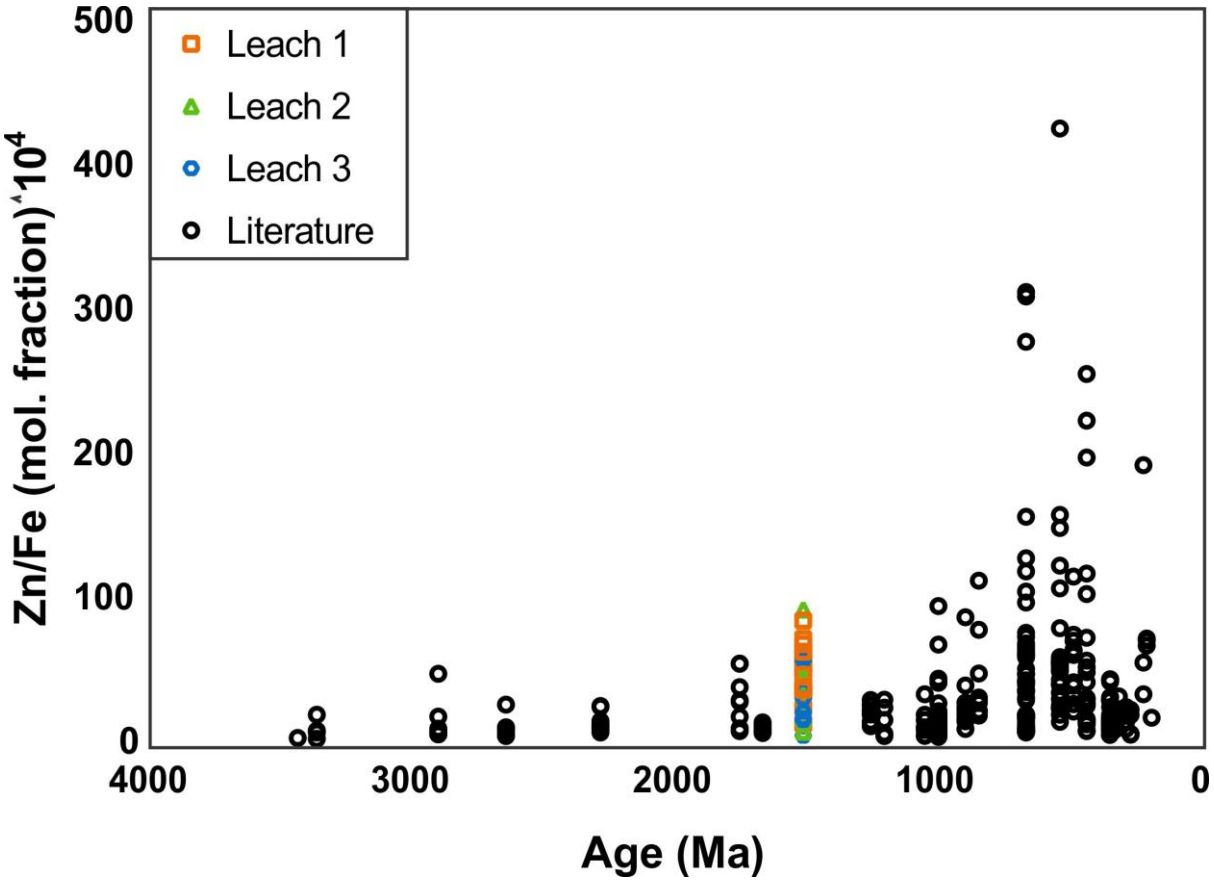

Figure 20: Zn/Fe ratios plotted against time for each carbonate analysis with literature (Liu et al., 2016) data containing 300 analyses. All of the Mount Rigg Carbonate leachates produced very similar values, displaying an O_2 poor environment.

EXTRACTING SEAWATER RARE EARTH ELEMENTS AND YTTRIUM (REY) PATTERNS

Carbonates and other hydrogenous materials such as marine chert and phosphorites are commonly used as a proxy for reconstructing seawater REY patterns at the time of deposition (Tostevin et al., 2016). REY are primarily injected into the oceans via rivers, wind-borne input and hydrothermal vents (Byrne & Kim, 1990; Douville et al., 1999; Tostevin et al., 2016). Their chemical properties and behaviour can result in characteristic distribution patterns when normalised to PAAS. Normalisation is done to remove natural variation in REY concentrations by comparing the data with the composition of the upper crust for which shale is a proxy. Rivers are the main source of REY and has a distinctively flat 'continental' distribution pattern. However, freshwater interactions with saline waters can quickly transform this pattern into a more typical seawater sequence. Seawater REY profiles are

typically smooth, with progressive enrichments in REE and a distinguishable negative Ce anomaly and positive Y anomaly (Zhong & Mucci, 1995). Hydrothermal inputs are secondary supplies of REY into the ocean and they carry a flat Heavy Rare Earth Elements (HREE) signal with a prominent Eu anomaly (Bau & Dulski, 1996). Therefore the preservation of seaweater anomalies in REY patterns from authigenic minerals can identify the deposition conditions, secondary alteration as well as improving confidence in our geochemical data.

Modern seawater REY patterns show a large positive Y anomaly (Y/Ho) with larger Y anomalies (40–80) mainly occurring in open marine settings while smaller anomalies (33–40) originate from near shore or restricted setting (De Baar et al., 1985; Bau et al., 1997). However, the understanding of Y anomalies are somewhat limited as the majority of earlier studies did not include Y measurements to complement REEs (De Baar et al., 1985, Tostevin et al, 2016). Y anomalies can vary with salinity, fractionation during chemical weathering and redox cycling (Liu & Byrne, 1997; Hill et al., 2000). Small enrichments of Gd habitually exists as an analytical artifact due to the increase of their relative stability in solution (Tostevin et al., 2016). Positive Eu anomalies are indicative of mixing with hydrothermal fluids (Meyer et al., 2012) while authigenic carbonates customarily carry a positive La anomaly (Figure 21b). REY data from all three leachates were normalised against PAAS. Each analyses from the leachates were then bootstrapped using the Monte Carlo Simulation approach (Figure 21a) and plotted to present a REY distribution pattern reflective of the deposition conditions of the Mount Rigg Carbonates. REY for all leachates display a consistent and similar pattern.

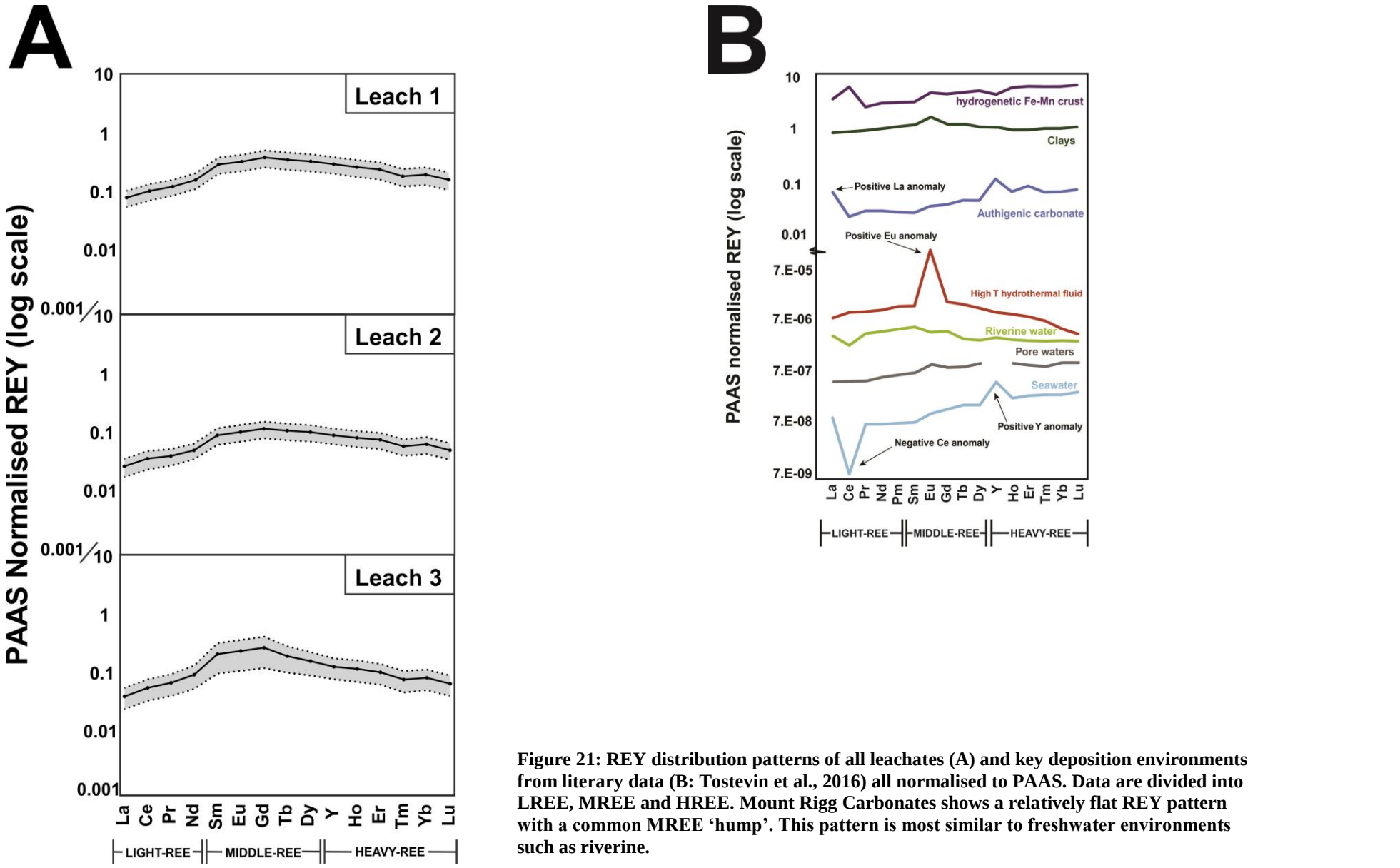

Figure 21: REY distribution patterns of all leachates (A) and key deposition environments from literary data (B: Tostevin et al., 2016) all normalised to PAAS. Data are divided into LREE, MREE and HREE. Mount Rigg Carbonates shows a relatively flat REY pattern with a common MREE 'hump'. This pattern is most similar to freshwater environments such as riverine.

The overall REY profile is relatively flat with the positive Ce anomalies previously discussed visible throughout the different plots. A ‘hump’ in the MREE can also be observed with minor positive Eu and Gd anomalies, although they are both well within range of variable seawater conditions. When compared with typical key natural environments from literary data (Figure 21b), the Mount Rigg Carbonates REY pattern look most similar to that of a freshwater environment.

When further compared to other freshwater environment analogues, the Mount Rigg Carbonates show remarkable likeness with lacustrine sediments (Figure 22) albeit carrying a slightly more prominent MREE signature. This is most likely due to the fluctuating solubility effect previously discussed as well as interferences with other ions of similar mass/charge ratio (Tostevin et al., 2016). The lack of La and Gd anomalies, flat REY patterns, as well as the absence of superchondritic Y anomalies all seem to indicate that the palaeoenvironment of the Mount Rigg Carbonates was not a typical open-marine, oxic basin setting but is instead a restricted, oxygen-poor and possibly lacustrine domain.

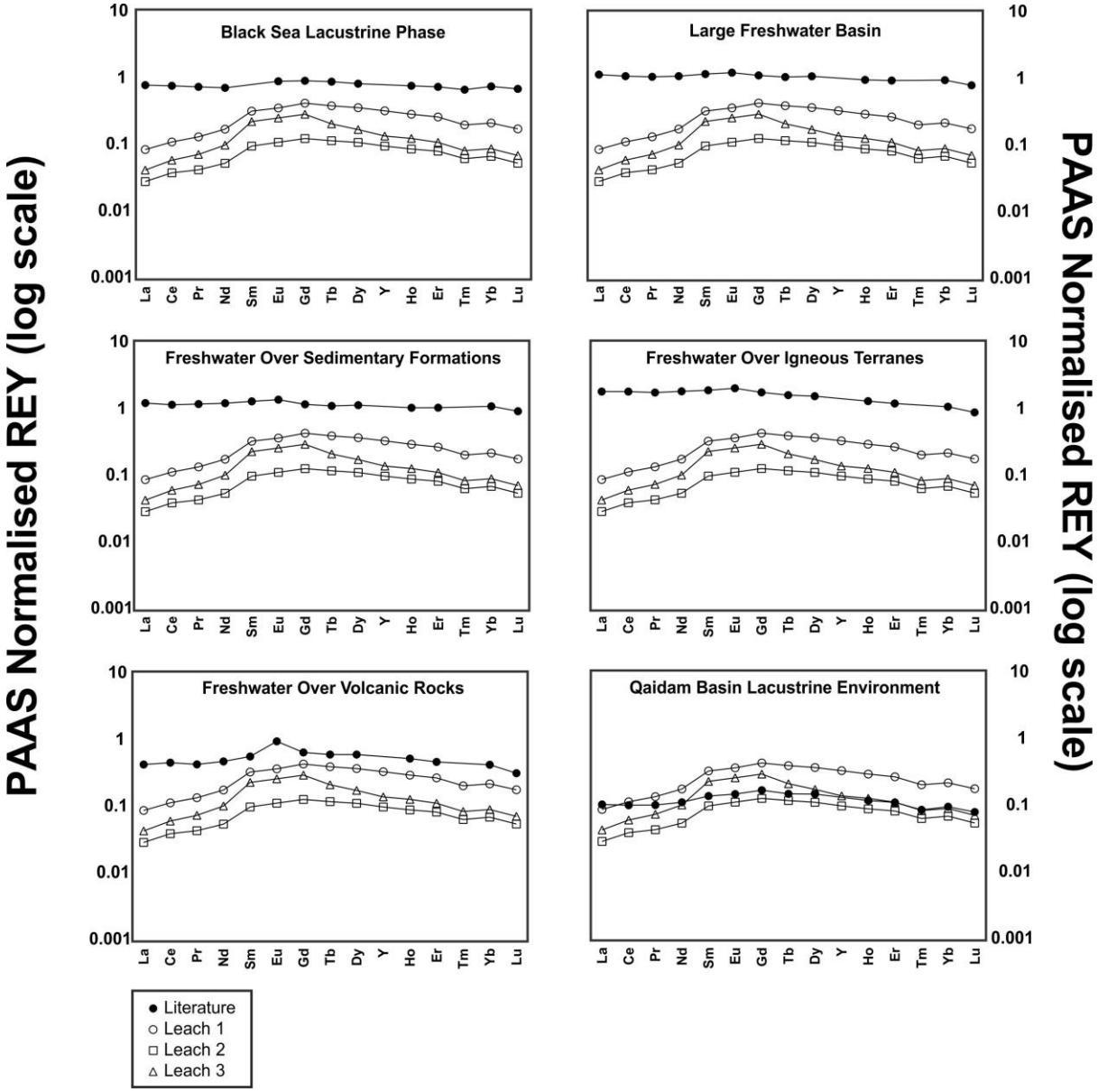

Figure 22: All leachates compared to modern analogues of fresh water environments from literature. All river basin data are from Bayon et al., (2015). Black sea lacustrine data are from Piper & Calvert, (2011). Qaidam Basin Lacustrine data are from Yang et al., (2014). Mount Rigg Carbonate REY distribution patterns resemble both lacustrine environments most.

Bullen (2017) and Munson (2016) have both made interesting comparisons between the Glyde and Wilton Packages and the modern day Black Sea, noting similar fluctuations in the water column chemistry such as varying salinities indicating limited water exchange, water stratification, an anoxic environment and periods of basin restriction. The Black Sea has also experienced temporal transitions between a lacustrine and marine environments during periods of extreme restriction (Piper & Calvert 2011). We suggest that the Mount Rigg Carbonates may also represent a similar transition environment.

However, Ce anomalies can be absent in deeper, fully anoxic waters with oxic surface waters hosting those negative anomalies above them (German et al., 1991). In some local modern Mn-rich waters, positive Ce anomalies develop beneath the Mn redoxcline (Bau et al., 1997, De Baar et al., 1988). Ce anomalies can also be hindered under excessive alkaline conditions and in the presence of strong Fe^{3+} binding compounds (Moller & Bau, 1993, Kraemer et al., 2015). Carbonate rocks have been previously observed to display a characteristic 'seawater' appearance despite undergoing restrictive basin conditions (Paula-Santos et al., 2018). The use of normalised REY distribution patterns as a palaeoenvironmental proxy is limited by the possibility that terrestrial waters are also capable of developing 'seawater' type REY distribution. To summarize, although REY compositions are useful tools to analyse changes in chemical composition of seawater, we must acknowledge that it should not be used as an unequivocal tool for such purpose as different marine environments can develop similarities and differences among them resulting in misguided palaeoenvironmental interpretations.

PALAEOENVIRONMENTAL AND TECTONIC IMPLICATIONS

When integrating both U–Pb age data with $\varepsilon_{Hf}(t)$ values in detrital zircons, all results indicates that the formations within the Lower Roper and the Mount Rigg Group from the McArthur Basin as well as the Tijunna and the Bullita Group from the Birrindudu Basin are sourcing from similar provenance regions. The provenance most similar to the sedimentary units discussed in this study is the Arunta Region, located south of the basin system. Older populations (ca. 2500 Ma) possibly originate from the juvenile Billabong Complex within the Tanami (Ahmad & Munson, 2013) while younger populations (ca. 1800 Ma) were interpreted to derive from units present in the Aileron Province (Leno et al., 2017).

The Bessie Creek Sandstone is stratigraphically adjacent to the boundary between the Maiwok and the Collara Subgroup (Figure 2) and has U–Pb data similar to the Arunta Region as well (Yang et al., 2018). However, up stratigraphy and into the Velkerri Formation, samples begin to have values reflecting easterly sources (Mount Isa Province). Further upwards into the top of the Maiwok Subgroup, the Moroak Sandstone and the Kyalla Formation exhibits data similar to the Arunta Region again. The subduction of the Mirning Ocean (Kirkland et al., 2017; Morrissey et al., 2017) that collided the West Australian Craton (WAC) into the combined North Australian Craton (NAC) and South Australian Craton (SAC) ca. 1.28 Ga have been suggested to correlate with the uplift of the Arunta, allowing it to become a source again for sands in the Moroak and the Kyalla (Yang et al., 2018).

However, this model does not explain how the Arunta Region was also a provenance source for sedimentary units stratigraphically below the Velkerri Formation. Results in this study have shown the units equivalent to and underneath the Collara Subgroup all exhibit data resembling the Arunta. Notably, Mount Isa-like data are largely absent in these formations. Therefore we propose a slight modification to the sequence of events put forward by Yang et al. (2018).

Pluton-related metamorphism and magmatic activity alongside widespread isotope resetting, shear zone reactivation and basin development ca. 1.50–1.45 Ga in the NAC have been correlated with similar events throughout the SAC and Laurentia. This suggests that Australia and Laurentia were still connected during the Mesoproterozoic (Morrissey et al., 2018). Hence we propose that the exposure of the Arunta Region occured in this earlier period, correlating with the events previously mentioned and enabling it to be a source for sands within and underneath the Collara Subgroup. Furthermore, we also suggest that the Mount Isa Province have yet to be uplifted at this time.

The Proterozoic rifting of North Australia Craton and Laurentia then occured ca. 1.45 Ga (Mulder et al., 2015). We propose the exhumation of the Mount Isa Province to occur throughout this process instead. Spikings et al. (2001) have previously reported that post-orogenic exhumation of the Mount Isa Province happened between 1.46 and 1.39 Ga. This is possibly reflected by the limited Mount Isa-like detritus within the Munyi and the Bessie Creek and the increase in such sources within the Velkerri Formation. The return to formations with data more similar to the Arunta could then suit the model proposed by Yang et al. (2018). These following tectonic scenarios are detailed in Figure 23 below.

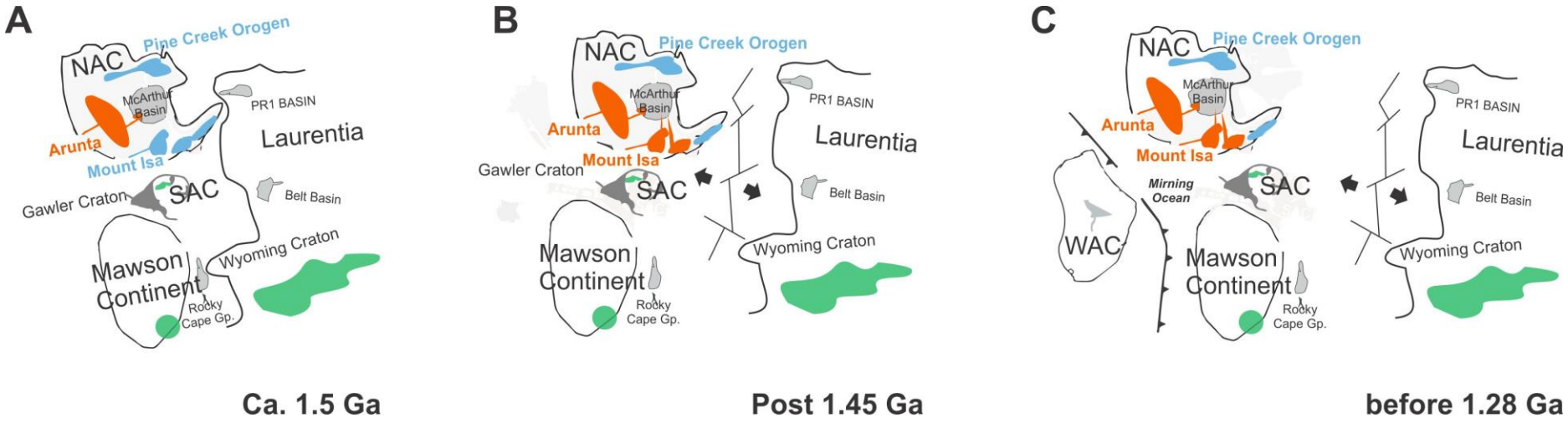

Figure 23: Tectonic scenario sketch showing deposition history of the Favenc and Wilton Packages modified after Smiths et al. (2014), Mulder et al. (2015), Morrissey et al. (2018) and Yang et al. (2018). (A) Uplift of the Arunta and its erosion, becoming a major source (orange) for the Favenc and Wilton Packages is interpreted to correlate with ca. 1.50 Ga pluton-related magmatism, isotope resetting of igneous rocks (shown in green) and a compilation of other widespread events at the time such as shear zone reactivation and rift basin development. No Mount Isa-like detritus are found in these units. (B) Separation of NAC and Laurentia exhuming south and southeastern margins of the NAC, particularly Mount Isa, which is reflected by detritus composition of the Velkerri Formation. (C) Collision between WAC and combination of NAC and SAC, exposing both the Arunta and Mount Isa and allowing them to become a source for sands again in the Moroak and Kyalla Formations.

This tectonic scenario would also have implications on the deposition palaeoenvironment of the Mount Rigg Carbonates. Munson (2016) and Bullen (2017) have suggested that the Wilton and Glyde Packages were both deposited in an enclosed marine environment. The basin was interpreted to be restricted by some land mass or chains of islands with limited connection to the open sea (Munson, 2016). This model is largely consistent with the tectonic scenario proposed in this study. If the widespread exhumation of NAC igneous provinces did occur ca. 1.45 Ga, the Mount Rigg Carbonates would have been restricted to the open sea by multiple sources south and east of the basin system. The basin would then have developed a fluctuating water balance (Munson et al., 2016). With a positive water balance (freshwater flow exceeding seawater), water stratification and anoxic conditions would arise, similar to the environment of the Black Sea. When water surfaces cannot rise above the elevation of the outlet sill, the sea will remain isolated from the global ocean and evolve over time into a lake (Yanchilina et al., 2017).

CONCLUSIONS

Using data from detrital zircons and carbonate-rich units, we have constrained the palaeoenvironment, geochronological and the tectonic geochemical evolution of the Mesoproterozoic greater McArthur Basin. U–Pb data of the Dook Creek Formation have resulted in an MDA of 1614 ± 78 Ma, with populations present ca. 1800 Ma, ca. 2100 Ma and ca. 2500 Ma. Older population grains exhibit more juvenile $\varepsilon_{Hf}(t)$ values while younger populations consists of more negative, crustal-like values. There is a remarkable resemblance between Dook Creek Formation detritus U–Pb, $\varepsilon_{Hf}(t)$, and REE data when compared to stratigraphic-equivalent units. Therefore these formations have been interpreted to be sourced from the same provenance; the Arunta Region. Further up stratigraphy into the Maiwok Subgroup, there is a change in provenance to more easterly sources (Mount Isa Region).

Using isotopic data from carbonate-rich facies, we have also constrained the palaeoenvironment and water column redox conditions. REY distribution patterns of the Mount Rigg Carbonates reflected a lacustrine environment. In addition, Ce anomalies, Y/Ho and Zn/Fe ratios have been interpreted to represent anoxic and restricted basin conditions. The palaeoenvironment of these units are comparable to the modern Black Sea, where restricted basin systems transition in and out of anoxic lacustrine environments controlled by a fluctuating water balance between freshwater and seawater flow.

A tectonic model slightly modified after Yang et al. (2018) has been developed to explain the changes in provenance and deposition environment. We argue that the Arunta Region was exhumed before the exposure of Mount Isa as there were initially no visible data from sands reflecting easterly sources. This process has been interpreted to correlate with widespread pluton-related magmatism, isotope resetting, shear-zone reactivation and basin development ca. 1.5 Ga (Morrissey et al. 2018). The rifting between NAC, SAC and the Gawler Craton with Laurentia, exhumation of Mount Isa, as well as the subsequent tectonic activity then follows the model proposed by Yang et al. (2018). This tectonic model also fits with the palaeoenvironment interpreted for the Mount Rigg Carbonates. At the time of deposition, the basin would be restricted from the open ocean by a number of southerly and easterly provinces. When water levels cannot overcome the elevation outlet of the sill, the region will become completely isolated from the open ocean and over time evolve into a lacustrine environment.

ACKNOWLEDGMENTS

I would like express my gratitude to everyone who has helped me academically and personally throughout the year. Dr. Morgan Blades, Dr. Alan Collins and Dr. Grant Cox for their continual support and guidance in this project. Thank you to Bo Yang, Dr. Juraj Farkas and David Bruce for their general advice and input. The McArthur and Amadeus Basin research group for great times in Alice Springs. Many thanks to Sarah Gilbert at Adelaide Microscopy and Galen Halverson and Thi Hao Bui for their help during the zircon and carbonate geochemistry analyses. Thank you to ARC Linkage partners: the Northern Territory Geological Survey, Origin, Santos and Imperial Oil and Gas for providing funding for this project. Last but not least, thank you to the honours crew for an incredible year and I wish you all the best in your future.

REFERENCES

ABBOTT, S. T., SWEET, I. P., PLUMB, K. A., YOUNG, D. N., CUTOVINOS, A., FERENCZI, P. A., . . . PIETSCH, B. A. (2001). *Roper Region: Urapunga and Roper River Special, Northern Territory (Second Edition). 1:250000 geological map series explanatory notes, SD 53-10, 11.* Darwin: Northern Territory Geological Survey.
AHMAD, M., & MUNSON, T. J. (2013). *Geology and mineral resources of the Northern Territory.* NTGS.
BAILEY, T., MCARTHUR, J., PRINCE, H., & THIRLWALL, M. (2000). Dissolution methods for strontium isotope stratigraphy: whole rock analysis. *Chemical Geology*, 313-319.
BANNER, J. L., & HANSON, G. N. (1990). Calculation of simultaneous isotopic and trace element variations during water-rock interactoin with applications to carbonate diagenesis. *Geochimica et Cosmochimica Arte*, 3123-3137.
BANNER, J. L., HANSON, G. N., & MEYERS, W. J. (1988). Rare earth element and Nd isotopic variations in regionally extensive dolomites from the Burlington-Keokuk Fomation (Mississippian): implications for REE mobility during carbonate diagenesis. *Journal of Sedimentary Research*, 415-432.
BARBEY, P., ALLE, P., BROUAND, M., & ALBAREDE, F. (1995). Rare-earth patterns in zircons from the Maaslu granite and Tibetan slab migmatites (Himalaya): Insights in the origin and evolution of a crustally derived granite magma. *Chemical Geology*, 1-17.
BAU, M., & DULSKI, P. (1996). Distribution of yttrium and rare-earth elements in the Penge and Kuruman iron-formations, Transvaal Supergroup, South Africa. *Precambrian Research*, 37-55.
BAYON, G., SAMUEL, T., CHARLOTTE, S., ANDRE, L., SYLVAIN, B., SANDRINE, C., . . . BARRAT, J.-A. (2015). Rare earth elemens and neodynium isotopes in world river sediments revisited. *Geochimica et Cosmochimica Acta*, 17-38.
BLADES, M.L. (2013, November). The Age and Origin of the Western Ethiopian Shield. South Australia, Adelaide: University of Adelaide.
BLAKE, D. H., HODGSON, I. M., & SMITH, P. A. (1975). *Geology of the Birrindudu and Tanam 1:250000 sheet areas, Northern Territory.* . Canberra: Bureau of Mineral Resources.
BLAKE, D. H., TYLER, I. M., & WARREN, R. G. (2000). *Gordon Downs, Western Australia. 1:250000 geological map series explanatory notes, SE 52-10.* Canberra: Australain Geological Survey Oranisation.
BULLEN, M. (2017, November). Isotopic Constraints on the Depositional Environment and Paleo-Redox Conditions of the Greater McArthur Basin, Northern Territory. Sourth Australia, Adelaide: University of Adelaide.
BYRNE, R. H., & KIM, K. H. (1990). Rare earth element scavenging in seawater. *Geochimica et Cosmochimica Acta*, 2645-2656.
CARSON, C. J. (2010). The Victoria and Birrindudu basins, a U-Pb SHRIMP study and review of resource potential. *Annual Geoscience Exploration Seminar (AGES).* Alice Springs: Northern Territory Geological Survey.
CASSIDY, E. (2018). Tectonic Geography of the Lower Roper Group, McArthur Basin, Northern Australia using detrital geochronology and shale geochemistry. South Australia, Adelaide: University of Adelaide.
CLOSE, D. (2014, March). *The McArthur Basin: NTGS' approach to a frontier petroleum basin with known base metal prospectivity*. Retrieved from https://geoscience.nt.gov.au/gemis/ntgsjspui/handle/1/82357
CLOSE, D. (2017, March). *Annual Geoscience Exploration Seminar (AGES) proceedings, Alice Springs, Northern Territory*. Retrieved from https://geoscience.nt.gov.au/gemis/ntgsjspui/handle/1/85106
COX, G. M., JARRET, A., EDWARDS, D., CROCKFORD, P. W., HALVERSON, G. P., COLLINS, A. S., . . . LI, Z.-X. (2016). Basin redox and primary productivity within the Mesoproterozoic Roper Seaway. *Chemical Geology*, 101-114.
CUTOVINOS , A., BEIER, P., KRUSE , P., ABBOT, S., DUNSTER, J., & BRESCIANINI, R. (2002). *Limbunya, Northern Territory (Second Edition). 1:250000 geological map series explanatory notes, SE 52-07.* Darwin: Northern Territory Geological Survey.
DABARD, M. P., LOI, A., & PEUCAT, J. J. (1996). Zircon typology combined with Sm-Nd whole-rock isotope analysis to study Brioverian sediments from tje Armorican Massif. *Sedimentary Geology*, 243-260.
DE BAAR, H. J., BREWER, P. G., & BACON, M. P. (1985). Anomalies in rare earth distributions in seawater: Gd and Tb. *Geochimica et Cosmochimica Acta*, 1961-1969.
DOUVILLE, E., BIENVENU, P., CHARLOU, J. L., DONVAL, J. P., FOUQUET, Y., APPRIOU, P., & GAMO, T. (1999). Yttrium and rare earth elements in fluids from various deep-sea hydrothermal systems. *Geochimica Cosmochimica Acta*, 627-643.
DUNSTER, J. N. (1998). *Reconnaissance of the Proterozoic rocks of the Victoria River regoin, North Ltd.* Northern Territory Geological Survey, Open File Company Report CR1998-0082.

ELDERFIELD, H., & GREAVES, M. (1981). Negative cerium anomalies in the rare earth element paterns of oceanic ferromanganese nodules. *Earth and Planetary Science Letters*, 163-170.
GEHRELS , H. (2014). Detrital zircon U-Pb geochronology applied to tectonics. *Annual Eath Planet Science*, 127-149.
GERMAN, C. R., HOLLIDAY, B. P., & ELDERFIELD, H. (1991). Redox cycling of rare earth elements in the suboxic zone of the Black Sea. *Geochimica et Cosmochimica Acta*, 3553-3558.
HAINES, P. W. (1994). The Balma and Habgood Groups, Northern McArthur Basin, Northern Teritory: Stratigraphy and correlations with the McArthur Group . *AusIMM Annual Conference.* Darwin: The Australian Institute of Mining and Metallurgy.
HALVERSON, G. P., WADE, B. P., HURTGEN, M. T., & BAROVICH, K. M. (2010). Neoproterozoic chemostratigraphy. *Precambrian Research* , 337-350.
HAWKESWORTH, C., & KEMP, T. (2006). A zircon perspective on the evolution of the continental crust: Insights from combined Hf and O isotopes. *Geochimica et Cosmochimica Acta*, 236.
HEAMAN, L. M., BOWINS, R., & CROCKET, J. (1990). The chemical composition of igneous zircon suites: Implications for geochemical tracer studies. *Geochimica et Cosmochimica Acta*, 1597-1607.
HILL, I. G., WORDEN, R. H., & MEIGHAN, I. G. (2000). Yttrium: the immobility-mobility transition during basaltic weathering. *Geology* , 923-926.
HINTON, R. W., & UPTON, B. G. (1991). The chemistry of zircon: variations within and between large crystals from syenite and alkali basalt xenoliths. *Geochimica et Cosmochimica Aca* , 3287-3302.
HOSKIN, P. W., & IRELAND, T. R. (2000). Rare earth element chemistry of zircon and its use as a provenance indicator. *Geology*, 627-630.
JACKSON, S. E., PEARSON, N. J., GRIFFIN, W. I., & BELOUSVA, E. A. (2004). The application of laser ablation-inductively coupled plasma-mass spectrometry to in situ U-Pb zircon geochronology. *Chemical Geology*, 47-69.
KIRKLAND, C.L., SMITHIES, R.H., SPAGGIARI, C.V., WINGATE, M.T.D., QUENTIN DE GROMARD, R., CLARK, C., GARDINER, N.J., BELOUSOVA, E.A. (2017). Proterozoic crustal evolution of the Eucla basement, Australia: implications for destruction of oceanic crust during emergence of Nuna. *Lithos*, 278–281, 427–444.
KRAEMER, D., KOPF, S., & BAU, M. (2015). Oxidative mobilization of cerium and uranium and enhanced release of 'imobile' high field strength elements from igneous rocks in the presence of the biogenic siderophore desferrioxamine. *Geochimica et Cosmochimica Acta*, 263-279.
KRALIK, M. (1982). Rb-Sr age determinations on Precambrian carbonate rocks of the Carpentarian McArthur Basin, Northern Territory, Australia. . *Precambrian Research*, 151-170.
KRUSE, P. D., SWEET, I. P., STUART-SMITH, P. G., PIETERS, P. E., & CRICK, I. H. (1994). *Katheine, Northern Teritory (Second Edition). 1:250000 geological map series explanatory notes, SD 53-09.* Darwin: Northern Territory Geological Survey.
LIU, C., WANG, Z., RAUB, T. D., MACDONALD, F. A., & EVANS, D. A. (2014). Neoproterozoic cap-dolostone deposition in stratified glacial meltwater plume. *Earth and Planetary Science Letters*, 22-32.
LIU, X. M., KAH, L. C., KNOLL, A. H., CUI, H., KAUFMAN, A. J., SHAHAR, A., & HAZEN, R. M. (2016). Tracing Earth's O2 evolution using Zn/Fe ratios in marine carbonates. *Geochemical Perspectives Letters*, 24-34.
LIU, X., & BYRNE, R. H. (1997). Rare earth and yttrium phosphate solubilities in aqueous solution. *Geochimica et Cosmochimica Acta*, 1625-1633.
LUDWIG, K. R. (2003). *Yser's Manual for Isoplot 3.00: a geochronological toolkitfor Microsoft Excel (No.4). Kenneth R. Ludwig.*
MORRISSEY, L. J., BAROVICH, K. M., HAND, M., & HOWARD, K. E. (2018). Magmatism and metamorphism at ca. 1.45 Ga in the northern Gawler Craton: The Australian record of rifting within Nuna (Colombia). *Geoscience Frontiers*, 1-21.
MEYER, E. E., QUICKSALL, A. N., LANDIS, J. D., LINK, P. K., & BOSTICK, B. C. (2012). Trace and rare earth elemental investigation of a Sturtian cap carbonate, Pocatello, Idaho: evidence for ocean redox conditions before and during carbonate deporition. *Precambrian Research*, 192-195.
MOLLER, P., & BAU, M. (1993). Rare-earth paterns with positive cerium anomaly in alkaline waters from Lake Van, Turkey . *Earth Planet Science Letters*, 671-676.
MULDER, J.A., HALPIN, J.A., & DACZKO, N.R., (2015). Mesoproterozoic Tasmania: Witness to the East Antarctica-Laurentia connection within Nuna. *Geology*, 759–769.
MUNSON, T. J. (2016). Sedimentary characterisation and correlation of the Wilton package, greater McArthur Basin . *Annual Geoscience Exploration Seminar (AGES) Proceedings.* Alice Springs: Northern Teritory Geolocial Survey.
NANCE, W. B., & TAYLOR, S. (1976). Rare earth element patterns and crustal evolution: Australian post-Archean sedimentary rocks. *Geochimica et Cosmochimica Acta*, 1539-1551.
PAGE, R. W., JACKSON, M. J., & KRASSAY, A. A. (2000). Constraining the sequence stratigraphy in northern Australian basins: SHRIMP U-Pb zircon geochronology between Mt Isa and McArthur River. *Australian Journal of Earth Sciences*, 431-460.

PAULA-SANTOS, G. M., FILHO, S. C., & BABINSKI, M. (2018). Rare earth elements of carbonate rocks from the Bambui Group, southern Sao Francisco Basin, Brazil, and their significance as paleoenvironmental proxies. *Precambrian Research*, 327-340.
PAYNE, J., PEARSON, N. J., GRANT, K. J., & HALVERSON, G. P. (2013). Reassessment of relative oxide formation rates and molecular interferences on in situ lutetium-hafnium analysis with laser ablation MC-ICP-MS. *Journal of Analytical Atomic Spectrometry*, 1068-1079.
PIPER, D. Z., & CALVERT, S. E. (2011). Holocene and late glacial palaeoceanography and paleolimnology of the Black Sea: Changing sediment provenance and basn hydrography over the past 20000 years. *Geochimica et Cosmochimca Acta*, 5597-5624.
PLUMB, K., & WELLMAN, P. (1987). McArthur Basin, Northern Territory: mapping of deep troughs using gravity magnetic anomalies. . *BMR Journal of Australian Geology and Geophysics* , 243-252.
PLUMB, K., DERRICK, G. M., & WILSON, I. H. (1980). Precambrian geology of the McArthur River-Mount Isa region, northern Australia. *The Geology and Geophysics of Northeastern Australia* , 71-88.
POURMAND, A., DAUPHAS, N., & IRELAND, T. J. (2012). A novel extraction chromatography and MC-ICP-MS technique for rapid analysis of REE, Sc and Y: Revising CI-chondrite and Post-Archean Australian Shale (PAAS) abundances. *Chemical Geology*, 38-54.
RAWLINGS, D. J. (1999). Stratigraphic resolution of a multiphase intracratonic basin system: the McArthur Basin, northern Australia. *Australian Journal of Earth Sciences*, 703-723.
RAWLINGS, D. J., HAINES, P. W., MADIGAN, T., PIETSCH, B. A., SWEET, I. P., PLUMB, K. A., & KRASSAY, A. A. (1997). *Arnhem Bay-Gove, Northern Territory (Second Edition). 1:250000 geological map series explanatory notes, SD 53-03, 04.* Darwin: Northern Territory Geological Survey.
RENO, B. L., WEISHEIT, A., BEYER, E. E., MCGLOIN, M. V., & KOSITCIN, N. (2017). Oroterozoic tectonothermal evolution of the northeastern sector of the Aileron Province. *Annual Geoscience Exploration Seminar* (pp. 36-41). Alice Springs: NT Geological Survey.
RUBATTO, D. (2002). Zircon trace element geochemistry: partitioning with garnet and the link between U--Pb ages and metamorphism. *Chemical Geology*, 123-138.
SHEN, Y., CANFIELD, D. E., & KNOLL, A. H. (2002). Middle Proerozoic Ocean Chemistry: Evidence From The McArthur Basin, Northern Australia. *American Journal of Science*, 81-109.
SLAMA, J., KOSLER, J., CONDON, D. J., CROWLEY, J. I., GERDES, A., HANCHAR, J. M., & SCHALTEGGER, U. (2008). Plesovice zircon--a new natural reference material for U-Pb and Hf isotopic microanalysis. *Chemical Geology*, 1-35.
SOUTHGATE, P. N., BRADSHAW, B. E., DOMAGALA, J., JACKSON, M. J., IDNURM, M., KRASSAY, A. A., . . .
TARLOWSKI, C. (2000). Chronostratigraphic basin framewok for Paleoproterozoic rocks (1730-1575 Ma) in northern Australia and implications for base-metal mineralisation. *Australian Journal of Earth Sciences*, 461-483.
SPENCER, C. J., & KIRKLAND, C. I. (2016). Visualizing the sedimentary response through the orogenic cycle: a multidemnsional scaling approach. . *Lithosphere*, 29-37.
SPIKINGS, R.A., FOSTER, D.A., KOHN, B.P., & LISTER, G.S., (2001). Post-orogenic (< 1500 Ma) thermal history of the Proterozoic Eastern Fold Belt, Mount Isa Inlier, Australia. *Precambr. Res.* 109 (1), 103–144.
TOSTEVIN, R., SHIELDS, G. A., TARBUCK, G. M., TIANCHEN, H., CLARKSON, M. O., & WOOD, R. A. (2016). Effective use of cerium anomalies as a redox proxy in carbonate-dominated marine settings. *Chemical Geology*, 146-162.
TRAIL, D., WATSON , B., & TAILBY, N. D. (2012). Ce and Eu anomalies in zircon as proxies for the oxidation state of magmas. *Geochimica et Cosmochimica Acta*, 70-87
VERMEESCH, P. (2013). Multi-sample comparison of detrital age distributions. *Chemical Geology*, 140-146.
WANG, Y., LIU, Y. G., & SCHMITT, R. (1986). Rare earth element geochemistry of South Atlantic deep sea sediments: Ce anomaly change at 54 My. *Geochimica et Cosmochimica Acta*, 1337-1355.
WATSON, E. B. (1996). Surface enrichment and trace element uptake during crystal growth. *Geochimica et Cosmochimica Acta*, 5013-5020.
WATSON, E. B., & HARRISON, T. M. (1983). Zircon saturation revisited: Temperature and composition effects in a variety of crustal magma types. *Earth and Planetary Science Letters*, 295-304.
WILDE, P., QUINBY-HUNT, M. S., & ERDTMANN, B. D. (1996). The whole-rock cerium anomaly: a potential indicator of eustatic sea-level changes in shales of the anoxic facies. *Sedimentary Geology*, 43-53.
Yanchilina, A., Ryan , W., McManus, J., Dimitrov, P., Dimitrov, D., Slavova, K., & Filipova-Marinova, M. (2017). Compilation of geophysical, geochronological and geochemical evidence indicates a rapid Mediterranean-derived submergence of the Black Sea's shelf and subsequent substantial salinification in the early Holocene. *Marine Geology*, 14-34.
YANG, Y., FANG, X., GALY, A., LI, M., APPEL, E., & LIU, X. (2014). Paleoclimatic significance of rare earth element record of the calcareous lacustrine sediments from a long core (SG-1) in the western Qaidam Basin, NE Tibetan Plateau. *Journal of Geochemical Exploration*, 223-232.

YANG, B., TODD, S. M., COLLINS, A. S., MUNSON, T. J., SCHOEMAKER, B., NICHOLLS, D., . . . GLORIE, S. (2018). Spatial and temporal variation in detrital zircon age provenance of the hydrocarbon-bearing upper Roper Group, Beetaloo Sub-basin, Northern Territory, Australia. *Precambrian Research*, 140-155.
YANG, B., COLLINS, A.S., BLADES, M.L., CAPOGRECO, N., PAYNE, J.L., MUNSON, T.J., COX, G.M. (2018) submitted. Middle-late Mesoproterozoic tectonic geography of the North Australia Craton: U–Pb and Hf isotopes of detrital zircons in the Beetaloo Sub-basin, Northern Territory, Australia. J*ournal of the Geological Society, London.*
ZHONG, S., & MUCCI, A. (1995). Partitioning of rare earth elements (REEs) between calcite and seawater solutions at 25C and 1 atm, and high dissolved REE concentrations. *Geochimcia et Cosmochimica Acta*, 443-453.

APPENDIX

Detrital zircon arrangement

MINERAL PREPARATION

1. Clean rock crusher and disc mill before and after use with compressed air gun and ethanol.
2. Crush rock using jaw crusher
3. Separate fractions with sieve using 79 μm and 479 μm mesh on an Endcotts EPL2000 super shaker.
4. Take coarse 479 μm fraction and re-crush on the disc mill.
5. Repeat and divide final fractions for each sample.

MINERAL SEPARATION

1. Separation was done in B29 Mawson Laboratories, Adelaide University.
2. Clean room and equipment before and after use with vacuum and ethanol wipe.
3. Pan samples to separate light and heavy grains.
4. Separate heavy fraction by magnetic strength using the FRANZ.
5. Final separation done using heavy liquids:
    i. Fill burette with methyl iodide.
    ii. Take top off funnel and pour remaining fraction of sample into burette.
    iii. Stir and allow separates to drop to the bottom.
    iv. Tap off and repeat until no more particles sink.
    v. Clean off heavy liquids using ethanol.
    vi. Zircon fraction is then dried on a hot plate and the separates are cleaned and kept.

ZIRCON PICKING AND MOUNT PREPARATION

1. Clean petri dish with ethanol. Place under microscope. Transfer zircon fraction onto dish,
2. Use a pick to take zircon and place onto Teflon mount base laced with a double sided tape.
3. Repeat for sufficient number of grains (~150).
4. Reconnect Teflon base with enclosement.
5. Coat with vaseline for ease of removal.
6. Mix expoxy resin mixture (epoxy 5g, hardner 0.5g) and add into mount, ensuring air pockets do not form.
7. Heat resin for 30 seconds on a 50˚C hotplate and let cool for 24 hours.
8. Remove epoxy mount with zircon grains from Teflon holder.
9. Bring grains to surface using repetition of sand paper and polishing lap.

Carbonate geochemistry arrangement

CRUSHING AND POWDER PREPARATION

1. Clean equipment before and after use with compressed air gun, ethanol and quartz blank to remove previous sample residue.
2. Break sample using hammer in sizeable pieces.
3. Place samples into ring mill using tungsten carbide.
4. Run for 1 minute.
5. Repeat for all samples.
6. Weigh out 75 mg of powder for each sample and place into glass septa vials.

SAMPLE CLEANING WITH WEAK ACID

1. Weigh centrifuge tube, record, re-zero scale.
2. Clean spatula with ethanol, use to scoop powder from vials, weigh and record.
3. Pipette 2.52 mL of 1 M ammonium acetate solution into tube.
4. Mix vile and leave for 1 hour.
5. Sonicate for 20 minutes, centrifuge for 10 minutes on 4000 rpm.
6. Discard supernatant and keep residue.

LEACHING PROCEDURE

1. Pipette 2.7 mL of 0.2 M acetic acid solution into centrifuge tubes with samples.
2. Mix, make sure solution doesn't touch lid.
3. Sonicate for 20 minutes, centrifuge for 10 minutes at 4000 rpm.
4. Keep supernatant for analysis and repeat steps with residue for further leaching.
5. Final leach, repeat steps but with 2% nitric acid.
6. Evaporate supernatant on 140˚C hotplate to prepare for diluting.
7. Dilute samples onto 1:1500 and 1:100000 leachates using 2% nitric acid following the equation:

$$Dilution\ Factor = \frac{Acid\ Mass + Sample\ Mass}{Sample\ Mass}$$

Detrital Zircon Data

URANIUM—LEAD DATA

Name	Final207/235	Final207/235 Prop2SE	Final206/238	Final206/238 Prop2SE	ErrorCorrelation 6/38 vs 7/35	Concordance
FF02_103	6.16	0.21	0.3784	0.01	0.29184	108.328968
FF02_23	11.53	0.52	0.509	0.016	0.098436	106.9786204
FF01_34	5.89	0.27	0.3703	0.012	0.43122	106.2860136
FF01_14	7.5	0.27	0.4147	0.012	0.47385	106.2767475
FF01_74	7.18	0.27	0.4069	0.012	0.436	106.2288749
FF01_38	4.657	0.17	0.321	0.0089	0.55353	105.4673721
FF02_68	5.74	0.23	0.3574	0.01	0.36229	105.4662379
FF01_3	11.34	0.4	0.4993	0.015	0.28816	104.9899396
FF01_42	5.55	0.21	0.3533	0.0098	0.34449	104.8977395
FF01_76	6.34	0.24	0.3775	0.011	0.73683	104.5615813
FF02_28	11.63	0.44	0.5054	0.014	0.45278	104.4391597

FF02_55	6.46	0.23	0.3805	0.01	0.17768	103.951976
FF02_16	5.33	0.2	0.3432	0.01	0.62291	103.7097654
FF01_54	5.914	0.2	0.3626	0.0097	0.46061	103.6921477
FF01_33	5.459	0.19	0.3461	0.0091	0.35889	103.4501348
FF01_55	6.2	0.29	0.3708	0.012	0.27134	103.1504065
FF01_56	5.74	0.22	0.3561	0.01	0.3105	103.0462185
FF02_61	11.44	0.4	0.4952	0.014	0.77436	102.9330163
FF01_7	10.94	0.4	0.485	0.014	0.70303	102.7016129
FF01_15	6.27	0.23	0.3717	0.011	0.42667	102.5692695
FF01_77	4.62	0.17	0.3172	0.0089	0.34804	102.3054755
FF01_41	11.96	0.51	0.503	0.016	0.39496	102.301092
FF01_19	5.49	0.19	0.3463	0.0092	0.44341	102.2957822
FF02_65	6.57	0.23	0.3784	0.01	0.44195	102.2244192
FF02_22	4.76	0.18	0.3216	0.0089	0.38527	102.21843
FF01_63	6.35	0.23	0.3714	0.011	0.34379	102.2044088
FF01_53	7.55	0.29	0.4061	0.011	0.24669	101.9498607
FF01_61	7.68	0.35	0.413	0.014	0.6508	101.7832647
FF02_101	6.3	0.24	0.3706	0.01	0.33201	101.7025538
FF01_40	5.56	0.21	0.3455	0.0096	0.29779	101.5400956
FF02_25	6.623	0.22	0.3794	0.0099	0.62019	101.5181195
FF02_123	5.34	0.26	0.343	0.013	0.56961	101.1720831
FF02_52	5.14	0.19	0.3327	0.0089	0.42178	101.1437908
FF01_28	5.77	0.2	0.3545	0.01	0.15523	101.1381273
FF02_132	4.513	0.15	0.3103	0.0084	0.29808	101.0446895
FF01_6	5.75	0.22	0.3524	0.01	0.62709	101.038961
FF02_69	10.79	0.41	0.4771	0.014	0.33071	101.0048232
FF01_57	5.23	0.19	0.3355	0.0088	0.36727	100.9750813
FF01_64	4.141	0.14	0.2953	0.0078	0.28997	100.9079903
FF01_62	5.58	0.22	0.3463	0.0095	0.39702	100.895208
FF01_4	5.06	0.19	0.3275	0.0099	0.57717	100.8287293
FF02_109	5.37	0.21	0.3385	0.011	0.75494	100.805153
FF02_39	11	0.38	0.48	0.013	0.55439	100.7578779
FF01_49	4.59	0.18	0.3114	0.0085	0.5397	100.3446295
FF02_79	3.947	0.14	0.2857	0.0077	0.46815	100.3097893
FF01_30	5.41	0.21	0.3398	0.0094	0.51397	100.1594049
FF02_83	11.31	0.45	0.4823	0.013	0.58782	100.1184366
FF01_31	5.98	0.24	0.3546	0.011	0.3809	100.0511771
FF01_17	5.41	0.22	0.3378	0.0099	0.45668	99.68186638
FF02_119	5.69	0.23	0.3447	0.0095	0.28237	99.53051643
FF02_112	5.28	0.2	0.3303	0.012	0.41033	99.19093851
FF01_88	4.51	0.18	0.3064	0.0091	0.73148	99.13644214
FF02_122	5.59	0.24	0.343	0.01	0.29118	99.1131977
FF01_25	5.59	0.28	0.3426	0.013	0.27987	98.85297185
FF02_34	6.16	0.25	0.3578	0.011	0.4552	98.79638917
FF02_19	4.605	0.16	0.3099	0.0089	0.52796	98.75070982
FF02_110	5.18	0.23	0.3281	0.011	0.66462	98.59762675
FF01_46	5.47	0.22	0.3388	0.011	0.67852	98.58786611
FF02_106	5.52	0.2	0.337	0.0088	0.45299	98.31932773
FF01_52	4.53	0.18	0.3024	0.009	0.084312	97.7599081
FF01_94	5.333	0.19	0.3311	0.0093	0.63018	97.10221286
FF01_81	5.095	0.17	0.3209	0.0085	0.61902	96.87331536
FF02_105	5.4	0.2	0.3317	0.0093	0.56837	96.64921466
FF01_9	5.47	0.2	0.3327	0.01	0.82703	96.55532359
FF02_48	4.924	0.17	0.3169	0.011	0.65459	96.41109299
FF02_15	7.09	0.33	0.373	0.014	0.68662	96.34831461
FF01_83	10.79	0.37	0.4618	0.013	0.42518	96.33714061
~~FF02_84~~	~~6~~	~~0.25~~	~~0.3499~~	~~0.0097~~	~~0.08134~~	~~96.26494024~~
FF01_12	4.805	0.16	0.3112	0.008	0.39533	96.14537445
FF01_26	5.15	0.2	0.3235	0.0093	0.59331	96.01275917
FF01_2	5.605	0.2	0.34	0.0094	0.52939	95.78466227
FF02_87	6.62	0.28	0.3654	0.01	0.52966	95.61696046
FF01_27	7.74	0.35	0.392	0.014	0.91316	95.57443004
FF01_8	11.08	0.43	0.4627	0.013	0.67202	95.19006982
FF02_73	5.39	0.22	0.3262	0.0091	0.34076	95.13598326
FF02_17	4.842	0.17	0.3098	0.0093	0.67931	95.08733624
FF02_108	5.86	0.21	0.3428	0.0093	0.63785	94.33962264
FF02_51	5.14	0.2	0.3213	0.0099	0.77232	94.27521008
FF01_35	5.2	0.3	0.325	0.015	0.83032	93.87966805
FF01_89	4.4	0.18	0.2925	0.0086	0.5839	93.65439093
FF01_86	4.836	0.16	0.3069	0.008	0.54177	93.54663774
FF01_92	3.943	0.15	0.2745	0.0078	0.51376	93.42498506
FF01_23	15.09	0.55	0.522	0.016	0.75799	93.40469613
FF01_58	4.789	0.17	0.3053	0.0092	0.52483	93.21021184
FF01_24	4.812	0.17	0.3067	0.0085	0.52858	92.98813376
FF01_37	11.06	0.39	0.4568	0.013	0.67383	92.94478528
FF01_44	5.006	0.17	0.3111	0.008	0.58889	92.5729443
FF02_29	9.58	0.39	0.426	0.014	0.58402	92.55362202
FF01_68	5.08	0.2	0.314	0.01	0.77677	92.43300053
FF02_120	4.96	0.18	0.3087	0.0085	0.45202	92.18085106
FF01_66	4.386	0.15	0.2881	0.0077	0.66272	91.73228346
FF01_80	5.157	0.18	0.3145	0.0085	0.56696	91.64504411
FF01_21	6.17	0.24	0.345	0.0099	0.30051	91.57491623

FF02_41	4.87	0.23	0.306	0.014	0.86693	91.13117366
FF01_32	6.31	0.23	0.344	0.0098	0.62561	89.87282148
FF01_75	10.41	0.39	0.4335	0.012	0.87623	89.85282727
FF02_124	5.7	0.26	0.327	0.013	0.85977	89.74358974
FF01_96	4.47	0.18	0.2916	0.0086	0.57221	89.66829799
FF01_82	5.2	0.19	0.3127	0.0091	0.48721	89.43877551
FF01_34	6.090033845	0.238974088	0.327575727	0.009998043	0.662198729	89.27230293
FF01_47	4.981	0.18	0.305	0.0085	0.47984	89.22996878
FF01_16	7.68	0.45	0.373	0.017	0.91971	89.19037199
FF02_66	4.262	0.16	0.2779	0.0095	0.57769	88.81394042
FF02_98	4.988	0.18	0.3007	0.0084	0.5615	88.22916667
FF01_48	4.33	0.17	0.2807	0.0088	0.67582	88.18984547
FF02_24	5.19	0.2	0.3075	0.0088	0.65775	87.89420142
FF02_12	5.577	0.2	0.3202	0.0092	0.75891	87.87432499
FF01_51	4.781	0.16	0.2955	0.0081	0.58484	87.60504202
FF01_79	4.769	0.17	0.2934	0.0077	0.53973	87.44725738
FF01_13	4.423	0.16	0.2829	0.0085	0.7449	86.99186992
FF01_72	5.303	0.18	0.3097	0.008	0.59292	86.74638764
FF02_118	5.09	0.19	0.3039	0.0094	0.60072	86.71399594
FF02_45	4.927	0.17	0.2996	0.008	0.75333	86.65982555
FF02_75	5.19	0.25	0.305	0.013	0.90558	86.4209995
FF02_99	9.36	0.38	0.4011	0.013	0.70964	85.7199211
FF02_113	9.23	0.34	0.3999	0.013	0.71809	85.61264822
FF01_65	5.06	0.18	0.2993	0.0083	0.66476	85.44719555
FF01_90	3.889	0.13	0.2617	0.007	0.64806	85.40478905
FF01_78	4.177	0.15	0.273	0.0078	0.57669	85.34577387
FF01_45	4.43	0.21	0.279	0.012	0.84025	84.79657388
FF02_11	4.75	0.18	0.2906	0.0085	0.41476	84.78597215
FF01_29	3.96	0.15	0.2608	0.0075	0.61481	84.73325766
FF02_57	4.207	0.16	0.2725	0.0075	0.5857	84.72449536
FF01_87	4.46	0.17	0.2791	0.0082	0.82548	84.72222222
FF01_1	4.06	0.16	0.2637	0.0084	0.84353	83.40707965
FF02_20	5.21	0.2	0.2987	0.0088	0.5814	83.20158103
FF02_131	4.91	0.33	0.292	0.014	0.4363	83.09008556
FF02_111	5.57	0.24	0.3086	0.011	0.37075	83.03785338
FF02_130	4.71	0.74	0.284	0.03	0.77272	82.81893004
FF02_88	4.73	0.22	0.2821	0.012	0.93049	82.42548818
FF01_11	6.56	0.23	0.331	0.0094	0.64919	81.6127603
FF02_96	5.4	0.2	0.3013	0.0091	0.80351	81.53846154
FF02_80	3.66	0.18	0.2495	0.0095	0.52272	81.38479001
FF01_20	9.44	0.37	0.3892	0.013	0.83075	81.32205995
FF02_115	4.53	0.19	0.2736	0.0095	0.77657	80.97207859
FF02_74	4.426	0.15	0.2717	0.0073	0.65299	80.88772846
FF01_85	3.95	0.14	0.2544	0.0075	0.81498	80.84163898
FF01_60	4.712	0.16	0.2809	0.0078	0.5298	80.75949367
FF02_47	6.35	0.22	0.3232	0.0089	0.74319	80.10657194
FF02_18	4.01	0.19	0.259	0.012	0.723	79.98921251
FF02_129	4.5	0.19	0.2719	0.0099	0.7183	79.71163749
FF02_27	3.886	0.15	0.2522	0.0087	0.85447	79.69179967
FF02_60	3.38	0.15	0.2312	0.0083	0.74688	79.19621749
FF02_95	3.827	0.13	0.2482	0.0068	0.56967	79.03761062
FF02_128	4.43	0.19	0.2686	0.0099	0.71782	78.59342916
FF02_53	4.74	0.22	0.275	0.012	0.83018	77.87170562
FF02_46	4.34	0.17	0.2642	0.0085	0.72772	77.83505155
FF02_127	3.73	0.16	0.2423	0.009	0.7931	77.82729805
FF02_13	7.7	0.27	0.3444	0.01	0.81277	77.74154097
FF01_10	3.481	0.11	0.2325	0.0062	0.48829	77.4137931
FF02_67	6.69	0.23	0.3224	0.0086	0.61224	77.29613734
FF02_63	3.71	0.16	0.2418	0.0084	0.85563	76.94429123
FF01_50	3.712	0.13	0.2402	0.007	0.81043	76.12513721
FF02_31	3.68	0.18	0.238	0.01	0.96264	75.95356551
FF01_18	5.21	0.19	0.2834	0.0082	0.86063	75.33989686
FF02_90	4.27	0.16	0.2596	0.0081	0.69927	75.29113924
FF01_43	3.891	0.14	0.245	0.0065	0.42975	75.18636848
FF02_50	8.77	0.32	0.3581	0.0099	0.53577	75.0475466
FF02_86	4.35	0.18	0.2592	0.0084	0.90483	74.88653555
FF02_1	7.69	0.28	0.3381	0.011	0.88837	74.88019169
FF02_92	8.11	0.34	0.342	0.013	0.77846	74.75422729
FF01_5	3.61	0.16	0.2326	0.0089	0.88037	74.5584989
FF01_67	16.56	0.61	0.4555	0.014	0.9098	74.46874038
FF02_8	3.014	0.11	0.2119	0.006	0.60366	74.35590174
FF01_71	3.58	0.21	0.2312	0.01	0.91382	73.88183324
FF01_69	5.72	0.23	0.2931	0.0094	0.84162	73.73107747
FF02_38	3.822	0.13	0.238	0.0071	0.57871	73.62520021
FF02_78	3.415	0.13	0.2275	0.0074	0.7978	73.53760446
FF01_22	3.429	0.12	0.2262	0.0063	0.60402	73.32589286
FF02_62	3.64	0.17	0.2331	0.0088	0.88779	73.11653117
FF02_133	4.196	0.15	0.2501	0.0076	0.47783	72.92089249
FF02_56	3.393	0.12	0.223	0.0059	0.61107	72.62038074
FF02_32	4.051	0.15	0.2427	0.0065	0.6853	71.83170857
FF02_102	7.86	0.28	0.3316	0.0095	0.42111	71.77795031
FF02_5	3.89	0.17	0.2366	0.0083	0.86846	71.60817182

FF02_116	3.744	0.12	0.2326	0.0065	0.64919	71.38314785
FF01_36	6.67	0.23	0.3059	0.0079	0.5846	71.22153209
FF02_36	3.74	0.21	0.2299	0.0096	0.61475	71.13127001
FF01_70	3.53	0.16	0.2257	0.0089	0.87728	71.07976126
FF02_30	3.99	0.17	0.2394	0.0084	0.94033	70.72671443
FF02_121	3.174	0.12	0.2134	0.006	0.70204	70.69160998
FF02_59	7.3	0.28	0.3158	0.0098	0.74667	70.5225369
FF02_97	9.28	0.34	0.3483	0.01	0.75217	70.16393443
FF02_43	4.519	0.16	0.2516	0.007	0.41594	69.30787589
FF02_58	4.259	0.15	0.2443	0.0067	0.73965	69.25725529
FF02_2	4.18	0.18	0.2422	0.008	0.76378	69.10528917
FF02_77	3.351	0.12	0.2158	0.0063	0.79274	68.72270742
FF02_6	3.88	0.17	0.2316	0.009	0.81627	68.2790224
FF02_114	6.99	0.36	0.303	0.013	0.89262	67.8614098
FF02_40	3.56	0.19	0.2226	0.011	0.92488	67.60858189
FF02_33	3.33	0.15	0.2124	0.0075	0.84789	67.20867209
FF02_21	6.5	0.25	0.2918	0.0083	0.805	66.69361358
FF02_91	4.05	0.16	0.2333	0.0079	0.78768	66.17647059
FF02_14	2.714	0.09	0.188	0.0048	0.5885	65.71936057
FF01_59	2.711	0.093	0.1863	0.0049	0.75415	64.34833431
FF02_64	2.767	0.11	0.1888	0.0063	0.88999	64.3187067
FF02_125	14.2	1.7	0.382	0.024	0.9492	63.49693252
FF02_76	3.361	0.12	0.2061	0.0058	0.56547	62.47412008
FF02_93	3.126	0.13	0.1977	0.006	0.83613	62.43954863
FF02_85	4.268	0.16	0.2291	0.0058	0.33191	61.37517305
FF02_7	3.173	0.13	0.1954	0.0086	0.85934	61.29204485
FF02_26	3.228	0.13	0.1996	0.0073	0.72557	61.26502875
FF01_93	2.73	0.14	0.1824	0.0072	0.92932	61.22102883
FF02_49	2.699	0.11	0.1799	0.0059	0.86799	60.15801354
FF02_37	3.745	0.15	0.2113	0.0065	0.71623	59.63302752
FF02_117	3.19	0.26	0.194	0.013	0.98078	58.56922285
FF02_82	3.55	0.17	0.2016	0.0062	0.4266	58.4486166
FF02_9	3.722	0.15	0.2067	0.0061	0.66787	57.77671756
FF02_35	3.7	0.16	0.2028	0.0088	0.5444	56.80840898
FF01_84	2.681	0.093	0.1729	0.0049	0.57475	55.84556824
FF02_126	5.28	0.35	0.235	0.016	0.94354	54.88051843
FF01_95	1.98	0.14	0.1433	0.0085	0.96931	53.77888819
FF02_81	4.21	0.17	0.2083	0.0068	0.86257	53.31010453
FF02_89	2.085	0.092	0.1457	0.005	0.84662	52.2673031
FF02_72	4.89	0.18	0.2166	0.0063	0.39534	51.34037368
FF02_104	4.63	0.25	0.2123	0.011	0.77208	50.53061224
FF02_54	5.53	0.2	0.2179	0.0061	0.28822	47.4076837
FF02_10	3.262	0.12	0.1724	0.0048	0.67848	46.73962608
FF02_94	4.31	0.2	0.1867	0.0062	0.64926	44.19070513
FF02_44	9.92	0.41	0.2549	0.0086	0.62765	43.77618193
FF02_71	7.12	0.25	0.2271	0.0067	0.7154	43.64659166
~~FF02_134~~	~~7.48~~	~~0.29~~	~~0.2263~~	~~0.0063~~	~~0.083154~~	~~42.62560778~~
FF02_135	4.06	0.16	0.1772	0.0082	0.91003	41.89189189
FF02_70	3.361	0.14	0.1499	0.0058	0.73135	36.11892326

REE DATA (STANDARDIZED TO CHONDRITE VALUES)

Analysis Name	La	Ce	Pr	Nd	Sm	Eu	Gd	Tb	Dy	Ho	Er	Tm	Yb	Lu
Z_FF01_12	53.12236	290.8497	310.5263	401.9272	627.451	340.6897	688.5645	801.0695	1037.402	1286.219	1680.967	2003.922	2629.412	3181.102
Z_FF01_14	38.39662	232.0261	211.5789	278.3726	475.1634	270.6897	554.7445	655.0802	811.0236	918.7279	1135.952	1286.275	1629.412	1850.394
Z_FF01_15	106.7511	157.6797	116	134.0471	136.6013	70.86207	156.2044	203.2086	293.7008	440.2827	659.8187	869.8039	1274.706	1681.102
Z_FF01_16	8.691983	44.44444	14.73684	19.05782	29.47712	13.48276	65.69343	98.93048	158.2677	244.6996	381.2689	500	714.7059	946.063
Z_FF01_19	459.9156	593.1373	457.8947	522.4839	988.2353	625.8621	1168.37	1556.15	1874.016	2021.201	2513.595	2980.392	3882.353	4574.803
Z_FF01_2	24.21941	127.6144	135.7895	176.6595	266.6667	145	316.3017	432.8877	635.0394	878.0919	1233.837	1563.529	2007.647	2444.882
Z_FF01_21	119.4093	704.2484	691.5789	914.3469	1307.19	770.6897	1333.333	1521.39	1850.394	2261.484	2858.006	3278.431	3923.529	4185.039
Z_FF01_23	24.38819	127.2876	143.1579	185.2248	290.1961	128.1034	448.6618	597.861	847.2441	1167.845	1536.556	1757.647	2257.059	2673.228
Z_FF01_24	9.915612	73.03922	52.84211	73.8758	128.1046	74.48276	156.2044	201.6043	268.1102	379.8587	613.8973	1044.706	1711.765	2244.094
Z_FF01_25	21.77215	107.6797	124.9474	167.4518	302.6144	175.6897	388.3212	500.8021	616.9291	690.8127	816.9184	902.3529	1081.765	1212.598
Z_FF01_27	4.978903	46.89542	29.26316	38.5439	70.58824	37.24138	115.8151	170.8556	260.2362	377.0318	554.0785	709.0196	978.2353	1212.992
Z_FF01_28	22.02532	128.9216	126.3158	174.7323	342.4837	181.8966	516.3017	778.0749	1259.843	1938.163	2888.218	3482.353	4400	5051.181
Z_FF01_32	9.620253	55.06536	59.47368	85.43897	161.4379	80.17241	272.5061	408.2888	668.1102	1053.004	1607.251	2015.686	2847.059	3629.921
Z_FF01_33	41.77215	49.5098	34.73684	35.11777	39.86928	7.172414	81.26521	120.0535	200	313.9576	461.6314	584.7059	815.2941	1052.362
Z_FF01_34	40.50633	204.7386	206.8421	265.0964	401.9608	233.7931	509.4891	617.6471	818.8976	1051.237	1390.332	1639.216	2112.353	2555.118
Z_FF01_35	5.991561	42.81046	36.21053	46.25268	83.66013	43.62069	147.4453	212.2995	355.1181	542.4028	800	996.0784	1388.235	1755.906
Z_FF01_37	102.5316	102.9412	63.15789	66.59529	95.42484	35.34483	212.6521	333.1551	544.8819	793.2862	1137.764	1399.608	1842.353	2251.969
Z_FF01_38	156.5401	799.0196	850.5263	1098.501	1640.523	934.4828	1630.17	1780.749	2059.055	2243.816	2610.272	2866.667	3476.471	3826.772
Z_FF01_4	0.924051	25.4902	5.473684	7.601713	23.13725	8.448276	70.3163	118.984	208.2677	348.5866	534.139	678.4314	948.8235	1220.472

Z_FF01_46	26.58228	83.16993	71.57895	98.92934	162.0915	77.93103	234.0633	316.8449	474.4094	681.9788	984.8943	1226.275	1669.412	2114.173
Z_FF01_47	64.13502	357.8431	391.5789	516.06	823.5294	451.7241	856.4477	1013.369	1244.094	1413.428	1740.181	1976.471	2417.647	2732.283
Z_FF01_52	66.24473	295.7516	367.3684	449.6788	614.3791	296.5517	700.7299	868.984	1149.606	1530.035	2048.338	2494.118	3223.529	3830.709
Z_FF01_53	18.77637	95.26144	113.3684	151.8201	297.3856	166.5517	363.017	446.5241	543.3071	613.0742	782.4773	964.7059	1341.176	1661.417
Z_FF01_55	0.274262	14.54248	0.715789	1.905782	10.65359	8.655172	38.24818	67.94118	124.685	231.2721	427.7946	649.0196	1095.882	1728.346
Z_FF01_61	143.4599	866.0131	930.5263	1271.949	2437.908	1506.897	3007.299	3860.963	4535.433	4607.774	5075.529	5513.725	6305.882	6602.362
Z_FF01_62	33.96624	197.7124	176.2105	236.8308	415.6863	227.2414	508.0292	653.7433	883.4646	1180.212	1770.393	2498.039	3917.647	5444.882
Z_FF01_63	3.248945	22.71242	17.89474	38.97216	118.3007	33.10345	327.4939	512.0321	835.8268	1272.085	1745.015	2117.647	2723.529	3318.898
Z_FF01_66	4.978903	47.85948	26.31579	37.04497	65.94771	26.03448	117.2749	199.1979	350.3937	594.3463	952.2659	1305.882	1885.294	2444.882
Z_FF01_68	46.83544	251.634	267.3684	361.8844	592.1569	327.5862	696.3504	871.6578	1175.197	1427.562	1879.758	2250.98	2864.706	3322.835
Z_FF01_7	0.240506	32.4183	4.894737	15.13919	60.06536	30	177.6156	270.3209	437.7953	681.2721	1018.127	1306.667	1823.529	2366.142
Z_FF01_74	54.00844	258.1699	293.6842	361.8844	514.3791	274.1379	583.9416	660.4278	834.6457	973.4982	1214.502	1360.784	1705.882	2023.622
Z_FF01_75	35.44304	223.8562	222.1053	291.2206	443.1373	248.2759	467.1533	542.7807	677.1654	805.6537	1027.19	1215.686	1576.471	1862.205
Z_FF01_77	34.13502	155.719	147.0526	198.2869	330.719	185.6897	467.1533	597.861	833.0709	1118.375	1475.529	1745.098	2247.059	2700.787
Z_FF01_8	11.35021	69.11765	52.10526	68.09422	118.9542	63.7931	151.8248	195.4545	270.4724	364.1343	524.4713	679.2157	980	1263.78
Z_FF01_80	26.79325	128.7582	154.7368	203.212	323.5294	168.9655	394.1606	481.2834	627.5591	703.1802	841.6918	956.8627	1150.588	1342.52
Z_FF01_81	47.25738	248.366	277.8947	364.0257	547.7124	306.8966	540.146	585.5615	673.2283	720.8481	791.5408	823.5294	947.0588	972.4409
Z_FF01_82	59.91561	204.2484	206.3158	270.8779	462.7451	237.7586	639.9027	895.7219	1263.78	1701.413	2364.955	2800	3605.882	4200.787
Z_FF01_83	56.11814	121.8954	111.5789	146.6809	194.7712	103.4483	226.764	282.8877	395.6693	535.3357	755.287	974.5098	1351.765	1716.535
Z_FF01_86	262.4473	1519.608	1693.684	2413.276	4509.804	2765.517	5386.861	6978.61	7937.008	7685.512	8078.55	8313.725	9217.647	8677.165
Z_FF01_88	35.99156	180.8824	200	271.5203	473.2026	252.7586	555.2311	671.3904	862.9921	1056.537	1365.559	1592.157	2043.529	2354.331
Z_FF01_89	40.33755	187.7451	207.3684	301.9272	548.366	298.2759	704.1363	871.6578	1102.362	1197.88	1376.435	1443.137	1673.529	1834.646
Z_FF01_9	7.383966	45.91503	44.21053	62.52677	112.4183	57.41379	124.5742	165.7754	194.8819	226.1484	300.9063	361.9608	488.8235	610.2362
Z_FF01_92	10.16878	98.36601	71.78947	114.7752	263.3987	166.5517	384.9148	487.1658	646.8504	839.2226	1126.888	1394.51	1865.882	2318.898
Z_FF02_101	91.81435	699.35	771.5789	946.467	699.346	370.52	604.38	730.48	955.51	1183.75	1526.3	1776.47	2193.5	2476.4
Z_FF02_105	11.56118	85.458	80.73684	97.4304	81.3072	47.414	99.4647	134.76	200.79	291.166	419.34	544.314	766.47	1012.2
Z_FF02_106	1.565401	61.879	19.66316	47.9657	138.562	79.138	254.988	273.53	312.99	353.004	414.5	459.608	571.18	677.95
Z_FF02_108	2.067511	21.405	19.78947	25.9101	35.0327	15	84.1849	124.06	198.82	303.887	441.09	557.255	779.41	1006.7
Z_FF02_112	39.66245	218.95	327.3684	413.276	307.19	148.28	248.175	358.29	503.94	651.943	876.13	1105.88	1494.1	1826.8
Z_FF02_119	67.1308	410.13	553.6842	668.094	515.033	255.69	508.029	668.45	933.07	1208.48	1655.6	1968.63	2570.6	3019.7
Z_FF02_120	43.88186	349.67	414.7368	494.647	424.837	189.66	462.287	676.47	1003.9	1415.19	2048.3	2690.2	3705.9	4409.4
Z_FF02_123	6.329114	60.784	55.36842	73.8758	107.19	51.379	218.005	335.83	538.58	823.322	1181.9	1439.22	1901.8	2397.6
Z_FF02_124	43.45992	292.48	377.8947	479.657	418.954	218.97	452.068	598.93	787.4	1010.6	1335.3	1607.84	2105.9	2527.6
Z_FF02_132	2.447257	24.902	17.36842	22.0343	28.7582	10.776	65.0122	117.11	208.66	340.283	544.41	720.392	1015.3	1303.1
Z_FF02_15	38.52321	253.27	301.0526	357.602	300	158.28	300.243	397.06	537.8	708.481	980.06	1266.67	1826.5	2460.6
Z_FF02_16	237.9747	1535.9	1957.895	2366.17	2333.33	1387.9	2335.77	3128.3	3787.4	4116.61	4628.4	5050.98	5829.4	5566.9
Z_FF02_19	68.35443	534.31	587.3684	687.366	490.196	277.59	433.09	553.48	767.72	962.898	1317.2	1537.25	2005.9	2444.9
Z_FF02_22	28.90295	205.88	254.7368	299.786	250.327	126.72	286.618	427.81	625.59	909.894	1296.7	1596.08	2123.5	2641.7
Z_FF02_23	271.308	2186.3	2284.211	2700.21	2137.25	1160.3	1766.42	2240.6	2874	3344.52	4090.6	4729.41	5852.9	6381.9
Z_FF02_34	116.4557	823.53	968.4211	1171.31	869.281	444.83	715.328	911.76	1137.8	1356.89	1685.8	1956.86	2394.1	2712.6
Z_FF02_39	125.3165	759.8	911.5789	1115.63	866.013	413.79	825.791	1098.9	1492.1	1931.1	2444.7	2870.59	3576.5	3992.1
Z_FF02_48	85.65401	625.82	706.3158	845.824	633.987	337.93	545.012	705.88	921.26	1123.67	1462.2	1717.65	2129.4	2433.1
Z_FF02_51	107.173	671.57	910.5263	1098.5	836.601	381.03	784.428	983.96	1263.8	1531.8	1981.9	2282.35	2800	3169.3
Z_FF02_52	78.90295	328.43	387.3684	464.668	359.477	175.86	335.766	417.11	574.8	734.982	960.73	1125.49	1476.5	1633.9
Z_FF02_55	149.789	1258.2	1305.263	1584.58	1254.9	665.52	1094.89	1328.9	1692.9	1961.13	2410.9	2686.27	3276.5	3543.3
Z_FF02_61	61.18143	220.59	225.2632	261.242	205.229	101.21	190.754	256.68	359.45	491.166	743.81	996.471	1450.6	2003.9
Z_FF02_65	68.35443	416.67	542.1053	629.55	488.889	224.14	503.163	663.1	948.03	1302.12	1774	2145.1	2735.3	3315
Z_FF02_66	43.03797	305.56	364.2105	441.113	343.137	177.93	344.526	443.85	622.05	842.756	1111.8	1345.1	1717.6	2039.4
Z_FF02_69	70.88608	553.92	567.3684	713.062	550.98	296.55	523.601	705.88	1003.9	1340.99	1770.4	2133.33	2558.8	2866.1
Z_FF02_73	69.62025	429.74	611.5789	762.313	576.471	272.41	530.414	673.8	905.51	1091.87	1395.8	1588.24	1982.4	2189
Z_FF02_79	109.7046	746.73	901.0526	1083.51	777.778	406.9	701.703	895.72	1161.4	1469.96	1909.4	2223.53	2758.8	3220.5
Z_FF02_83	21.94093	156.37	186.3158	223.34	177.124	87.759	199.027	279.41	410.63	572.438	761.93	933.725	1218.8	1468.5
Z_FF02_84	222.3629	1462.4	1863.158	2291.22	1830.07	922.41	1678.83	2125.7	2744.1	3293.29	4126.9	4984.31	6300	7291.3
Z_FF02_87	0.506329	33.595	4.842105	8.07281	12.549	9.5862	30.7543	49.332	84.685	144.346	244.53	356.471	580.59	867.32

EPSILON HF DATA

Sample N	Hf176/Hf177	2 S.E.	Lu176/Hf177	U/Pb AGE

DS_FF01_02	0.281599539	2.87176E-05	0.001187174	1969
DS_FF01_03	0.281267691	3.1286E-05	0.000744841	2485
DS_FF01_04	0.281495937	2.42577E-05	0.000706687	1810
DS_FF01_06	0.281634978	2.79254E-05	0.000485192	1925
DS_FF01_07	0.281333766	2.81169E-05	0.000917698	2480
DS_FF01_08	0.281205862	1.91518E-05	0.000396302	2578
DS_FF01_09	0.281555805	2.43187E-05	0.000673792	1916
DS_FF01_12	0.281323952	3.85645E-05	0.00153561	1816
DS_FF01_14	0.281494627	2.27729E-05	0.000658424	2103
DS_FF01_15	0.281491211	2.78724E-05	0.000849636	1985
DS_FF01_16	0.281589578	2.33797E-05	0.000622688	2285
DS_FF01_19	0.281051521	3.85031E-05	0.001675338	1873
DS_FF01_21	0.28127634	2.71916E-05	0.000629175	2089
DS_FF01_23	0.281519655	2.86371E-05	0.001238564	2896
DS_FF01_24	0.280846167	2.71805E-05	0.000972226	1854
DS_FF01_25	0.281505696	3.86862E-05	0.000598728	1918
DS_FF01_26	0.281522832	2.2943E-05	0.000319262	1881
DS_FF01_27	0.281566014	2.66414E-05	0.0008153	2237
DS_FF01_28	0.281324086	4.07272E-05	0.001744218	1933
DS_FF01_30	0.278325757	0.001997773	0.003705813	1882
DS_FF01_31	0.281516602	3.39851E-05	0.001289317	1954
DS_FF01_32	0.281514075	3.1185E-05	0.001481728	2123
DS_FF01_33	0.281536958	3.04704E-05	0.001040953	1855
DS_FF01_35	0.281527819	2.40397E-05	0.000896429	1928
DS_FF01_37	0.281625091	2.3857E-05	0.000631898	2608
DS_FF01_38	0.281192323	3.16512E-05	0.001454443	1701
DS_FF01_40	0.28168907	6.78015E-05	0.002142435	1883
DS_FF01_42	0.28149603	2.50167E-05	0.000715765	1858
DS_FF01_47	0.281456439	2.84992E-05	0.000996414	1922
DS_FF01_49	0.28160291	2.95438E-05	0.001105789	1741
DS_FF01_52	0.281460997	4.17278E-05	0.001729561	1741
DS_FF01_53	0.281651714	2.39783E-05	0.000584667	2154
DS_FF01_54	0.281589907	2.34046E-05	0.000440749	1923
DS_FF01_55	0.281565611	2.94828E-05	0.000950555	1968
DS_FF01_57	0.281589059	2.72127E-05	0.0003321	1846
DS_FF01_61	0.281515382	7.13692E-05	0.002977609	2187
DS_FF01_63	0.281426091	3.79987E-05	0.001526944	1996
DS_FF01_64	0.281480338	1.76922E-05	3.20341E-05	1652

DS_FF01_66	0.281802746	2.96658E-05	0.001124563	1778
DS_FF01_74	0.281517728	2.77136E-05	0.000673136	2071
DS_FF01_75	0.281403443	3.08354E-05	0.000677742	2582
DS_FF01_76	0.281584424	2.53964E-05	0.000632234	1973
DS_FF01_77	0.281058007	2.54224E-05	0.00110177	1735
DS_FF01_80	0.281570227	2.38137E-05	0.000633083	1927
DS_FF01_81	0.281513796	2.75941E-05	0.000508849	1855
DS_FF01_82	0.281559366	3.34086E-05	0.001007471	1960
DS_FF01_88	0.281532192	7.0112E-05	0.00102973	1737
DS_FF01_89	0.281511035	3.45684E-05	0.001181506	1765
DS_FF01_92	0.281495479	2.54159E-05	0.000801527	1673

DS_FF02_101	0.28155693	2.37982E-05	0.000707002	1997
DS_FF02_105	0.281181614	2.48909E-05	0.000683476	1910
DS_FF02_106	0.281587426	2.73401E-05	0.000724713	1904
DS_FF02_108	0.281465295	2.23669E-05	0.000526693	2014
DS_FF02_112	0.281010921	4.56178E-05	0.000850505	1854
DS_FF02_119	0.281583957	3.7473E-05	0.001507573	1917
DS_FF02_120	0.281583957	3.7473E-05	0.001507573	1880
DS_FF02_122	0.281564901	3.64716E-05	0.00175787	1917
DS_FF02_123	0.281503307	3.52241E-05	0.001119522	1877
DS_FF02_124	0.281493875	3.02446E-05	0.001084375	2028
DS_FF02_132	0.281596397	2.15986E-05	0.000486442	1723
DS_FF02_15	0.2812245	3.87E-05	0.00161566	2136
DS_FF02_16	0.281622832	9.09751E-05	0.004096296	1833
DS_FF02_17	0.281489979	2.55831E-05	0.000813461	1832
DS_FF02_19	0.281525801	3.56983E-05	0.001688126	1761
DS_FF02_22	0.281470296	3.12669E-05	0.000787804	1758

DS_FF02_23	0.281259569	2.75945E-05	0.001167799	2479
DS_FF02_25	0.281179236	2.77409E-05	0.000801853	2042
DS_FF02_28	0.281668588	2.61907E-05	0.000897504	2523
DS_FF02_29	0.281617927	3.406E-05	0.001616407	2471
DS_FF02_34	0.281480305	1.89554E-05	0.000491038	1994
DS_FF02_39	0.281611969	3.06854E-05	0.001310699	2507
DS_FF02_41	0.281320277	5.32201E-05	0.002705513	1883
DS_FF02_48	0.28146091	3.55286E-05	0.001145038	1839
DS_FF02_51	0.281450163	2.7199E-05	0.000802565	1904
DS_FF02_52	0.281482534	2.64096E-05	0.0007282	1836
DS_FF02_55	0.281523198	2.50971E-05	0.000340563	1999
DS_FF02_61	0.281340535	2.7602E-05	0.001049452	2523
DS_FF02_65	0.281426844	9.23932E-05	0.001025319	2023
DS_FF02_66	0.281476143	2.74781E-05	0.000962556	1779
DS_FF02_68	0.281638321	3.77785E-05	0.001729962	1866
DS_FF02_69	0.2816069	3.36016E-05	0.001971009	2488
DS_FF02_73	0.281623378	2.77185E-05	0.000780167	1912
DS_FF02_79	0.281593833	2.67026E-05	0.000948766	1614
DS_FF02_83	0.281613132	3.83939E-05	0.001438738	2533
DS_FF02_87	0.28157587	2.09876E-05	0.000503862	2099

Carbonate Geochemistry Data

LEACH 1

		La		Ce		Pr		Nd		Sm		Eu		Gd		Tb		Dy		Y		Ho		Er		Tm		Yb		Lu	
Depth (m)	Sample	ppm	SN	ppm	SN	ppm	SN	ppm	SN	ppm	SN	ppm	SN	ppm	SN	ppm	SN	ppm	SN	ppm	SN	ppm	SN	ppm	SN	ppm	SN	ppm	SN	ppm	SN
252.5	BR01-1	8.226496	0.216487	27.4949	0.343686	1.770298	0.19891	7.212042	0.225376	1.992103	0.355733	0.535365	0.486714	2.711781	0.576975	0.398762	0.517873	2.219107	0.504343	18.15066	0.648238	0.425317	0.425317	1.094876	0.377543	0.137307	0.274615	0.860214	0.307219	0.128716	0.257432
310	BR03-1	3.917274	0.103086	10.67245	0.133406	1.406596	0.158269	7.10096	0.221905	2.936581	0.524747	0.734773	0.667975	4.068039	0.86554	0.540436	0.701865	2.54639	0.578725	15.33842	0.547801	0.412825	0.412825	0.958217	0.33042	0.107746	0.215492	0.586377	0.20942	0.083695	0.16739
312.9	BR04-1	3.184852	0.083612	8.650833	0.108135	1.066985	0.119886	4.96244	0.155701	1.610421	0.287575	0.364045	0.33095	1.894953	0.403182	0.256785	0.333487	1.292998	0.293863	8.058007	0.287786	0.235988	0.235988	0.585233	0.201804	0.073032	0.146064	0.430272	0.153669	0.063068	0.126135
321.05	BR05-1	5.105449	0.134354	13.66862	0.170858	1.698616	0.190856	8.079151	0.252473	2.620777	0.467996	0.598587	0.54417	2.916763	0.620588	0.42805	0.555909	2.293467	0.521243	12.74196	0.45507	0.411853	0.411853	1.080369	0.372541	0.139398	0.278796	0.80369	0.287032	0.124972	0.249944
325.38	BR06-1	4.399911	0.115787	10.20293	0.127537	1.227596	0.137932	5.771274	0.180352	1.970147	0.351812	0.436939	0.397217	2.197121	0.467473	0.299309	0.388713	1.534551	0.348762	9.198475	0.328517	0.276066	0.276066	0.693636	0.239185	0.08291	0.16582	0.481261	0.171879	0.073023	0.146047
328.1	BR07-1	9.284309	0.244324	24.74563	0.30932	3.328372	0.373974	15.7024	0.4907	5.256769	0.938709	1.104784	1.004349	5.805193	1.235147	0.873996	1.13506	4.643732	1.055394	25.00919	0.893185	0.827297	0.827297	2.174052	0.749673	0.294949	0.589097	1.804095	0.64432	0.264759	0.529518
334.57	BR08-1	4.764501	0.125382	12.37189	0.154649	1.548013	0.173934	7.246151	0.226442	2.370516	0.423306	0.529903	0.48173	2.671653	0.568437	0.381516	0.495475	1.930627	0.438779	10.93703	0.390608	0.335049	0.335049	0.864708	0.296175	0.105107	0.210214	0.650339	0.232264	0.088709	0.177417
339.8	BR09-1	5.927007	0.155974	17.03829	0.212979	2.124617	0.238721	9.269636	0.289676	2.358099	0.421089	0.463905	0.421731	2.21063	0.470347	0.339973	0.441523	1.881806	0.427683	10.08065	0.360023	0.354729	0.354729	0.972253	0.33526	0.135513	0.271027	0.863851	0.308518	0.126582	0.253164
350	BR11-1	7.03338	0.185089	18.4194	0.230243	2.153229	0.241936	9.827082	0.307096	3.276843	0.585151	0.748138	0.680125	4.090179	0.870251	0.621943	0.807718	3.383718	0.769027	19.69988	0.703567	0.622554	0.622554	1.658967	0.572058	0.217545	0.435091	1.284338	0.458692	0.178361	0.356722
358.45	BR12-1	1.84521	0.048558	6.022921	0.075287	0.806421	0.090609	3.929615	0.1228	1.578186	0.281819	0.352117	0.320107	1.574402	0.334979	0.235945	0.306423	1.201018	0.272959	5.889303	0.210332	0.207397	0.207397	0.562967	0.194127	0.082967	0.165934	0.532931	0.190332	0.074263	0.148526
360.3	BR13-1	4.383235	0.115348	12.03047	0.150381	1.692224	0.190138	7.891432	0.246607	2.360328	0.421487	0.504364	0.458512	2.575983	0.548082	0.36327	0.471779	1.916314	0.435526	12.07538	0.431264	0.339037	0.339037	0.899547	0.310189	0.111276	0.222551	0.646754	0.230984	0.091415	0.18283
366	BR14-1	5.012336	0.131904	15.15534	0.189442	2.157613	0.242428	10.41336	0.325417	3.790096	0.676803	0.842948	0.766316	3.98046	0.846906	0.617593	0.802069	3.290696	0.747885	17.97143	0.641837	0.57854	0.57854	1.515035	0.522702	0.202126	0.404251	1.242829	0.443868	0.180436	0.360873
373.1	BR15-1	7.82589	0.205944	23.17364	0.28967	3.037908	0.341338	14.12429	0.441384	4.59126	0.819868	1.039476	0.944978	5.190209	1.1043	0.825063	1.071511	4.537033	1.031144	25.47044	0.909659	0.831005	0.831005	2.249836	0.775806	0.300154	0.600307	1.773031	0.633225	0.257607	0.515215
382.75	BR16-1	1.37529	0.036192	3.446143	0.043077	0.457122	0.051362	2.220159	0.06938	0.795885	0.142122	0.206493	0.187721	0.825745	0.17569	0.121008	0.157153	0.624531	0.141939	3.583322	0.127976	0.10932	0.10932	0.273779	0.094406	0.034939	0.069878	0.177424	0.063366	0.025354	0.050709
482.2	BR17-1	0.261488	0.006881	1.023282	0.012791	0.173054	0.019444	0.911811	0.028494	0.233968	0.041784	0.072547	0.065952	0.211308	0.044959	0.03366	0.043715	0.195942	0.044532	1.103063	0.039396	0.034424	0.034424	0.092562	0.031918	0.01018	0.02036	0.069685	0.024887	0.010344	0.020687
486.75	BR18-1	0.391575	0.010305	1.098354	0.013729	0.179498	0.020168	0.868377	0.027137	0.224006	0.040001	0.050499	0.045908	0.222911	0.047428	0.032781	0.042573	0.164799	0.037454	1.090177	0.038935	0.031453	0.031453	0.084557	0.029158	0.011627	0.023254	0.056326	0.020116	0.010151	0.020301
489.7	BR19-1	1.721535	0.045304	4.892299	0.061154	0.67821	0.076203	3.167065	0.098971	1.120898	0.20016	0.207192	0.188356	1.0611	0.225766	0.159729	0.20744	0.879125	0.199801	4.77741	0.170622	0.157963	0.157963	0.40729	0.140445	0.053763	0.107526	0.323462	0.115522	0.046366	0.092733
505.6	BR20-1	0.650184	0.01711	1.488845	0.018611	0.270266	0.030367	1.370134	0.042817	0.316831	0.056577	0.061324	0.05575	0.339082	0.072145	0.051044	0.066291	0.34058	0.077405	3.054926	0.109104	0.073629	0.073629	0.217448	0.074982	0.028598	0.057196	0.181014	0.064648	0.026084	0.052168
511.38	BR21-1	4.410188	0.116058	12.02965	0.150371	1.552263	0.174412	7.326281	0.228946	2.22918	0.398068	0.44056	0.400509	2.179757	0.463778	0.323707	0.420398	1.744679	0.396518	9.671067	0.345395	0.316802	0.316802	0.812486	0.280167	0.102801	0.205603	0.59038	0.21085	0.081105	0.16221
514.7	BR22-1	0.61226	0.016112	1.325052	0.016563	0.243587	0.027369	1.076449	0.033639	0.220926	0.039451	0.047236	0.042941	0.245753	0.052288	0.034365	0.04463	0.234332	0.053257	2.112629	0.075451	0.052264	0.052264	0.161794	0.055791	0.020719	0.041438	0.133351	0.047625	0.022231	0.044462
520.85	BR23-1	0.691094	0.018187	1.549397	0.019367	0.265627	0.029846	1.130396	0.035325	0.224065	0.040012	0.047857	0.043507	0.247368	0.052631	0.03886	0.050468	0.228418	0.051913	2.335102	0.083396	0.052721	0.052721	0.148374	0.051164	0.020364	0.040728	0.106663	0.038094	0.016878	0.033756
535.25	BR26-1	0.541396	0.014247	1.62506	0.020313	0.231637	0.026027	0.893633	0.027926	0.174643	0.031186	0.029324	0.026658	0.169926	0.036154	0.023801	0.03091	0.147109	0.033434	0.954761	0.034099	0.028843	0.028843	0.071893	0.024791	0.011528	0.023056	0.065933	0.023548	0.011839	0.023677
543.75	BR28-1	0.791992	0.020842	2.33684	0.02921	0.399071	0.044839	2.041002	0.063781	0.725158	0.129492	0.118977	0.108161	0.704366	0.149865	0.115663	0.150211	0.692573	0.157403	3.952577	0.141163	0.13545	0.13545	0.35922	0.123869	0.050045	0.100089	0.340571	0.121633	0.05039	0.10078
551.37	BR29-1	0.938302	0.024692	2.636138	0.032952	0.390864	0.043917	1.704883	0.053278	0.455769	0.081387	0.098939	0.089945	0.443617	0.094387	0.071739	0.093168	0.458875	0.10429	2.695412	0.096265	0.09086	0.09086	0.236164	0.081436	0.034728	0.069456	0.215214	0.076062	0.031392	0.062784
127.07	MV18-1	0.124494	0.003276	0.458383	0.00573	0.069161	0.007771	0.312714	0.009772	0.076365	0.013637	0.015342	0.013947	0.083533	0.017773	0.012017	0.015607	0.076367	0.017356	0.383066	0.013681	0.012231	0.012231	0.034966	0.012057	0.003952	0.007905	0.02548	0.0091	0.002961	0.005923
143.4	MV34-1	0.69757	0.018357	1.987833	0.024848	0.297515	0.033429	1.376558	0.043017	0.484934	0.086595	0.092637	0.084215	0.46041	0.097959	0.071639	0.093038	0.377789	0.085861	1.962336	0.070083	0.064473	0.064473	0.162819	0.056144	0.020129	0.040258	0.119092	0.042533	0.014489	0.028978
145.4	MV35-1	0.65687	0.017286	2.075184	0.02594	0.296909	0.03337	1.374435	0.042951	0.418658	0.07476	0.071548	0.065044	0.380602	0.080979	0.056057	0.072801	0.312299	0.070977	1.679532	0.059983	0.053487	0.053487	0.137341	0.047359	0.018773	0.037547	0.106724	0.038116	0.016368	0.032736
146	MV36-1	0.252008	0.006632	0.890243	0.011128	0.171294	0.019247	0.918276	0.028696	0.301828	0.053898	0.055616	0.05056	0.28791	0.061258	0.037476	0.04867	0.182847	0.041556	1.135648	0.040559	0.028297	0.028297	0.071751	0.024742	0.00708	0.01416	0.036065	0.01288	0.005728	0.011456
152.2	MV37-1	0.28898	0.007605	0.925628	0.01157	0.163425	0.018362	0.789395	0.024669	0.230907	0.041233	0.036799	0.033453	0.208874	0.044441	0.029485	0.038292	0.152608	0.034684	0.861543	0.030769	0.027654	0.027654	0.063915	0.02204	0.006984	0.013967	0.037695	0.013462	0.005291	0.010583
153.05	MV38-1	0.077921	0.002051	0.252631	0.003158	0.038744	0.004353	0.186442	0.005826	0.05466	0.009761	0.00999	0.009082	0.050796	0.010808	0.008366	0.010865	0.041793	0.009499	0.241166	0.008613	0.007862	0.007862	0.018806	0.006485	0.002158	0.004316	0.013098	0.004678	0.001284	0.002568

LEACH 2

		La		Ce		Pr		Nd		Sm		Eu		Gd		Tb		Dy		Y		Ho		Er		Tm		Yb		Lu	
Depth (m)	Sample	ppm	SN	ppm	SN	ppm	SN	ppm	SN	ppm	SN	ppm	SN	ppm	SN	ppm	SN	ppm	SN	ppm	SN	ppm	SN	ppm	SN	ppm	SN	ppm	SN	ppm	SN
252.5	BR01-2	1.935414	0.050932	7.135945	0.089199	0.427028	0.047981	1.703019	0.053219	0.4849	0.086589	0.118398	0.107634	0.630111	0.134066	0.091251	0.118507	0.50631	0.11507	4.222931	0.150819	0.094737	0.094737	0.256071	0.0883	0.032735	0.065469	0.211179	0.075421	0.028454	0.056909
310	BR03-2	1.827696	0.048097	5.309193	0.066365	0.656204	0.073731	2.914819	0.091088	1.032561	0.184386	0.246374	0.223977	1.271126	0.270452	0.183732	0.238613	0.907262	0.206196	5.123255	0.182973	0.1526	0.1526	0.376546	0.129844	0.043456	0.096911	0.240306	0.065824	0.03436	0.068761
312.9	BR04-2	2.396349	0.063062	7.053006	0.088163	0.774237	0.086993	3.293141	0.102911	0.963151	0.171991	0.210193	0.191084	1.077239	0.2292	0.152601	0.198183	0.81805	0.18592	4.687436	0.167408	0.142496	0.142496	0.363825	0.125457	0.049274	0.096546	0.296036	0.105727	0.039722	0.079444
321.05	BR05-2	3.377701	0.088887	9.940689	0.124259	1.133662	0.127378	4.942439	0.154451	1.466852	0.261938	0.334425	0.304023	1.59587	0.339547	0.258948	0.336297	1.395482	0.317155	7.280804	0.260029	0.253201	0.253201	0.688337	0.237358	0.096772	0.193544	0.577112	0.206111	0.079131	0.158262
325.38	BR06-2	0.387948	0.010209	0.906154	0.011327	0.103528	0.011632	0.442756	0.013836	0.139901	0.024982	0.030169	0.027426	0.151061	0.032141	0.021972	0.028535	0.11805	0.02683	0.668776	0.023885	0.020228	0.020228	0.053164	0.018333	0.007063	0.014126	0.040218	0.014364	0.005859	0.011719
328.1	BR07-2	2.629247	0.069191	7.715795	0.096447	0.942347	0.105882	3.993707	0.124803	1.304862	0.233011	0.267764	0.243422	1.348481	0.286911	0.213017	0.276645	1.163567	0.264447	6.003939	0.214426	0.206415	0.206415	0.547484	0.188788	0.073952	0.147904	0.472107	0.16861	0.064574	0.129147
334.57	BR08-2	2.391793	0.062942	6.338477	0.079231	0.742083	0.08338	3.153729	0.098554	0.912068	0.162873	0.206693	0.189721	1.007019	0.214259	0.150298	0.195192	0.796285	0.180974	4.472821	0.159744	0.144311	0.144311	0.382502	0.131897	0.049689	0.099377	0.294273	0.105097	0.039931	0.079863
339.8	BR09-2	0.130324	0.00343	0.358511	0.004481	0.040465	0.004547	0.182841	0.005714	0.040302	0.007197	0.00744	0.006784	0.038344	0.008158	0.005703	0.007407	0.034108	0.007752	0.186818	0.005958	0.006154	0.006154	0.018567	0.006402	0.003053	0.006106	0.015873	0.005669	0.001506	0.003012
350	BR11-2	2.563886	0.067471	6.882299	0.086029	0.755523	0.08489	3.231999	0.101	0.970833	0.173363	0.231936	0.210851	1.187971	0.25276	0.192071	0.249443	1.06077	0.241084	6.334504	0.226232	0.200241	0.200241	0.556489	0.191893	0.071503	0.143006	0.446811	0.159575	0.058858	0.117717
358.45	BR12-2	0.450547	0.011856	1.83219	0.022902	0.336564	0.037816	2.233688	0.069803	1.203247	0.214865	0.273316	0.24847	1.238425	0.263495	0.129743	0.168498	0.486811	0.110639	1.657321	0.05919	0.067265	0.067265	0.145896	0.050309	0.016959	0.033918	0.096645	0.034516	0.013955	0.027911
360.3	BR13-2	0.774162	0.020373	2.294431	0.02866	0.297014	0.033372	1.333545	0.041673	0.377393	0.067392	0.078543	0.071402	0.405486	0.086274	0.05967	0.077493	0.319127	0.072529	1.884009	0.067286	0.058272	0.058272	0.144567	0.048651	0.020099	0.041796	0.117606	0.042002	0.016214	0.032428
366	BR14-2	0.691947	0.018209	2.081889	0.026024	0.272862	0.030659	1.364391	0.042637	0.459869	0.082119	0.090233	0.08203	0.460079	0.097889	0.065791	0.085442	0.347586	0.078997	1.786002	0.063786	0.05839	0.05839	0.156433	0.053942	0.021174	0.042347	0.125402	0.044786	0.016193	0.032387
373.1	BR15-2	2.164416	0.056958	6.27022	0.078378	0.808215	0.090811	3.611235	0.112851	1.149632	0.205291	0.265735	0.241577	1.228711	0.261428	0.203518	0.26431	1.123526	0.255347	6.2575	0.223482	0.207254	0.207254	0.564029	0.194493	0.073444	0.146889	0.456714	0.163112	0.068859	0.137719
382.75	BR16-2	0.910831	0.023969	2.22527	0.027816	0.285456	0.032074	1.383582	0.043237	0.484456	0.08651	0.125866	0.114424	0.488165	0.103065	0.071295	0.092592	0.371916	0.084526	2.140876	0.07646	0.064983	0.064983	0.161462	0.055677	0.020213	0.040426	0.111654	0.039877	0.017465	0.03493
482.2	BR17-2	0.122058	0.003212	0.46687	0.005861	0.07081	0.007956	0.348964	0.010905	0.092998	0.016607	0.042334	0.036485	0.093675	0.020995	0.015218	0.019764	0.0882	0.020046	0.543585	0.019414	0.016804	0.016804	0.043506	0.015002	0.006016	0.012032	0.035751	0.012768	0.005058	0.010116
486.75	BR18-2	0.062028	0.002159	0.245759	0.003072	0.040089	0.004504	0.198052	0.006189	0.045407	0.008108	0.007513	0.00683	0.057916	0.012323	0.008458	0.010985	0.04516	0.010264	0.2686	0.009593	0.00875	0.00875	0.020722	0.007145	0.002462	0.004924	0.01597	0.005704	0.00195	0.003899
489.7	BR19-2	0.64353	0.016935	1.94489	0.024311	0.245446	0.027578	1.068814	0.034025	0.448655	0.080117	0.09562	0.087109	0.477485	0.101593	0.061191	0.105443	0.437514	0.099435	2.242473	0.080068	0.078158	0.078158	0.211104	0.072795	0.026603	0.053206	0.178529	0.06376	0.02287	0.045741
505.6	BR20-2	0.577831	0.015206	1.169782	0.014622	0.219648	0.02468	1.053734	0.032929	0.247627	0.044219	0.055512	0.050465	0.315563	0.067141	0.048609	0.063129	0.332065	0.075469	3.020659	0.107881	0.073174	0.073174	0.233274	0.080439	0.030626	0.061252	0.195432	0.069797	0.029871	0.059741
511.38	BR21-2	1.25467	0.033018	3.544747	0.044309	0.414429	0.046565	1.92127	0.06004	0.578246	0.103258	0.111636	0.101487	0.567702	0.120788	0.083734	0.108745	0.469066	0.106606	2.590118	0.092504	0.089359	0.089359	0.242954	0.083777	0.031143	0.062285	0.194595	0.069498	0.025287	0.050575
514.7	BR22-2	0.288213	0.007585	0.6036	0.007545	0.110945	0.012466	0.508307	0.015885	0.111043	0.019829	0.023855	0.021686	0.124859	0.026566	0.020851	0.027079	0.137332	0.031212	1.158009	0.041357	0.026557	0.026557	0.0933	0.032172	0.011966	0.023933	0.069443	0.024801	0.011323	0.022647
520.85	BR23-2	0.313752	0.008257	0.722836	0.009035	0.12119	0.013617	0.54598	0.017062	0.111739	0.019953	0.024906	0.022642	0.137564	0.029269	0.022085	0.028682	0.147311	0.03348	1.237925	0.044212	0.028802	0.028802	0.082489	0.028445	0.011353	0.022705	0.058571	0.020918	0.010381	0.020763
535.25	BR26-2	0.323966	0.008525	1.015114	0.012689	0.136363	0.015322	0.581305	0.018168	0.115564	0.020636	0.021118	0.019198	0.12342	0.02626	0.018979	0.026548	0.095004	0.021592	0.628878	0.02246	0.021268	0.021268	0.054467	0.018782	0.008451	0.016903	0.05231	0.018682	0.008307	0.016615
539.1	BR27-2	0.235813	0.006206	0.691452	0.008643	0.106892	0.01201	0.453117	0.01416	0.127761	0.022814	0.021939	0.019945	0.105752	0.0225	0.018042	0.023431	0.107172	0.024357	0.683435	0.024408	0.02218	0.02218	0.059949	0.020672	0.007273	0.014545	0.043887	0.015674	0.00668	0.01336
543.75	BR28-2	0.445384	0.011721	1.304857	0.016311	0.215091	0.024167	1.111565	0.034736	0.390341	0.069704	0.075775	0.068886	0.45807	0.097462	0.079195	0.102851	0.490686	0.111519	2.854551	0.101948	0.102714	0.102714	0.292121	0.100731	0.04213	0.084259	0.261081	0.093243	0.040574	0.081148
551.37	BR29-2	0.531769	0.013994	1.570725	0.019634	0.234343	0.026331	1.077739	0.033679	0.284052	0.050724	0.064293	0.058448	0.295498	0.062872	0.044541	0.057846	0.25987	0.059061	1.523048	0.054395	0.049337	0.049337	0.13633	0.04701	0.019748	0.039496	0.118856	0.042449	0.018197	0.036394
127.07	MV18-2	0.409054	0.010765	1.589394	0.019867	0.246422	0.027913	1.200584	0.037518	0.370188	0.066105	0.053641	0.048765	0.330931	0.070411	0.046612	0.060535	0.256695	0.05834	1.330924	0.047533	0.041573	0.041573	0.107419	0.037041	0.011941	0.023881	0.068473	0.024455	0.009763	0.019526
143.4	MV34-2	0.264873	0.00697	0.748307	0.009354	0.127025	0.014273	0.674179	0.021068	0.2396	0.042766	0.04795	0.043591	0.231387	0.049231	0.034758	0.04514	0.204095	0.046385	0.917323	0.032762	0.028188	0.028188	0.069909	0.024107	0.008794	0.017588	0.047605	0.017002	0.007281	0.014563
145.4	MV35-2	0.065566	0.001725	0.243543	0.003044	0.033096	0.003719	0.15835	0.004948	0.051557	0.009207	0.009496	0.008633	0.047906	0.01021	0.007011	0.009106	0.03638	0.008268	0.185081	0.00661	0.006486	0.006486	0.014985	0.005167	0.001726	0.003451	0.011525	0.004116	0.001595	0.003189
146	MV36-2	0.090703	0.002387	0.365471	0.004568	0.074912	0.008417	0.377552	0.011798	0.131261	0.023439	0.023704	0.021549	0.116268	0.024738	0.016097	0.020905	0.077569	0.017629	0.436263	0.015581	0.011712	0.011712	0.027651	0.009535	0.00325	0.006499	0.019545	0.00698	0.002342	0.004685
152.2	MV37-2	0.062975	0.001657	0.258907	0.003236	0.051409	0.005776	0.284191	0.006881	0.086877	0.015514	0.015616	0.014197	0.068184	0.014507	0.011591	0.015053	0.061434	0.013962	0.330265	0.011795	0.009194	0.009194	0.024803	0.008553	0.002287	0.004574	0.015014	0.005362	0.00298	0.005961
153.05	MV38-2	0.03017	0.000794	0.119427	0.001493	0.019715	0.002215	0.104938	0.003279	0.036257	0.006475	0.006097	0.005543	0.029528	0.006283	0.004103	0.005329	0.023877	0.005427	0.142518	0.00509	0.005294	0.005294	0.009429	0.003251	#VALUE!	#VALUE!	0.00592	0.002114	0.000985	0.001969

LEACH 3

		La		Ce		Pr		Nd		Sm		Eu		Gd		Tb		Dy		Y		Ho		Er		Tm		Yb		Lu	
Depth (m)	Sample	ppm	SN	ppm	SN	ppm	SN	ppm	SN	ppm	SN	ppm	SN	ppm	SN	ppm	SN	ppm	SN	ppm	SN	ppm	SN	ppm	SN	ppm	SN	ppm	SN	ppm	SN
252.5	BR01-3	3.937273	0.103612	16.61605	0.207701	1.227535	0.137925	5.397766	0.17493	1.431379	0.255603	0.332135	0.301941	1.639648	0.348861	0.201501	0.26169	0.954767	0.216992	6.535639	0.233416	0.166585	0.166585	0.393372	0.135645	0.046359	0.092717	0.264327	0.094402	0.037589	0.075178
310	BR03-3	2.599717	0.068414	7.860799	0.09826	0.937971	0.10539	4.169822	0.130307	1.26181	0.225323	0.297842	0.270766	1.429961	0.304247	0.212205	0.27559	1.125238	0.255736	6.054834	0.216244	0.195718	0.195718	0.50182	0.173041	0.06292	0.12584	0.380683	0.135958	0.049259	0.098519
312.9	BR04-3	4.76321	0.125348	13.94319	0.17429	1.568479	0.176234	6.74005	0.210627	2.013132	0.359488	0.433649	0.394227	2.191567	0.466291	0.303169	0.393726	1.612478	0.366472	9.323421	0.332979	0.295412	0.295412	0.739026	0.254837	0.097762	0.195225	0.587167	0.209702	0.079387	0.158775
321.05	BR05-3	1.460551	0.038436	4.289888	0.053625	0.504664	0.056704	2.160656	0.067521	0.652157	0.116457	0.141827	0.128934	0.696954	0.148288	0.105086	0.136475	0.602971	0.137039	2.954043	0.105502	0.103675	0.103675	0.284979	0.098269	0.039173	0.078345	0.245269	0.087596	0.032357	0.064714

325.38	BR06-3	2.19368	0.057728	5.393211	0.067415	0.65009	0.073044	3.049666	0.095302	1.155291	0.206302	0.252495	0.229541	1.210739	0.257604	0.146261	0.18995	0.687914	0.156344	3.7197	0.132846	0.116193	0.116193	0.298942	0.103084	0.034462	0.068925	0.203951	0.07284	0.028583	0.057165
328.1	BR07-3	1.289036	0.033922	3.846455	0.048081	0.462727	0.051992	1.94716	0.060849	0.618344	0.110419	0.118124	0.107385	0.636245	0.135371	0.102701	0.133378	0.536228	0.12187	2.762007	0.098643	0.094857	0.094857	0.252645	0.087119	0.03488	0.069761	0.21836	0.077986	0.031606	0.063211
334.57	BR08-3	0.427924	0.011261	1.195857	0.014948	0.148402	0.016674	0.652907	0.020403	0.240754	0.042992	0.054768	0.049789	0.266816	0.056769	0.038889	0.04531	0.17624	0.040055	0.934082	0.03336	0.029991	0.029991	0.075847	0.026154	0.009425	0.01885	0.058521	0.0209	0.008037	0.016074
339.8	BR09-3	0.404144	0.010635	1.126882	0.014086	0.121484	0.01365	0.499839	0.01562	0.10139	0.018105	0.017634	0.016091	0.073562	0.015651	0.011941	0.015508	0.064374	0.01463	0.308423	0.011015	0.012296	0.012296	0.032525	0.011215	0.00422	0.008441	0.028765	0.010273	0.003844	0.007688
350	BR11-3	5.698001	0.149947	15.18966	0.189871	1.733245	0.194747	7.352969	0.22978	2.381527	0.425273	0.529499	0.481362	2.731368	0.581142	0.423339	0.549791	2.298082	0.522291	13.20623	0.471651	0.41518	0.41518	1.131678	0.390234	0.154181	0.308363	0.87991	0.314253	0.129085	0.258169
358.45	BR12-3	2.963706	0.077992	12.10162	0.15127	2.090344	0.23487	13.1294	0.410294	6.898791	1.231927	1.541704	1.401549	7.322857	1.600608	0.778236	1.010696	2.97971	0.677207	10.66825	0.381009	0.396716	0.396716	0.834437	0.287787	0.09476	0.189521	0.540689	0.193109	0.071796	0.143593
360.3	BR13-3	0.233353	0.006141	0.651913	0.008149	0.082858	0.00931	0.385971	0.012062	0.111978	0.019996	0.022348	0.020316	0.105028	0.022346	0.016531	0.021469	0.081024	0.018415	0.305756	0.018063	0.016009	0.016009	0.04226	0.014572	0.004837	0.009674	0.032842	0.011729	0.005273	0.010546
366	BR14-3	4.699509	0.123671	14.44798	0.1806	2.00317	0.225075	10.18611	0.318316	3.614386	0.645426	0.729877	0.663525	3.467028	0.737666	0.462571	0.600742	2.334063	0.530469	12.02326	0.429402	0.404917	0.404917	1.03623	0.357321	0.139951	0.279901	0.837684	0.299173	0.114314	0.228628
373.1	BR15-3	0.818683	0.021544	2.710988	0.033887	0.426548	0.047927	2.235606	0.069863	0.752954	0.134456	0.174528	0.158661	0.675297	0.14368	0.090155	0.117085	0.438532	0.099666	2.09904	0.074966	0.070813	0.070813	0.185306	0.063899	0.022319	0.044637	0.134523	0.048044	0.01874	0.037481
382.75	BR16-3	0.580939	0.015288	1.756863	0.021961	0.313525	0.035228	1.883536	0.05886	0.712915	0.127306	0.173499	0.157726	0.666813	0.141875	0.080696	0.1048	0.345361	0.078491	1.575282	0.05626	0.049587	0.049587	0.110632	0.038149	0.009543	0.019086	0.056637	0.020227	0.006268	0.012535
482.2	BR17-3	0.189945	0.004999	0.722501	0.009031	0.112436	0.012633	0.555252	0.017352	0.149756	0.026742	0.034342	0.085765	0.152463	0.032439	0.021432	0.027833	0.110208	0.025047	0.607941	0.021712	0.020124	0.020124	0.057356	0.019847	0.007327	0.014654	0.04441	0.015861	0.007045	0.01409
486.75	BR18-3	0.038109	0.001003	0.131625	0.001645	0.019382	0.002178	0.096796	0.003025	0.030872	0.005513	0.004003	0.003639	0.022593	0.004807	0.003691	0.004793	0.013274	0.003017	0.093767	0.003349	0.002986	0.002986	0.008027	0.002768	#VALUE!	#VALUE!	0.004831	0.001725	0.00065	0.0013
489.7	BR19-3	0.448402	0.0118	1.401135	0.017514	0.181059	0.020344	0.862026	0.026938	0.332176	0.059317	0.063793	0.057994	0.327198	0.069617	0.04977	0.064436	0.228084	0.065474	1.473918	0.05264	0.049769	0.049769	0.136096	0.04693	0.016371	0.032742	0.107721	0.038472	0.015192	0.030383
505.6	BR20-3	0.070479	0.001855	0.140091	0.001751	0.024819	0.002789	0.121957	0.003811	0.029911	0.005341	0.00616	0.0056	0.032402	0.006894	0.004056	0.005268	0.02448	0.005564	0.256484	0.00916	0.006122	0.006122	0.01727	0.005955	0.00221	0.00442	0.016	0.005714	0.002301	0.004601
511.38	BR21-3	1.025658	0.026991	3.055053	0.038188	0.336825	0.037846	1.474274	0.046071	0.419559	0.074921	0.085611	0.077828	0.399016	0.084897	0.063907	0.082996	0.368272	0.083698	1.980095	0.070718	0.071123	0.071123	0.192768	0.066472	0.025118	0.050236	0.159811	0.057075	0.022167	0.044334
514.7	BR22-3	1.019762	0.026836	1.811581	0.022645	0.34998	0.039324	1.587264	0.049602	0.366969	0.06553	0.076192	0.069265	0.389697	0.082914	0.059517	0.077295	0.374244	0.085055	3.540217	0.126436	0.085801	0.085801	0.255779	0.0882	0.034188	0.068375	0.222283	0.079387	0.033163	0.066326
520.85	BR23-3	0.492655	0.012965	1.052605	0.013158	0.178387	0.020044	0.805003	0.025156	0.180599	0.03225	0.036989	0.033626	0.201148	0.042797	0.02956	0.038389	0.175808	0.039956	1.78214	0.063648	0.037261	0.037261	0.108676	0.037474	0.013946	0.027891	0.081865	0.029238	0.012361	0.024722
535.25	BR26-3	3.445908	0.090682	11.04709	0.138089	1.685437	0.189375	7.269401	0.227169	1.504896	0.268731	0.266239	0.242035	1.49292	0.317643	0.203433	0.264199	1.070813	0.243367	6.194045	0.221216	0.190459	0.190459	0.463374	0.159784	0.056158	0.112316	0.328254	0.117234	0.049172	0.098344
539.1	BR27-3	0.374685	0.00986	1.063427	0.01328	0.15511	0.017428	0.677715	0.021179	0.174741	0.031204	0.031335	0.028486	0.174454	0.037118	0.028096	0.036489	0.17276	0.039264	1.087288	0.038832	0.033639	0.033639	0.095185	0.032822	0.012912	0.025824	0.080977	0.02892	0.0124	0.024799
543.75	BR28-3	0.319242	0.008401	0.920126	0.011502	0.149101	0.016753	0.767647	0.023989	0.25864	0.046186	0.051597	0.046907	0.287584	0.061188	0.046115	0.05989	0.285209	0.06482	1.635068	0.058395	0.056594	0.056594	0.161601	0.055724	0.021597	0.043195	0.148688	0.053103	0.02406	0.04812
551.37	BR29-3	1.426287	0.037534	4.059325	0.050742	0.605632	0.068049	2.695338	0.084229	0.660888	0.118016	0.143652	0.130593	0.67785	0.144223	0.102018	0.132491	0.560685	0.127428	3.302278	0.117938	0.105559	0.105559	0.286121	0.098663	0.036406	0.072812	0.233787	0.083496	0.035916	0.071833

CARBON AND OXYEN ISOTOPES

Depth (m)	Sample	13C	18O
310	BR03-1	-2.49	-9.66
312.9	BR04-1	-1.92	-9.42
321.05	BR05-1	-1.77	-10.11
325.38	BR06-1	-0.94	-8.70
328.1	BR07-1	-0.72	-8.46
334.57	BR08-1	-1.94	-8.49
339.8	BR09-1	-1.06	-5.51
350	BR11-1	-1.58	-7.41
358.45	BR12-1	-2.60	-10.70
360.3	BR13-1	-3.39	-11.33
366	BR14-1	-3.23	-11.10
373.1	BR15-1	-3.50	-12.89
382.75	BR16-1	-2.03	-7.18
482.2	BR17-1	-0.49	-5.27
486.75	BR18-1	0.25	-7.43
489.7	BR19-1	0.27	-5.25
505.6	BR20-1	0.21	-8.11
511.38	BR21-1	-3.21	-11.05
514.7	BR22-1	0.69	-5.70
520.85	BR23-1	0.55	-7.13
535.25	BR26-1	0.63	-5.58
539.1	BR27-1	0.43	-5.98
543.75	BR28-1	1.26	-7.90
551.37	BR29-1	-0.27	-8.30

MAJOR ELEMENTS

LEACH 1

		Mn			Sr			Al			Zr			Ni			Sc			Zn			Fe		
Depth (m)	Sample	ppm	wt %	mol fraction	ppm	wt %	mol fraction	ppm	wt %	mol fraction	ppm	wt %	mol fraction	ppm	wt %	mol fraction	ppm	wt %	mol fraction	ppm	wt %	mol fraction	ppm	wt %	mol fraction
252.5	BR01-1	7189.599	0.71896	0.013071997	103.6384	0.010364	0.000117771	409.72	0.040972	0.001517481	0.520422	5.2E-05	5.78247E-07	0.686505	6.87E-05	1.16952E-06	6.945974	0.000695	1.54355E-05	4.080777	0.000408	6.18299E-06	3001.3	0.30013	0.005359464
310	BR03-1	1457.953	0.145795	0.002650823	41.25015	0.004125	4.68752E-05	37.32331	0.003732	0.000138234	0.009849	9.85E-07	1.09434E-08	0.166297	1.66E-05	2.83301E-07	0.284614	2.85E-05	6.32477E-07	3.624056	0.000362	5.49099E-06	2765.185	0.276518	0.00493783
312.9	BR04-1	825.938	0.082594	0.001501705	37.09166	0.003709	4.21496E-05	27.00257	0.0027	0.00010001	0.091206	9.12E-06	1.0134E-07	1.777074	0.000178	3.02738E-06	0.163625	1.64E-05	3.63611E-07	4.542475	0.000454	6.88254E-06	772.2205	0.077222	0.001378965
321.05	BR05-1	688.6328	0.068863	0.00125206	36.16697	0.003617	4.10988E-05	26.38753	0.002639	9.77316E-05	0.025373	2.54E-06	2.81919E-08	0.19291	1.93E-05	3.28638E-07	0.109944	1.1E-05	2.44319E-07	3.089228	0.000309	4.68065E-06	469.8251	0.046983	0.000838973
325.38	BR06-1	672.4025	0.06724	0.00122255	44.3201	0.004432	5.03637E-05	22.84185	0.002284	8.45994E-05	0.088735	8.87E-06	9.85942E-08	0.301512	3.02E-05	5.13649E-07	0.283103	2.83E-05	6.29118E-07	2.340655	0.000234	3.54645E-06	337.2848	0.033728	0.000602294
328.1	BR07-1	823.8135	0.082381	0.001497843	50.97976	0.005098	5.79315E-05	43.55723	0.004356	0.000161323	0.407664	4.08E-05	4.5296E-07	0.397136	3.97E-05	6.76552E-07	1.283856	0.000128	2.85301E-06	3.616587	0.000362	5.47968E-06	899.6499	0.089965	0.001606518
334.57	BR08-1	518.565	0.051856	0.000942845	41.91203	0.004191	4.76273E-05	12.38559	0.001239	4.58726E-05	0.04337	4.34E-06	4.81892E-08	0.251231	2.51E-05	4.27991E-07	0.142085	1.42E-05	3.15745E-07	4.589271	0.000459	6.95344E-06	469.8925	0.046989	0.000839094
339.8	BR09-1	639.9566	0.063996	0.001163557	30.72098	0.003072	3.49102E-05	532.5353	0.053254	0.001972353	0.102912	1.03E-05	1.14347E-07	0.402994	4.03E-05	6.86531E-07	2.379138	0.000238	5.28697E-06	4.964756	0.000496	7.52236E-06	1281.189	0.128119	0.002287838
350	BR11-1	1031.565	0.103156	0.001875572	29.36682	0.002937	3.33714E-05	50.95913	0.005096	0.000188738	0.261237	2.61E-05	2.90263E-07	0.304607	3.05E-05	5.18921E-07	1.117197	0.000112	2.48266E-06	#####	#####	#####	#####	#####	#####
358.45	BR12-1	443.7362	0.044374	0.000806793	9.719692	0.000972	1.10451E-05	538.9566	0.053896	0.001996136	0.273573	2.74E-05	3.0397E-07	0.264781	2.65E-05	4.51074E-07	0.949924	9.5E-05	2.11094E-06	#####	#####	#####	#####	#####	#####
360.3	BR13-1	689.2275	0.068923	0.001253141	29.50521	0.002951	3.35286E-05	90.94782	0.009095	0.000336844	0.045051	4.51E-06	5.00569E-08	0.217467	2.17E-05	3.70472E-07	0.390347	3.9E-05	8.67439E-07	5.464932	0.000546	8.2802E-06	660.8752	0.066088	0.001180134
366	BR14-1	852.042	0.085204	0.001549167	29.89492	0.002989	3.39715E-05	246.1618	0.024616	0.00091171	0.133261	1.33E-05	1.48068E-07	0.363422	3.63E-05	6.19118E-07	1.094807	0.000109	2.4329E-06	6.982177	0.000698	1.05791E-05	1309.049	0.130905	0.002337588
373.1	BR15-1	895.9971	0.0896	0.001629086	33.10649	0.003311	3.7621E-05	121.3028	0.01213	0.00044927	0.060242	6.02E-06	6.69356E-08	0.327551	3.28E-05	5.58008E-07	0.915668	9.16E-05	2.03482E-06	#####	#####	#####	#####	#####	#####
382.75	BR16-1	2011.72	0.201172	0.003657673	23.48903	0.002349	2.66921E-05	83.12794	0.008313	0.000307881	0.013393	1.34E-06	1.48808E-08	0.743122	7.43E-05	1.26597E-06	0.263605	2.64E-05	5.85788E-07	#####	#####	#####	#####	#####	#####
482.2	BR17-1	370.1597	0.037016	0.000673018	6.112818	0.000611	6.94638E-06	89.31596	0.008932	0.0003308	#VALUE!	#VALUE!	#VALUE!	0.257871	2.58E-05	4.39303E-07	0.129186	1.29E-05	2.87081E-07	5.092889	0.000509	7.7165E-06	1950.419	0.195042	0.003482891
486.75	BR18-1	400.253	0.040025	0.000727733	8.097519	0.00081	9.20173E-06	141.0433	0.014104	0.000522383	0.013485	1.35E-06	1.49833E-08	0.355589	3.56E-05	6.05774E-07	0.213247	2.13E-05	4.73882E-07	######	######	######	######	######	######
489.7	BR19-1	748.676	0.074868	0.001361229	7.21184	0.000721	8.19527E-06	1121.86	0.112186	0.004155038	0.223792	2.24E-05	2.48658E-07	0.491087	4.91E-05	8.36604E-07	1.040823	0.000104	2.31294E-06	18.2978	0.00183	2.77239E-05	4388.158	0.438816	0.007835996
505.6	BR20-1	255.8476	0.025585	0.000465177	5.164016	0.000516	5.8682E-06	65.32299	0.006532	0.000241937	0.018369	1.84E-06	2.04097E-08	0.3258	3.26E-05	5.55025E-07	0.19687	1.97E-05	4.37489E-07	7.444716	0.000744	1.12799E-05	1804.564	0.180456	0.003222435
511.38	BR21-1	1038.76	0.103876	0.001888654	29.32369	0.002932	3.33224E-05	115.362	0.011536	0.000427267	0.016918	1.69E-06	1.87974E-08	0.135608	1.36E-05	2.31019E-07	1.086755	0.000109	2.41501E-06	8.711118	0.000871	1.31987E-05	2003.843	0.200384	0.003578292
514.7	BR22-1	151.5165	0.015152	0.000275485	6.042918	0.000604	6.86695E-06	79.3697	0.007937	0.000293962	0.045248	4.52E-06	5.0276E-08	0.387625	3.88E-05	6.6035E-07	0.213514	2.14E-05	4.74476E-07	######	######	######	######	######	######
520.85	BR23-1	194.2116	0.019421	0.000353112	6.441461	0.000644	7.31984E-06	44.82712	0.004483	0.00016602	0.016546	1.65E-06	1.83848E-08	0.247117	2.47E-05	4.20983E-07	0.141684	1.42E-05	3.14852E-07	7.887723	0.000789	1.19511E-05	1093.602	0.10936	0.00195286
535.25	BR26-1	272.3651	0.027237	0.000495209	33.24807	0.003325	3.77819E-05	76.92057	0.007692	0.000284891	#VALUE!	#VALUE!	#VALUE!	0.355976	3.56E-05	6.06433E-07	0.225261	2.25E-05	5.0058E-07	10.35377	0.001035	1.56875E-05	1319.344	0.131934	0.002355971
539.1	BR27-1	#VALUE!	#VALUE!	#VALUE!	#VALUE!	#VALUE!	#VALUE!	#VALUE!	#VALUE!	#VALUE!	#VALUE!	#VALUE!	#VALUE!	#VALUE!	#VALUE!	#VALUE!	#VALUE!	#VALUE!	#VALUE!	#VALUE!	#VALUE!	#VALUE!	#VALUE!	#VALUE!	#VALUE!
543.75	BR28-1	563.9508	0.056395	0.001025365	4.771236	0.000477	5.42186E-06	176.7237	0.017672	0.000654532	0.033875	3.39E-06	3.76391E-08	0.877589	8.78E-05	1.49504E-06	0.750072	7.5E-05	1.66683E-06	#VALUE!	#VALUE!	#VALUE!	#VALUE!	#VALUE!	#VALUE!
551.37	BR29-1	1257.205	0.12572	0.002285827	10.58391	0.001058	1.20272E-05	253.2174	0.025322	0.000937842	0.075553	7.56E-06	8.39477E-08	0.741843	7.42E-05	1.26379E-06	0.71749	7.17E-05	1.59442E-06	#VALUE!	#VALUE!	#VALUE!	#VALUE!	#VALUE!	#VALUE!

LEACH 2

		Mn			Sr			Al			Zr			Ni			Sc			Zn			Fe		
Depth (m)	Sample	ppm	wt %	mol fraction	ppm	wt %	mol fraction	ppm	wt %	mol fraction	ppm	wt %	mol fraction	ppm	wt %	mol fraction	ppm	wt %	mol fraction	ppm	wt %	mol fraction	ppm	wt %	mol fraction
252.5	BR01-2	1690.173	0.169017	0.003073041	24.80431	0.00248	2.81867E-05	352.6984	0.03527	0.00130629	0.187104	1.87E-05	2.07893E-07	0.40095	4.01E-05	6.83049E-07	1.681611	0.000168	3.73691E-06	5.560699	0.000556	8.4253E-06	1095.097	0.10951	0.001955531
310	BR03-2	1056.639	0.105664	0.001921161	13.3607	0.001336	1.51826E-05	74.92325	0.007492	0.000277494	0.03296	3.3E-06	3.66222E-08	0.095196	9.52E-06	1.62174E-07	0.313298	3.13E-05	6.96217E-07	5.345818	0.000535	8.09972E-06	7825.187	0.782519	0.013973548
312.9	BR04-2	455.316	0.045532	0.000827847	21.49068	0.002149	2.44212E-05	34.22248	0.003422	0.00012675	0.0293	2.93E-06	3.2556E-08	0.224769	2.25E-05	3.82911E-07	0.348605	3.49E-05	7.74677E-07	2.188256	0.000219	3.31554E-06	1113.995	0.111399	0.001989276
321.05	BR05-2	350.3356	0.035034	0.000636974	18.38441	0.001838	2.08914E-05	74.55211	0.007455	0.000276119	0.680691	6.81E-05	7.56323E-07	0.104061	1.04E-05	1.77276E-07	0.644394	6.44E-05	1.43199E-06	2.110282	0.000211	3.1974E-06	386.328	0.038633	0.000689871
325.38	BR06-2	53.41504	0.005342	9.71183E-05	3.484197	0.000348	3.95931E-06	11.81516	0.001182	4.37599E-05	0.014437	1.44E-06	1.60417E-08	0.023924	2.39E-06	4.07565E-08	0.087904	8.79E-06	1.95342E-07	######	######	######	######	######	######
328.1	BR07-2	193.2352	0.019324	0.000351337	12.47203	0.001247	1.41728E-05	74.27391	0.007427	0.000275089	0.118685	1.19E-05	1.31872E-07	0.086083	8.61E-06	1.46649E-07	0.834197	8.34E-05	1.85377E-06	1.684842	0.000168	2.55279E-06	369.0037	0.0369	0.00069465
334.57	BR08-2	235.0158	0.023502	0.000427301	19.18225	0.001918	2.1798E-05	52.37137	0.005237	0.000193968	0.030145	3.01E-06	3.34947E-08	0.190356	1.9E-05	3.24286E-07	0.232732	2.33E-05	5.17182E-07	1.954743	0.000195	2.96173E-06	368.0376	0.038804	0.000692924
339.8	BR09-2	24.13625	0.002414	4.38841E-05	0.673491	6.73E-05	7.6533E-07	57.74543	0.005775	0.000213872	#VALUE!	#VALUE!	#VALUE!	#VALUE!	#VALUE!	#VALUE!	0.06996	7E-06	1.55468E-07	0.491587	4.92E-05	7.44829E-07	118.0234	0.011802	0.000210756
350	BR11-2	362.8444	0.036284	0.000659717	9.374886	0.000937	1.06533E-05	93.97201	0.009397	0.000348044	0.11247	1.12E-05	1.24966E-07	0.120381	1.2E-05	2.05079E-07	0.521069	5.21E-05	1.15793E-06	######	######	######	######	######	######
358.45	BR12-2	168.1414	0.016814	0.000305712	2.514254	0.000251	2.85711E-06	309.0152	0.030902	0.001144501	0.259287	2.59E-05	2.88097E-07	0.141182	1.41E-05	2.40515E-07	0.270316	2.7E-05	6.00702E-07	######	######	######	######	######	######
360.3	BR13-2	298.503	0.02985	0.000542733	5.341553	0.000534	6.06995E-06	94.41295	0.009441	0.000349678	0.039219	3.92E-06	4.35762E-08	0.106405	1.06E-05	1.81269E-07	0.212174	2.12E-05	4.71497E-07	2.590085	0.000259	3.92437E-06	736.1401	0.073614	0.001314536
366	BR14-2	235.9766	0.023598	0.000429048	4.57671	0.000458	5.20081E-06	109.3786	0.010938	0.000405106	0.037648	3.76E-06	4.1831E-08	0.152414	1.52E-05	2.59649E-07	0.301327	3.01E-05	6.69615E-07	2.070618	0.000207	3.1373E-06	553.8533	0.055385	0.000989024
373.1	BR15-2	275.4708	0.027547	0.000500856	9.429126	0.000943	1.07149E-05	146.396	0.01464	0.000542207	0.095365	9.54E-06	1.05961E-07	0.114712	1.15E-05	1.95421E-07	0.481815	4.82E-05	1.0707E-06	######	######	######	######	######	######
382.75	BR16-2	1449.228	0.144923	0.002634961	16.85462	0.001685	1.9153E-05	67.38697	0.006739	0.000249581	#VALUE!	#VALUE!	#VALUE!	0.472723	4.73E-05	8.0532E-07	0.193047	1.93E-05	4.28992E-07	8.915345	0.000892	1.35081E-05	1258.086	0.125809	0.002246583
482.2	BR17-2	212.3848	0.021238	0.000386154	3.775386	0.000378	4.29021E-06	39.21883	0.003922	0.000145255	#VALUE!	#VALUE!	#VALUE!	0.1848	1.85E-05	3.1482E-07	0.070387	7.04E-06	1.56417E-07	2.571603	0.000257	3.89637E-06	1049.797	0.10498	0.001874637
486.75	BR18-2	137.0924	0.013709	0.000249259	3.058127	0.000306	3.47514E-06	35.58175	0.003558	0.000131784	0.010741	1.07E-06	1.19348E-08	0.094583	9.46E-06	1.61129E-07	0.058962	5.9E-06	1.31072E-07	4.561004	0.000456	6.91061E-06	789.4458	0.078945	0.001409725
489.7	BR19-2	466.5326	0.046653	0.000848241	4.275083	0.000428	4.85805E-06	340.8139	0.034081	0.001262274	0.066066	6.61E-06	7.34064E-08	0.282836	2.83E-05	4.81834E-07	0.599835	6E-05	1.33297E-06	8.036432	0.000804	1.21764E-05	2903.444	0.290344	0.005184721
505.6	BR20-2	278.8482	0.027885	0.000506997	5.684524	0.000568	6.45969E-06	52.35957	0.005236	0.000193924	#VALUE!	#VALUE!	#VALUE!	0.110768	1.11E-05	1.88702E-07	0.254803	2.55E-05	5.66229E-07	3.776887	0.000378	5.72256E-06	2342.015	0.234201	0.004182169
511.38	BR21-2	490.6667	0.049067	0.000892121	9.88432	0.000988	1.12322E-05	83.01555	0.008302	0.000307465	0.013647	1.36E-06	1.51636E-08	#VALUE!	#VALUE!	#VALUE!	0.497906	4.98E-05	1.10646E-06	3.700988	0.00037	5.60756E-06	1670.712	0.167071	0.002983415
514.7	BR22-2	85.5375	0.008554	0.000155523	3.504505	0.00035	3.98239E-06	40.45978	0.004046	0.000149851	0.024392	2.44E-06	2.71022E-08	0.104087	1.04E-05	1.77321E-07	0.132142	1.32E-05	2.93648E-07	######	######	######	######	######	######
520.85	BR23-2	104.1869	0.010419	0.000189431	3.800783	0.00038	4.31907E-06	31.63071	0.003163	0.000117151	#VALUE!	#VALUE!	#VALUE!	#VALUE!	#VALUE!	#VALUE!	0.079715	7.97E-06	1.77145E-07	1.272992	0.000127	1.92878E-06	620.087	0.062009	0.001107298
535.25	BR26-2	191.5175	0.019152	0.000348214	5.351378	0.000535	6.08111E-06	43.94635	0.004395	0.000162764	#VALUE!	#VALUE!	#VALUE!	#VALUE!	#VALUE!	#VALUE!	0.202128	2.02E-05	4.49174E-07	3.166566	0.000317	4.79783E-06	1038.847	0.103885	0.001855084
539.1	BR27-2	215.062	0.021506	0.000391022	3.324059	0.000332	3.77734E-06	98.8026	0.00988	0.000365936	#VALUE!	#VALUE!	#VALUE!	0.196317	1.96E-05	3.34441E-07	0.073268	7.33E-06	1.62817E-07	10.81235	0.001081	1.63623E-05	1013.451	0.101345	0.001809734
543.75	BR28-2	482.7838	0.048278	0.000877789	3.808186	0.000381	4.32748E-06	78.58499	0.007858	0.000291056	0.011697	1.17E-06	1.29963E-08	0.26165	2.62E-05	4.45741E-07	0.602454	6.02E-05	1.33879E-06	######	######	######	######	######	######
551.37	BR29-2	753.3524	0.075335	0.001369732	5.774611	0.000577	6.56206E-06	204.4396	0.020444	0.000757184	0.133415	1.33E-05	1.48239E-07	0.362992	3.63E-05	6.18384E-07	0.431464	4.31E-05	9.5881E-07	######	######	######	######	######	######

LEACH 3

		Mn			Sr			Al			Zr			Ni			Sc			Zn			Fe		
Depth (m)	Sample	ppm	wt %	mol fraction	ppm	wt %	mol fraction	ppm	wt %	mol fraction	ppm	wt %	mol fraction	ppm	wt %	mol fraction	ppm	wt %	mol fraction	ppm	wt %	mol fraction	ppm	wt %	mol fraction
252.5	BR01-3	1378.679	0.137868	0.00250669	22.19161	0.002219	2.52177E-05	1278.731	0.127873	0.00473604	0.330453	3.3E-05	3.6717E-07	1.236034	0.000124	2.10568E-06	1.168366	0.000117	2.59637E-06	6.147271	0.000615	9.31405E-06	3633.05	0.363305	0.00648759
310	BR03-3	1820.245	0.182024	0.003309536	19.08989	0.001909	2.16931E-05	155.0289	0.015503	0.000574181	0.143957	1.44E-05	1.59952E-07	0.232628	2.33E-05	3.963E-07	0.51068	5.11E-05	1.13484E-06	5.554965	0.000555	8.41661E-06	16416.45	1.641645	0.029315068
312.9	BR04-3	1001.204	0.10012	0.00182037	37.91111	0.003791	4.30808E-05	163.9254	0.016393	0.000607131	0.862891	8.63E-05	9.58767E-07	0.329557	3.3E-05	5.61427E-07	1.020153	0.000102	2.26701E-06	4.390169	0.000439	6.65177E-06	3941.848	0.394185	0.007039014
321.05	BR05-3	171.4056	0.017141	0.000311646	20.1335	0.002013	2.2879E-05	60.69611	0.00607	0.0002248	0.05432	5.43E-06	6.03552E-08	0.09085	9.09E-06	1.5477E-07	0.694014	6.94E-05	1.54225E-06	0.582116	5.82E-05	8.81994E-07	325.3551	0.032536	0.000580991
325.38	BR06-3	287.3107	0.028731	0.000522383	23.51331	0.002351	2.67197E-05	153.0734	0.015307	0.000566939	0.13761	1.38E-05	1.529E-07	0.157978	1.58E-05	2.69128E-07	0.657221	6.57E-05	1.46049E-06	1.351263	0.000135	2.04737E-06	397.8726	0.039787	0.000710487
328.1	BR07-3	101.2523	0.010125	0.000184095	16.15335	0.001615	1.83561E-05	71.14153	0.007114	0.000263487	0.068561	6.86E-06	7.61787E-08	#VALUE!	#VALUE!	#VALUE!	0.569494	5.69E-05	1.26554E-06	0.604302	6.04E-05	9.15609E-07	373.8507	0.037385	0.00066759
334.57	BR08-3	62.67422	0.006267	0.000113953	17.54911	0.001755	1.99422E-05	22.03314	0.002203	8.16042E-05	0.042213	4.22E-06	4.69032E-08	#VALUE!	#VALUE!	#VALUE!	0.106809	1.07E-05	2.37354E-07	0.533867	5.34E-05	8.08889E-07	230.2001	0.02302	0.000411072
339.8	BR09-3	50.19326	0.005019	9.12605E-05	5.771337	0.000577	6.55834E-06	76.63378	0.007663	0.000283829	#VALUE!	#VALUE!	#VALUE!	#VALUE!	#VALUE!	#VALUE!	0.126821	1.27E-05	2.81824E-07	######	######	######	######	######	######
350	BR11-3	864.4137	0.086441	0.001571661	20.00965	0.002001	2.27382E-05	465.8084	0.046581	0.001725216	0.220234	2.2E-05	2.44704E-07	0.472432	4.72E-05	8.04824E-07	1.449553	0.000145	3.22123E-06	######	######	######	######	######	######
358.45	BR12-3	689.0106	0.068901	0.001252747	9.067098	0.000907	1.03035E-05	1121.852	0.112185	0.004155007	0.118526	1.19E-05	1.31695E-07	0.455424	4.55E-05	7.7585E-07	1.515569	0.000152	3.36793E-06	######	######	######	######	######	######
360.3	BR13-3	82.15776	0.008216	0.000149378	9.393328	0.000939	1.06742E-05	21.12294	0.002112	7.82331E-05	0.015364	1.54E-06	1.70706E-08	#VALUE!	#VALUE!	#VALUE!	0.061929	6.19E-06	1.3762E-07	0.622642	6.23E-05	9.43397E-07	154.0042	0.0154	0.000275007
366	BR14-3	1584.887	0.158489	0.002881612	25.17323	0.002517	2.86059E-05	244.2385	0.024424	0.000904587	0.171151	1.71E-05	1.90168E-07	1.1968	0.00012	2.03884E-06	2.478113	0.000248	5.50692E-06	######	######	######	######	######	######
373.1	BR15-3	166.7042	0.01667	0.000303099	5.019031	0.000502	5.70344E-06	95.72158	0.009572	0.000354524	0.093084	9.31E-06	1.03427E-07	0.137042	1.37E-05	2.33462E-07	0.298794	2.99E-05	6.63987E-07	######	######	######	######	######	######
382.75	BR16-3	531.5639	0.053156	0.00096648	9.712797	0.000971	1.10373E-05	67.24241	0.006724	0.000249046	0.089782	8.98E-06	9.97574E-08	0.294235	2.94E-05	5.01252E-07	0.108892	1.09E-05	2.41981E-07	4.262545	0.000426	6.4584E-06	618.4074	0.061841	0.001104299
482.2	BR17-3	232.8133	0.023281	0.000423297	6.148593	0.000615	6.98704E-06	62.94893	0.006295	0.000233144	0.053018	5.3E-06	5.89084E-08	0.33614	3.36E-05	5.72641E-07	0.137965	1.38E-05	3.0659E-07	4.026158	0.000403	6.10024E-06	1033.52	0.103352	0.001845571
486.75	BR18-3	44.686	0.004469	8.12473E-05	3.913452	0.000391	4.4471E-06	32.07094	0.003207	0.000118781	0.01527	1.53E-06	1.69672E-08	#VALUE!	#VALUE!	#VALUE!	0.029341	2.93E-06	6.52029E-08	1.228196	0.000123	1.8609E-06	326.661	0.032666	0.000583323
489.7	BR19-3	273.8745	0.027387	0.000497954	4.421103	0.000442	5.02398E-06	107.6567	0.010766	0.000398728	0.019322	1.93E-06	2.14685E-08	0.173526	1.74E-05	2.95615E-07	0.309507	3.1E-05	6.87794E-07	3.746025	0.000375	5.6758E-06	574.5578	0.057456	0.001025996
505.6	BR20-3	22.68812	0.002269	4.12511E-05	1.192555	0.000119	1.35518E-06	17.95432	0.001795	6.64975E-05	0.016448	1.64E-06	1.82758E-08	#VALUE!	#VALUE!	#VALUE!	0.018042	1.8E-06	4.00942E-08	#VALUE!	#VALUE!	#VALUE!	#VALUE!	#VALUE!	#VALUE!
511.38	BR21-3	385.9566	0.038596	0.000701739	20.30736	0.002031	2.30765E-05	45.02813	0.004503	0.000166771	0.02427	2.43E-06	2.69665E-08	0.093027	9.3E-06	1.58479E-07	0.466059	4.66E-05	1.03569E-06	2.989552	0.000299	4.52962E-06	520.0618	0.052006	0.000928682
514.7	BR22-3	261.4379	0.026144	0.000475342	12.28061	0.001228	1.39552E-05	121.5607	0.012156	0.000450225	0.23319	2.33E-05	2.591E-07	0.569332	5.69E-05	9.69901E-07	0.465029	4.65E-05	1.0334E-06	######	######	######	######	######	######
520.85	BR23-3	126.135	0.012613	0.000229336	3.177391	0.000318	3.61067E-06	17.00523	0.001701	6.29623E-05	0.032116	3.21E-06	3.56848E-08	0.095178	9.52E-06	1.62143E-07	0.086138	8.61E-06	1.91419E-07	0.806057	8.06E-05	1.2213E-06	151.947	0.015195	0.000271334
535.25	BR26-3	1162.527	0.116253	0.002113686	23.83913	0.002384	2.70899E-05	150.1733	0.015017	0.000556197	0.224736	2.25E-05	2.49707E-07	0.692333	6.92E-05	1.17944E-06	1.309806	0.000131	2.91068E-06	7.857632	0.000786	1.19055E-05	4934.354	0.493435	0.008811346
539.1	BR27-3	288.5433	0.028854	0.000524624	5.334695	0.000533	6.06215E-06	85.59003	0.008559	0.000317	0.034609	3.46E-06	3.84542E-08	0.286729	2.87E-05	4.88465E-07	0.560259	5.6E-05	1.24502E-06	7.137499	0.000714	1.08144E-05	1297.848	0.129785	0.002317585
543.75	BR28-3	248.3193	0.024832	0.00045149	2.290062	0.000229	2.60234E-06	49.05862	0.004906	0.000181699	0.0859	8.59E-06	9.54447E-08	0.115504	1.16E-05	1.9677E-07	0.419031	4.19E-05	9.3118E-07	10.17554	0.001018	1.54175E-05	555.2713	0.055527	0.000991556
551.37	BR29-3	1087.527	0.108753	0.001977321	10.60262	0.00106	1.20484E-05	56.3459	0.005635	0.000208689	0.043202	4.32E-06	4.80025E-08	0.54118	5.41E-05	9.21941E-07	0.524369	5.24E-05	1.16527E-06	23.83086	0.002383	3.61074E-05	211.3316	0.021133	0.000377378